THE HONG KONG
POLYTECHNIC UNIVERSITY
香港理工大學
Pao Yue-kong Library
包玉剛圖書館

Copyright Undertaking

This thesis is protected by copyright, with all rights reserved.

By reading and using the thesis, the reader understands and agrees to the following terms:

1. The reader will abide by the rules and legal ordinances governing copyright regarding the use of the thesis.
2. The reader will use the thesis for the purpose of research or private study only and not for distribution or further reproduction or any other purpose.
3. The reader agrees to indemnify and hold the University harmless from and against any loss, damage, cost, liability or expenses arising from copyright infringement or unauthorized usage.

If you have reasons to believe that any materials in this thesis are deemed not suitable to be distributed in this form, or a copyright owner having difficulty with the material being included in our database, please contact lbsys@polyu.edu.hk providing details. The Library will look into your claim and consider taking remedial action upon receipt of the written requests.

Pao Yue-kong Library, The Hong Kong Polytechnic University, Hung Hom, Kowloon, Hong Kong

http://www.lib.polyu.edu.hk

The Hong Kong Polytechnic University

Department of Industrial and Systems Engineering

Development of Nickel-free Barrier Coating for the Electroplating Industry

A Thesis submitted in Fulfilment

of the Requirements

for the Degree of

Master of Philosophy

by

Siu Cho Lung

June 2003

Pao Yue-kong Library
PolyU • Hong Kong

CERTIFICATE OF ORIGINALITY

I hereby declare that this thesis is my own work and that, to the best of my knowledge and belief, it reproduces no material previously published or written nor material which has been accepted for the award of any other degree or diploma, except where due acknowledgement has been made in the text.

_____(Signed)

Siu Cho Lung (Name of Student)

ABSTRACT

The European Union has been an important market for our watches, spectacle frames and jewellery. Nickel was used as the electroplated barrier coating to control the migration of the basis metal to the gold and gold alloy over-plated decorative. Since 1994, the Council of European Union has controlled the used of nickel in objects intended to be in contact with skin. The search for a barrier coating to replace Nickel has been a popular research topic over the years. Palladium and copper tin alloys have been explored but the price of the former and the temperature instability of the latter have caused concerned to the industry. Cobalt is less toxic in terms of skin toxicity and has low solubility for copper. Cobalt and its alloys have been proved to be good barriers for copper diffusion. However, the corrosion resistance of cobalt is worse than nickel. The main aim of this project is to develop binary and ternary electroplated cobalt alloys as barrier coatings which possess both good barrier and corrosion resistant properties. The plating solution compositions and the process conditions were investigated. The barrier and corrosion resistant properties for a range of coatings were compared.

By using citrate as complexing agent, the cobalt-molybdenum(Co-Mo), cobalt-phosphorus(Co-P) and cobalt-molybdenum-phosphorus(Co-Mo-P) alloy

coatings were successfully developed and electrodeposited. The Co-Mo with 31.6% of molybdenum and Co-P with 22.1 % P were optimized. By combining the Co-Mo and Co-P plating baths, the Co-Mo-P bath was obtained. The coating contains 8% Mo and 20% phosphorus.

To study the diffusion property, the interdiffusion coefficients of copper/barrier were determinated. The micro-profiling and Boltzmann-Matano Method were used to obtain the interdiffusion coefficients. It was found that the interdiffusion coefficients for nickel are higher than that of the cobalt base alloys. The results of this project have indicated the potentials of these alloys as effective and economical substitutes for nickel.

ACKNOWLEDGEMENTS

Many people have given helps and guidance to the author during the course of this research work and the author would like to mention some of them help. The most concrete assistance came from the author's supervisor Dr. H. C. Man (Department of Industrial and Systems Engineering) and co-supervisor Dr. C. H. Yeung (Department of Applied Biology and Chemical Technology) who provided many insightful suggestions and comments and provided the author with a whole range of new emotion and experiences that the author could not have previously anticipated and understood.

The author would also like to express his gratitude to Dr. W. Y. Ng for his encouragement to the author during his stay at the Hong Kong Polytechnic University.

The author would also like to thank all the staff members of ABCT at Hong Kong Polytechnic University for their help and cooperation throughout the author's stay in their Instrumental Analysis Laboratory and Industrial Chemistry Laboratory.

The financial support from the Research Committee of the Hong Kong Polytechnic University (project no. V793), which was essential for the author's graduate studies, is acknowledged.

Paper to be submitted for journal publication

1. Electrodeposition of Co-Mo-P barrier coating for Cu/Au system.

2. Interdiffusion coefficients of various cobalt base alloy coatings for Cu/Au system

LIST OF TABLES

LIST OF FIGURES

TABLE OF CONTENTS

Chapter 1 Introduction

1.1 Introduction

Gold is used extensively as the decorative coatings for watches, spectacles and jewelleries of which copper and its alloys are frequently used as base metals. Gold has aesthetic appearance and good corrosion resistance. Due to economical reasons, thin gold plating normally applied. When gold is plated on the copper and its alloys, copper will migrate to the gold layer and similarly gold will diffuse into the base metal. When copper diffuses to the top of the coating, it is tarnished by air and gold coating thus loses its aesthetic appearance. The copper/barrier coating/gold system is commonly used in electroplating industry and the barrier coating serves to block diffusion of copper into the gold overplate.

Traditionally, nickel and its alloys were used as the electroplated barrier coating to control the migration of copper to the over-plated gold coating. However, when the gold plated jewellery or watches are in direct contact with human skin, body perspiration migrates though crystal boundaries of the gold coating and interacts with nickel layer and as a result nickel ions are released. Nickel ions cause dermatitis and nickel allergy. A survey was conducted by the University of Barcelona and found that a high percentage of women were allergic to nickel ions after prolong exposure [1]. In view of the allergic effect of nickel in skin, the Commission of the European Union

(EU) has implemented controls, on the use of nickel for products directly in contact with the human body. For articles with direct contact to human bodies which have Ni^{2+} ions release rates of more than 0.5 $\mu g/cm^2$/week are prohibited [2].

The search for replacements of nickel as barrier coating has been actively pursued [3]. Palladium [4] and copper/tin [5] coatings have been used in the last few years as nickel substitute. The rapid hiking on the cost of palladium in the last couple of years and other teething problems such as hydrogen inclusion and high stress problems have also worried manufacturers. Copper/tin alloy coating can be a good barrier at low temperature. However, losses of the barrier property at high temperature, high internal stress and sublimation in high vacuum-temperature problems limit its use.

The aim of this project is to develop nickel-free barrier materials for the electroplating industry. Because low solubility of copper in cobalt, cobalt coatings are efficient copper barrier coatings [6]. Chow Kam Moon [7] studied the barrier effectiveness of nickel, palladium, palladium-iron, cobalt and cobalt-tungsten and found that cobalt and cobalt-tungsten are better than nickel in terms of barrier property. Cobalt and its alloys can be used as copper barrier. The severity on skin allergy is about 1/100 of nickel [8].

However, cobalt is less resistant to corrosion than nickel. The alloys of cobalt

can be tailored made to give excellent barrier property and corrosion resistant property. Molybdenum is known to increase corrosion resistant property in metal alloying. Phosphorus can be co-deposited with iron group metal such as nickel and cobalt to form amorphous coatings. The amorphous coatings have high corrosion resistance because they are free of crystal defects [9]. Many investigators have studied the deposition of cobalt-molybdenum [10,11] and cobalt-phosphorus [12], but little investigation has been reported on the deposition of cobalt-molybdenum-phosphorus.

1.2 Objectives of this project

The objective of this project: (1) to investigate the electroplating conditions of cobalt-molybdenum, cobalt-phosphorus and cobalt-molybdenum-phosphorus alloy coatings; (2) to compare the coating properties such as diffusion barrier property, corrosion resistance, crystal structure and internal stress these coatings; (3) to compare the diffusion barrier behavior of those coatings has also been studied. Diffusion barrier properties of electrodeposits with that nickel and to evaluate their suitability as an alternative to nickel as diffusion barrier for copper diffusion in electroplating industry; (4) to develop a semi-quantitative method and an apparent diffusion coefficient to compare the barrier performance of those coating.

Chapter 2 Literature and Theory Review

2.1 Diffusion in copper/gold system

Diffusion is an irreversible and spontaneous reaction in a system to achieve equilibrium though the elimination of concentration gradients of the atomic species comprising the couple [13]. Atoms or molecules within a material move to new sites and the net movement is from the direction of regions of low concentration in order to achieve homogeneity of the solution, which may be a liquid, solid or gas.

Diffusion can result in degradation of the properties of a deposit, particularly at the basis metal interface. In a gold/copper system, intermetallics form at room temperature over time and bulk lattice diffusion occurs at 200 to 250°C. For example, one month of exposure at 250°C is sufficient to allow copper to diffuse extensively though 2.5 μm of gold overplate and at 500°C only three days are required for similar penetration of 25 μm of gold [14]. In the case of gold plated jewellery and watches, underlying copper can diffuse through the thin gold deposit to the surface where it oxidizes, and lose their aesthetic appearance. An effective way to retard diffusion is to use a barrier coating. Certain metals are used as barrier coatings which tend to block transport of the substrate metal into the noble metal overplate.

2.2 Nickel and Nickel-free Barrier Coatings

Nickel and nickel alloys as a layer between copper and the gold overplate are known to inhibit the diffusion of copper into the gold. M. Antler [15] observed that nickel inhibit the diffusion of copper into gold very effectively. Pickering et al [16] observed that Ni-8 wt % phosphorous deposits can withstand copper diffusion at 400°C for 19 days. However, nickel is a skin allergen and carcinogeneity of specific nickel compounds has aroused concerns [17,18]. The Commission of the European Union (EU) has implemented the control on the use of nickel for products directly in contact with the human body. Thus, substitutes for nickel as the diffusion barrier are highly desirable.

As the control for the use of nickel in skin contact object, many laboratories and manufacturers are searching for substitute for nickel. Palladium [4] and copper/tin [5] coatings have been used in the last few years as nickel replacement. Palladium is one of the precious metals, which has higher corrosion resistance. Chow Kam Moon [7] observed that palladium barrier is not as effective as nickel. Moreover, the rapid hiking on the cost of palladium in the last couple of years has plagued the manufacturers. Copper/tin alloy coating is one of developed nickel-free barriers. However, at over 80°C, the interdiffusion of copper, tin and gold become dominated [19]. Other problems such as high internal stress and sublimation in high vacuum-

temperature during ion plating limit their application.

2.3 Cobalt as Nickel-free Barrier Coating

Very few studies have been made on the use of electroplated cobalt and its alloys as barrier coatings. Cobalt and Cobalt-Tungsten have been suggest as a good substitute for, and even better than nickel, as the diffusion barrier material between copper and gold [7]. The excellent barrier property is based on of their mutual insolubility at low temperature, as indicated by the Cu-Co phase diagram [6]. It prevents copper from diffusing through the cobalt crystal grains. It is also less severe on skin allergy problem [8] and has not been controlled.

Chemically, cobalt bears close resemblance to nickel. The nickel plating bath can become cobalt plating bath when replace nickel salts by cobalt salts [20]. Although cobalt has excellent barrier property and better skin compatibility, there are two disadvantages on the use of cobalt as the replacement of nickel. The cobalt is more costly and less resistant to corrosion than nickel.

However, cobalt is capable to form alloy with a number of metals and non-metals in electroplating process such as molybdenum [21] and phosphorus [12]. Binary and ternary alloys of cobalt can be tailored made to give excellent barriers possessing synergistic characters with the other components, and provide good physical and anti-corrosion properties [22].

2.4 Cobalt-Molybdenum Alloy Plating

This is believed that high melting point metals such as molybdenum and tungsten are good barrier materials [23]. Molybdenum has a high melting point of 2610°C and is also known to increase anti-corrosion property in metal alloying. The oxides of molybdenum serve as very good passive coatings to prevent corrosion. Alloys containing 2-3% molybdenum, such as 316 stainless steel, can have enhanced corrosion resistance. There is no conclusive evidence that pure molybdenum has been deposited consistently from aqueous solutions. W. P. Price and O. W. Brown [24] obtained steel-gray deposits on iron or copper cathode at 50°C and 36 A/dm^2 from a molybdenum oxides-sulfuric acid solution. However, the complex procedures for preparing the bath solution and the decrease plating rates during working cause difficulty for industrializing the process.

Although this is less possible for obtaining pure molybdenum from aqueous solutions, molybdenum can be co-deposited with iron group metals by induced co-deposition [25]. Molybdenum co-deposited with cobalt can form amorphous coatings. The amorphous coatings have high corrosion resistance and good barrier coating because they are free of crystal defects [9]. An amorphous alloy coating can be formed when the molybdenum content is more than 15% (atomic) [26].

A large variety of baths have been investigated for the electrodeposition of

molybdenum alloys [10,11]. Typical bath compositions and conditions by several investigators for preparing cobalt-molybdenum alloys are listed in Table 2.4.1.

Citrate is a well-known complexing agent in electroplating process and citrate type of plating bath for alloys of molybdenum, both acidic [27] and alkaline [28], have been proposed. The alkaline citrate Co-Mo bath can produce ten times higher molybdenum content coatings with higher cathode efficiency than acid bath does. The coating is bright but cracked. Yukimi [29] suggested pulse current for deposition of amorphous cobalt-molybdenum coating. Yntema [30] describes the deposition of cobalt-molybdenum and iron-molybdenum alloys from sodium hydroxide-sodium carbonate solution containing dextrose. Cobalt can form a blue complex with hydroxide and dextrose. The baths used by Holt [31] gave cobalt alloy containing 4 to 17% (weight percent) and iron alloys containing 12 to 34 % (weight) molybdenum. Myers [32] describes the deposition of molybdenum with iron-group alloys from pyrophosphate solution that can produce an alloy containing 50% molybdenum.

Table. 2.4.1 Typical Cobalt-Molybdenum Alloy Plating Baths

Bath	Bath Composition			Temp. (°C)	Cathode Current Density (A/dm^2)	Cathode Efficiency (%)	Mo Content (%)
	Compound	Conc. (g/l)	pH				
Acidic Citrate	Cobalt Sulphate	60.0	3	25	5	27	4
	Sodium Molybdate	5					
	Citric acid	66					
	Aqueous Ammonia	to pH					
Alkaline Citrate	Cobalt Sulphate	85.0	10.5	25	10	60	40
	Sodium Molybdate	48.0					
	Sodium Citrate	105.0					
	Aqueous Ammonia	to pH					
Free Alkaline	Cobalt Sulphate	10.0	-	25	0.2	-	17
	Sodium Molybdate	20.0					
	Sodium Hydroxide	250.0					
	Sodium Carbonate	80.0					
	Dextrose	20.0					
Pyro-phosphate	Cobalt Sulphate	9.6	8	22	4	20	50
	Molybdic Oxide	20.0					
	Sodium Pyrophosphate	60.0					
	Sodium Bicarbonate	80.0					

2.5 Cobalt-Phosphorus Alloy Plating

Phosphorus is a non-metal and it cannot be deposited alone from an aqueous solution. Similar to molybdenum, phosphorus can be co-deposited with iron group metals [12] to form amorphous alloy coating [33]. The nickel-phosphorus and cobalt-phosphorus alloys were first deposited by electroless plating process developed by Brenner and Riddel [34].

The electropdeposition of cobalt and nickel alloys were suggested by Brenner [35]. Some electroplating baths have been investigated for the depositions of Ni-P and Co-P alloys. The bath compositions and conditions for preparing nickel-phosphorus alloys and cobalt-phosphorus alloys are listed in Table 2.5.1 and Table 2.5.2.

In summary, the baths for electroplating of Ni-P and Co-P alloys are usually strongly acidic. They work in a relatively high temperature and no complexing agent has been used. They produce coatings with phosphorus content ranging from 0.8 to 15%. The phosphorous acid is the main phosphorus source for the coatings and some formulations use sodium hypophosphite as phosphorus source.

The high acidity and operating temperature for these baths, the problems associated with corrosion on the base metal and the plating equipment worried electroplaters. In this study, it is proposed to introduce citric acid as a complexing agent and pH buffer for cobalt-phosphorus plating. Sodium hypophosphite as

phosphorus source is proposed in this project. Although phosphorous acid is now available commercially, it not as common as sodium hypophosphite. Sodium hypophosphite is widely used as a reducing agent in common electroless plating processes.

Table. 2.5.1 Typical Nickel-Phosphorus and Cobalt- Phosphorus Alloy Plating Baths

No.	Bath Composition			Temp. (°C)	Cathode Current Density (A/dm^2)	P Content (%)	References
	Compound	Conc. (g/l)	pH				
1	Nickel Sulfate	150.0	0.5-1	75-95	5-40	12-15	[35]
	Nickel Chloride	45.0					
	Nickel Carbonate	15.0					
	Phosphoric Acid	50.0					
	Phosphorous Acid	40.0					
2	Nickel Sulphamate	300.0	1.5-2	50-60	2-4	10-15	[36]
	Nickel Chloride	15.0					
	Boric Acid	20.0					
	Phosphorous Acid	12.0					
3	Nickel Sulfate	14.0	-	80	2.5	9 (at. %)	[36]
	Sodium Chloride	16.0					
	Boric Acid	15.0					
	Sodium Hypophosphite	5.0					
4	Cobalt Chloride	180.0	0.5-1	75-95	5-40	9-11	[35]
	Cobalt Carbonate	15.0					
	Phosphoric Acid	50.0					
	Phosphorous Acid	40.0					
5	Cobalt Chloride	240.0	1.5-2	75-95	5-30	0.8-1.2	[35]
	Formic Acid	45.0					
	Phosphorous Acid	2.0					

2.6 Cobalt-Molybdenum-Phosphorus Alloy Plating

Cobalt-molybdenum-phosphorus alloy can be obtained by electroless plating [37]. Molybdenum trioxide is the catalytic poison of electroless nickel-plating process [38] and slows down the plating rate. A typical cobalt-molybdenum-phosphorus electroless bath contains only 0.04 g/l ammonium molybdate and produces a coating contains 1% molybdenum and 3% phosphorus [37].

No literature on electrodeposited cobalt-molybdenum-phosphorus ternary alloy is found. The addition of phosphorus increases the possibility of forming amorphous coating. Adding a phosphorus source such as hypophosphite in citrate type cobalt-molybdenum bath may produce a cobalt-molybdenum-phosphorus ternary alloy coating.

2.7 Plating Range Tests

The plating range tests are used as a measure to predict electroplating bath ability before production. They are designed to cover a wide current density range on one cathode, permitting studies to be made of the interrelation between plating characteristics and current density. Plating range tests may be used to control any bath constituent which, when varied in concentration, produces a definite visual change in the appearance of the test deposit. The Hull cell illustrated in figure 2.7.1 is the most generally used device for plating range tests [39].

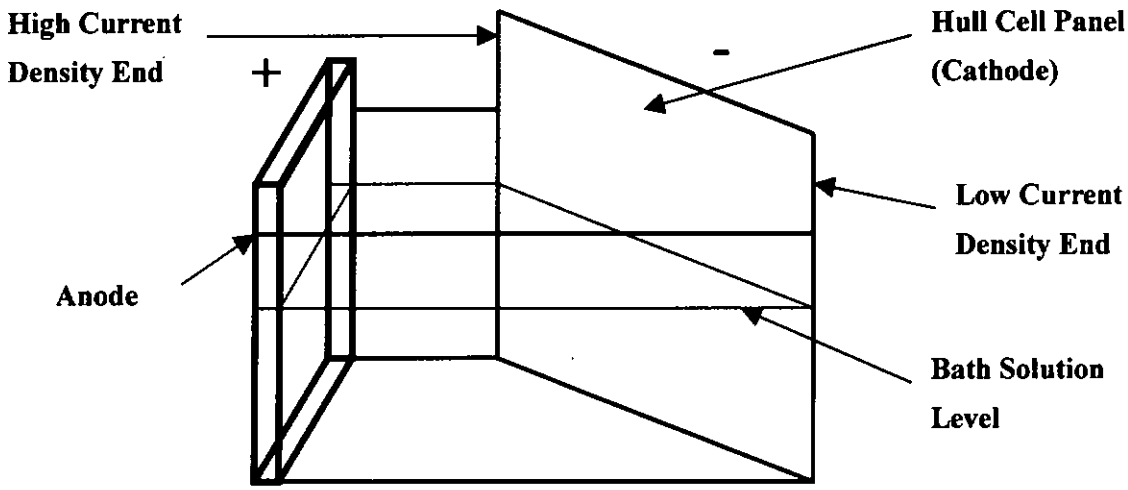

Fig. 2.7.1 The Diagram of Hull Cell

The Hull cell is constructed so that the cathode is maintained at a fixed acute angle with respect to the anode placed at the opposite end of the cell. Therefore, current density changes regularly across the width of the cathode. The current density scale approaches zero at the low current density edge of the cathode to infinite high current density on the opposite or high current density edge. The Hull cell usually has a solution volume of 267ml. This volume was selected for ease of calculating additions to the cell. This is because two grams per 267ml of any chemical addition equivalent to 1 oz per gal. The current density at any vertical plane on the cathode may be found by referring to equation 2.7.1.

$$i_{(L)} = I_{appl}(5.10 - 5.24 \log L) \qquad (2.7.1)$$

$i_{(L)}$ = Current density at a distance L (A/dm^2)

I_{appl} = Total cell current employed (A)

L = Length along the panel from High Current Density End (cm)

2.8 Determination of interdiffusion Coefficients by the Boltzmann-Matano Method

The interdiffusions of copper/barrier couples were studied by determination of the concentration-distance profile after heat treatment at different temperature. The problems associated with diffusion in a concentration gradient can be handled by Boltzmann-Matano method [40,41]. A chemical interdiffusion coefficient D is introduced that varies along the concentration gradient in the diffusion zone of Cu/barrier couple. Hence, chemical diffusivities were calculated from the concentration versus distance data at different copper concentration. Arrhenius plots (log diffusivity versus reciprocal temperature) can be constructed.

Heat treatment at temperature T leads to planar interdiffusion at the interface between two metal layers A and B. As interdiffusion proceeds, metal A will develop a profile of fractional atomic concentration $c_A(x)$. $D_{AB}(x)$ describes the progress of A atoms at a particular depth x measured from the original interface, where the host matrix is a mixture of A and B atoms in the proportion $c_A(x) : c_B(x)$. Exchange of two A atoms does not contribute to observed diffusing flux of species A. However, in a random vacancy diffusion process, the probability of successful replacement of a B atom with one type A will be proportional to $c_B(x)$. Therefore, the effective transport of species A from the interface, due to the combined migration both A and B atoms, is described by $D_{AB}(x)$, where

$$D_{AB}(x) = D_A c_A + D_B c_B \tag{2.8.1}$$

D_A and D_B can be deduced by measuring D_{AB} at several known concentrations (c_A, c_B) and then solve for D_A and D_B, for which the variation in D_{AB} with varying concentration can be handled by a method first proposed by Boltzmann. Fick's second law for one-dimensional diffusion is generalized to allow explicitly for variation in D by writing it in the form below

$$\frac{\partial c}{\partial t} = \frac{\partial}{\partial x}\left(D\frac{\partial c}{\partial x}\right) = D\frac{\partial^2 c}{\partial x^2} + \frac{\partial D(c)}{\partial c}\left(\frac{\partial c}{\partial x}\right)^2 \tag{2.8.2}$$

Assume a solution of the form

$$c = c\left(xt^{\frac{-1}{2}}\right) \tag{2.8.3}$$

And define $y = x\, t^{-1/2}$. Now by differentiation we obtain

$$\frac{\partial c}{\partial t} = \frac{dc}{dy}\frac{\partial y}{\partial t} = -\frac{1}{2}\frac{x}{t^{\frac{3}{2}}}\frac{dc}{dy} = -\frac{y}{2t}\frac{dc}{dy}$$

$$\frac{\partial c}{\partial x} = \frac{dc}{dy}\frac{\partial y}{\partial x} = t^{\frac{-1}{2}}\frac{dc}{dy}$$

$$\frac{\partial^2 c}{\partial x^2} = \frac{1}{t}\frac{\partial^2 c}{\partial y^2}$$

$$\frac{\partial D}{\partial x} = t^{\frac{-1}{2}}\frac{dD}{dy} \tag{2.8.4}$$

$$\frac{\partial c}{\partial t} = \frac{D}{t}\frac{\partial^2 c}{\partial y^2} + \frac{1}{t}\frac{dD}{dy}\frac{dc}{dy} = -\frac{y}{2t}\frac{dc}{dy} \tag{2.8.5}$$

$$\frac{d\left(D\frac{dc}{dy}\right)}{dy} = -\frac{y}{2}\frac{dc}{dy}$$

Solving for D and substituting for y, equation 2.8.6 was obtained

$$\tilde{D} = -\frac{1}{2}\frac{dy}{dc}\int_{c}^{c_0} y\,dc = \frac{1}{2t}\frac{dx}{dc}\int_{c}^{c_0} x\,dc \tag{2.8.6}$$

The interdiffusion coefficient, $\tilde{D}$ reflects the average of the overall movement of all constituents diffusing in concentration gradient.

Two homogeneous semi-infinite cylinders of different chemical composition that intimately joined at a mutual planar interface can be used as the model. For such configuration it becomes obvious that at $x = \pm\infty$, $dc/dx = 0$ and hence, equation 2.8.6 is undetermined as a result of the face that $c = 0$ or $c = c_0$ for each of arbitrary number of constituents. Consequently, equation 2.8.7 can be written

$$\frac{1}{2}\int_{c_0}^{c} y\,dc = \tilde{D}\frac{dc}{dy} = -\frac{1}{2}\int_{c_0}^{c} x\,dc \tag{2.8.7}$$

hence

$$\tilde{D} = -\frac{1}{2}\frac{dc}{dy}\int_{c_0}^{c} x\,dc \tag{2.8.8}$$

However, x must run from $-\infty$ to $+\infty$ for equation 2.8.8 to valid, and $x = 0$ must define a surface such that depletion of a particular constituent to the left of it must exactly equal the accumulation on the right. This is simply the requirement of the existence of a conservation of mass surface, which is named Matano interface. As a result of this

condition, t can be written equal to a constant

$$\int_{c_0}^{c_1} x dc - \int_{c'}^{c_1} x dc = 0 \text{ or} \tag{2.8.9}$$

$$\int_{c_0}^{c_1} x dc = \int_{c'}^{c_1} x dc \tag{2.8.10}$$

This situation is show a graphically in Figure 2.8.1.When the diffusion coefficient is independent of composition, $c_1 = c_0/2$ the Matano interface, after corrections for change in molar volumes, corresponds to the original interface. This is seldom if ever the case, although this condition is closely approached when the two members of the diffusion couple are of nearly the same composition. In actual practice, different elements diffuse with different velocities and furthermore are dependent upon composition. Values of D are computed graphically; for example, dx/dc is determined by drawing the tangent to the experimental measured diffusion profile at c'_1, the composition of interest, and the integration performed graphically:

$$D_{c=c'_1} = \frac{1}{2t}\frac{dx}{dc}\bigg|_{c=c'_1} \int_{c'}^{c_1} x dc$$

This method may be extended to other concentrations if one component is far more mobile than the rest by applying the graphical method shown in figure 2.8.2. Hence, equation 2.8.11 is obtained:

$$D_{c=c'_1} = -\frac{1}{2t}\frac{dx}{dc}\bigg|_{c=c'_1} \int_{0}^{c_1} x dc \tag{2.8.9}$$

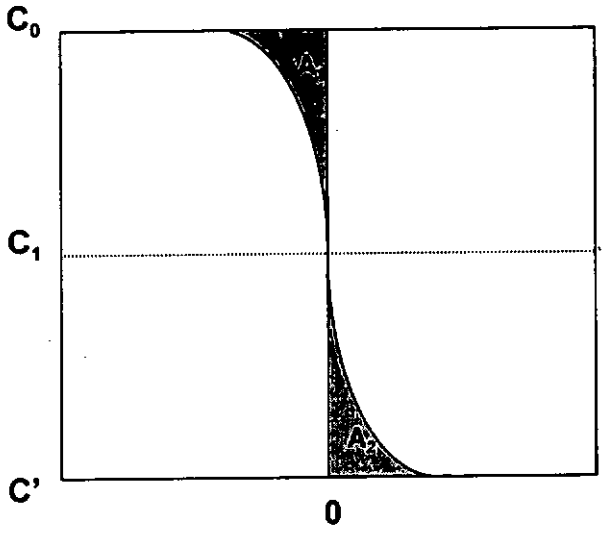

Fig. 2.8.1 Illustrating the Matano interface as defined by the areas A_1=A_2 for a specific constituent.

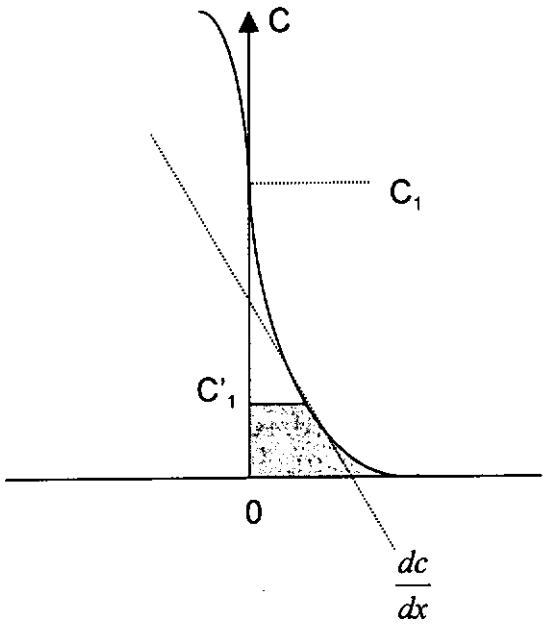

Fig. 2.8.2 Calculation of the chemical diffusion coefficient when only constituent is appreciably mobile.

By repetition of the process at a series of temperatures, Arrhenius plots for D_{AB}, D_A and D_B may be obtained, leading to experimental values for activation energies Q_{AB}, Q_A and Q_B.

2.9 Determination of Internal Stress by Spiral Contractometer

The properties of the coating surface will affect the apparance, the hardness, the ductility and the corrosion resistance. One of the important properties is the stress of the coating[42]. A residual stress may be defined as a stress within a material that is not subjected to load or temperature yet remains in internal equilibrium. Residual stress or so called internal stress in coating can cause adverse effects on properties. They may be responsible for peeling, tearing and blistering of the deposits. They may result in warping or cracking of deposits.

Internal stress appears to be unrelated to any physical property of a metal, such as strength, ductility, brightness, etc. In a deposit, it manifests itself by the latter being either stretch or compressed as compared with its normal state. When stretched, the deposit is in tension and tends to contract, whilst when compressed, it tends to expand. The nature of internal stress and their magnitude depend on the particular metal being deposited, on the operating parameters and on the composition of the electrolyte.

The structural cause of internal stress is not yet fully understood. However, there is some evidence that the coalescence of grains or parts of grains growing laterally

from different nucleation centers is a cause. The stress field around oriented arrays of dislocations produced by the coalescence or other growth process can add up to produce a macrostress. Changes in concentrations, distribution, or arrangement subsequent to incorporation of such foreign substances as hydrogen, basic colloids, or reaction productions from additions to the plating bath comprise another possible cause of macrostress [43].

The spiral contractometer[44] is one of the instruments which is suitable for production control and research. It is commercially available for stress measurement. The spiral contractometer manufactured by Yamamoto-MS Company was used in this study. It is based on the change of radius of curvature of a helix as the helix is plated. The stress in the deposit causes the helix to wind more tightly or to unwind, depending on the whether the deposit stress is compressive or tensile. The change in the radius of curvature is actually measured by angular displacement of one end of the helix while the other end is held rigid. The reading of the pointer on the top of the instrument is magnified by the gears. The torsional angle can be read out with the meter and calculate internal stress by the equation 2.9.1.

$$\sigma_E = k \times \left(\frac{2}{B \times S}\right) \times \left(\frac{\alpha}{D}\right) \times \left(1 + \frac{D}{S}\right) \qquad (2.9.1)$$

σ_E = Internal Stress (kg/mm^2)

k = Spiral Constant (mm g / degree)

α = Torsional Angle (degree)

D = Deposit Thickness (μm)

B = Spiral Plate Width (mm)

S = Spiral Plate Thickness (mm)

Since D/S is tends to zero, the equation will simplify to equation 2.9.2.

$$\sigma_E = k \times \left(\frac{2}{B \times S}\right) \times \left(\frac{\alpha}{D}\right) \tag{2.9.2}$$

For calibration, the helix is stretched a load and a torsional angle for the load is found.

$$K = k \times \left(\frac{2}{B \times S}\right) \tag{2.9.3}$$

$$k = \frac{g \times \frac{R}{2}}{\alpha'}$$

where:

g = Load (g)

R = Diameter of Helix (degree)

α' = Torsional Angle for Load g (degree)

B = Spiral Plate Width (mm)

S = Spiral Plate Thickness (mm)

The deposit thickness can be obtained by 2.9.4.

$$D = \left(\frac{G}{R \times h \times \pi \times \rho}\right) \times 10^6 \tag{2.9.4}$$

D = Deposit Thickness (μm)

R = Diameter of Helix (mm)

h = Length of Helix (mm)

π = Constant 3.14

ρ = Coating Density (g / cm^3)

Finally the equation become:

$$\sigma_E = K \times \left(\frac{\alpha}{D} \right) \tag{2.9.5}$$

For each plating experiment, K is a constant and can be found by equation 2.9.3. After obtaining the thickness and torsional angle, the internal stress for each coating thickness can be calculated by equation 2.9.5.

2.10 X-ray Diffraction Studies

X-ray diffraction techniques are used to identify the phases present in samples and to provide information on the grain size, texture and lattice parameter. High-energy (20kV) electron beam is directed into a water-cooled metal target for generation of X-rays. As electrons are decelerated in the target, most of the electron beam energy is lost in collisions that set the atom in motion and produce heat that must dissipated through the cooling water. The decelerated electron caught in the electric fields of the atom produces X-ray of a continum of all energies between zero and the excitation potential, and is termed as white ratiation. Some target electrons are knocked out of their orbitals, and the stored energy is released as the electrons from other orbitals drop into the vacant orbital, for which these electron transitions are

quantized and have specific wavelength, 0.15406nm, and the target is easily cooled for high efficiency. For copper radiation, a nickel foil absorbs most of the white radiation and the other characteristic peaks, transmitting essentilly pure Kα radiation. A proportional detector filed with xenon gas is used for detection of X-rays as it is particularly good for detecting X-ray radiation that has the wavelength of Cu or longer.

Characteristics of a sample can be determined from the collection of angles at which h the diffracted X-ray beams are detected. The lattice of the sample reflects the size and shape of the unit cells and their periodic arrangement in space. The lattice is fundamental to the geometry of any diffraction experiment. Interference of the scattered X-rays in most directions results in cancellation and absence of detectable beams; however, in a few selected directions, reinforcement of all the scattered rays occurs, and a strong beam result. These are the diffracted beams. Because the crystal is periodic in three dimension, the lattice sites act as the scattering centers. Each scattering center emits rays in all directions, and resulting diffracted rays define a family of cones in space. The three-dimensional lattice of scattering centers restricts a diffraction experiment severely, and diffraction can only occur when the incident beam makes precisely the correct angle relative to the crystal.

2.11 Corrosion Test

2.11.1 Anti-perspiration Test

Some of metal-finished articles such as consumer goods are required to be resistant to degradation as a result of contact with human perspiration. Artificial perspiration is a simulation of human sweat and this is to monitor the metal coating corrosion resistance to perspiration. The samples were dipped in artificial perspiration for a period of time. The metal coating is corroded and dissolved in artificial perspiration. By analyzing the metal concentration in the artificial perspiration, the corrosion rate of the metal coating can be determined [45].

The concentration of metal ions in artificial perspiration may be very low. The method to analysis metal ions down to ppm level is needed. The most common method is Flame Atomic Absorption Spectroscopy (Flame AAS). However, the sodium ion in artificial perspiration emits strong band giving serious interference. The Differential Pulse Anodic Stripping technique is a powerful tool for trace metal analysis. It provides a suitable analysis technique for the anti-perspiration test [22].

Anodic stripping voltammerty is a two-step technique. The first step is deposition step and second step is stripping step. The deposition step is for preconcentration of substance from a dilute solution is most performed at a constant potential for a definite time. A hanging mercury drop electrode was used throughout

the experiment and the metal is deposited on it. A potential was selected cathodic enough so that the metal ion could be reduced to the mercury electrode. Between the deposition and stripping process, there is rest period for metal to become homogenenous on the electrode. The stripping step consists of scanning the potential anodically. When the potential reaches the oxidative potential of metal-ion couple, the particular metal is reoxidizied back to the solution and current flows. In our study, the linear D.C. ramp is applied and fixed pules height is superimposed on this ramp. The total current is sampled just before application of the pulse and again at the pulse. The output is the difference between these reading.

2.11.2 DC Polarization Measurements

Electrochemical methods are useful for determining in corrosion rates of metal within a short period of time. Since application of high potentials to operating systems may be risky, linear polarization techniques with low current-potential applications around corrosion potential values are the most widely used electrochemical methods. This technique is one of the most used techniques for studying metal corrosion [46]. The potential would be scanned linearly around corrosion potential (E_{corr}) as a function of time and the current monitored as the potential changes. When the potential is plotted as a function of the log of the current, portions of both the anodic and cathodic regions may be linear and follow a Tafel behavior. In cases, it is possible

to extrapolate these linear regions to where they should intersect, at the corrosion potential, and obtain a value for the corrosion current (I_{corr}).

The basis of the polarization resistance technique is the relation:

$$I_{corr} = \frac{b_a b_c}{2.3(b_a + b_c)}\left(\frac{dI}{d\phi}\right)_{\phi_{corr}} = \frac{b_a b_c}{2.3(b_a + b_c)}\frac{1}{R_p} = \frac{B}{R_p} \tag{2.11.1}$$

which is valid as long as the relation between current (I) and potential (ϕ) can expressed as:

$$I = I_{corr}\left\{\exp\frac{2.3(\phi - \phi_{corr})}{b_a} - \exp\frac{-2.3(\phi - \phi_{corr})}{b_c}\right\} \tag{2.11.2}$$

In equation 2.11.1 and 2.11.2, I_{corr} and ϕ_{corr} are corrosion current and corrosion potential, b_a and b_c are anodic and cathodic Tafel slopes, and $R_p = (d\phi/dI)\phi_{corr}$ is the slope of potential-current plot at corrosion potential. R_p is often called polarization resistance, which is equivalent to the change transfer resistance on the metal/electrolyte interface for the activation-controlled corrosion reactions. I in equation 2.11.1:

$$B = \frac{b_a b_c}{2.3(b_a + b_c)}$$

It is desirable to obtain simultaneously the Tafel slopes (b_a & b_c) and polarization resistance (R_p) in order to determine the corrosion current (I_{corr}). In doing so, one could accurately determine I_{corr} as function of time, electrolyte composition,

temperature or other parameters.

Analysis of polarization curves is summarized as following.

Combination of equation 2.11.1 and 2.11.2 leads to

$$I = \frac{1}{2.3}\frac{b_a b_c}{(b_a + b_c)}\frac{1}{R_p}\left\{\exp\left(\frac{2.3(\phi - \phi_{corr})}{b_a}\right) - \exp\left(\frac{-2.3(\phi - \phi_{corr})}{b_c}\right)\right\} \quad (2.11.3)$$

This can be written after rearrangement as:

$$2.3R_p I = \frac{b_a b_c}{(b_a + b_c)}\left\{\exp\left(\frac{2.3\Delta\phi}{b_a}\right) - \exp\left(\frac{-2.3\Delta\phi}{b_c}\right)\right\} \quad (2.11.4)$$

where $\Delta\phi = \phi - \phi_{corr}$

The I_{corr} can then be calculated from the measured polarization curve in the following four steps which are based on equation 2.11.1 and 2.11.2:

1. R_p is determined from:

$$\left(\frac{dI}{d\phi}\right)_{\phi_{corr}} = R_p^{-1}$$

By drawing a tangent at $\Delta\phi = 0$.

2. Multiply the current I measured at a certain value $\Delta\phi$ by 2.3 R_p and plot 2.3 R_p I Vs $\Delta\phi$

3. Determine from this plot the Tafel slopes (b_a & b_c) by curve fitting using theoretical curves calculated for various values of b_a & b_c.

4. Calculate I_{corr} from equation 2.11.1 using the R_p value determined in Step 1 and

the Tafel slopes determined in Step 3.

Several examples of computer programs have been described in the literature [47], where the application of statistics permits an automatic analysis of experimental data to obtain Tafel constants and calculate I_{corr} according to the Tafel extrapolation technique for measurement of corrosion kinetic parameters introduced by Stern [48] and Geary [49]. A commercial corrosion testing software is employed for the current studies [50].

Chapter 3 Experimental Procedures

3.1 Pretreatment Procedure

Copper panels for 250ml Hull cell were electrocleaned in alkaline cleaner. They were then activated in a 10% aqueous solution of sulfuric acid. All substrates were rinsed thoroughly by deionized water between each step.

3.2 Plating Range Test

A suitable anode was placed in Hull cell. Plating solution was kept at suitable temperature and then poured into the Hull Cell. The anode was connected to the positive pole and a cleaned testing panel was connected to negative pole of the DC power supply. The total current use for plating was kept at 2A and testing panel was electroplated for 5 minutes.

3.3 Cobalt-Molybdenum Bath

3.3.1 Citrate Cobalt-Molybdenum Bath

The plating conditions of citrate Co-Mo bath were tested by the Hull Cell test. The composition of Co-Mo layer is depended on the deposition parameters as well as on the variation of electrolyte concentrations. The cobalt(II) sulfate and citric acid content in the electrolyte was kept constant at 60g/l and 180g/l, respectively. Sodium molybdate content varied from 5 to 30g/l. The solution pH was adjusted by aqueous ammonia to 3. The plating temperature was kept at 65°C. The alloy compositions

were then determined by Energy Dispersive X-ray Spectroscopy (EDS) (Oxford Link ISIS).

3.3.2 Free Alkaline Cobalt-Molybdenum Bath

The optimization for free alkaline Co-Mo bath was done by orthogonal experiment design. The $L_{18}(3^7)$ orthogonal table was used. The experiment design was shown as below:

Table 3.3.1 The factors and levels of free alkaline Co-Mo bath in orthogonal experiment design.

Factor	1 Cobalt Sulphate $CoSO_4$ (mol dm^{-3})	2 Sodium Molybdate Na_2MoO_4 (mol dm^{-3})	3 Potassium hydroxide KOH (mol dm^{-3})	4 Potassium Carbonate K_2CO_3 (mol dm^{-3})	5 Glucose $C_6H_{12}O_6$ (mol dm^{-3})	6 Temp. (°C)	7. Current density I_d (A dm^{-2})
Level 1	0.05	0.1	2.0	0.4	0.1	25	0.4
Level 2	0.1	0.2	4.0	0.8	0.2	35	1.0
Level 3	0.2	0.25	6.0	1.2	0.3	45	5.0

Table 3.3.2 $L_{18}(3^7)$ orthogonal table

Test \ Factor	1	2	3	4	5	6	7
1	1	1	1	1	1	1	1
2	1	2	2	2	2	2	2
3	1	3	3	3	3	3	3
4	2	1	1	2	2	3	3
5	2	2	2	3	3	1	1
6	2	3	3	1	1	2	2
7	3	1	2	1	3	2	3
8	3	2	3	2	1	3	1
9	3	3	1	3	2	1	2
10	1	1	3	3	2	2	1
11	1	2	1	2	3	3	2
12	1	3	2	1	1	1	3
13	2	1	2	3	1	3	2
14	2	2	3	1	2	1	3
15	2	3	1	2	3	2	1
16	3	1	3	2	3	1	2
17	3	2	1	3	1	2	3
18	3	3	2	1	2	3	1

The alloy compositions were then determined by EDS.

3.4 Cobalt-Phosphorus Bath

The plating conditions of citrate Co-P bath were tested by the Hull Cell test. The composition of Co-P layer is depended on the deposition parameters as well as on the variation of electrolyte concentrations. The cobalt sulfate and citric acid content in the electrolyte was kept constant at 60g/l and 180g/l, respectively. Sodium hypophosphite content was varied from 5 to 30g/l. The solution pH was adjusted by aqueous ammonia to 3. The plating temperature was kept at 65°C. The alloy compositions were then determined by Energy Dispersive X-ray Spectroscopy.

3.5 Cobalt-Molybdenum-Phosphorus Bath

The plating conditions of Co-Mo-P bath were tested by the Hull Cell tests. The composition of Co-Mo-P layer is depended on the deposition parameters as well as on the variation of electrolyte concentrations. The cobalt(II) sulphate content was varied from 5 to 30g/l. The citric acid content varied from 30 to 220g/l, respectively. Sodium molybdate content was varied from 5 to 30g/l. Sodium hypophosphite content was varied from 5 to 30g/l. The solution pH was adjusted by aqueous ammonia to form 2 to 4. The plating temperature was kept at 65°C. The alloy compositions were then determined by Energy Dispersive X-ray Spectroscopy.

3.6 Diffusion Experiments

3.6.1 Copper/Barrier Systems

The plated samples with were cut into 2 cm × 2 cm and heat treated at temperatures ranging from 400°C to 800°C in an evacuated quartz tube under vacuum. The samples were treated for time interval ranging form 0.75 to 168 hours. After the heat treatment, the samples were micro-sectioned and ground with 150, 320 and 600 grit silicon carbide papers and polished successively using 1 μm and 0.3μm alumina powder. Samples were cleaned ultrasonically between each successive polishing step.

Energy Dispersive X-ray Spectroscopy was employed for obtaining the chemical composition value using the Link ISIS program [51] in which ZAF corrections were

made for atomic number, absorption and fluorescence effects. Concentration-versus-distance profiles were obtained.

The chemical interdiffusion coefficients were calculated using Boltmann-Matano method. With this analysis the value of $\tilde{D}$ is determined as a function of concentration and is given as:

$$D_{c=c'_1} = -\frac{1}{2t}\frac{dx}{dc}\bigg|_{c=c'_1} \int_0^{c_1} x dc$$

where t = time of diffusion, $\left(\frac{dx}{dc}\right)_{c_1}$ = reciprocal slope of the concentration-distance profile evaluated at c_1, $\int_0^{c_1} x dc$ = area between the profile and the Matano interface from c = 0 to c = c_1 concentration lines and c_1 = any concentration between 0 to 100%. Concentration-distance data points with different diffusion times were fitted into a polynomial curve using computer software TableCurve produced by AISN Software. Then the position of the Matano interface and the evalution of the Matano solution at different concentrations were calculated numerically. Diffusion annealing schedule for Cu/Barrier diffusion couples is listed Table 3.6

Table. 3.6 Heat Treatment Schedule for Copper/Barrier Diffusion Couples

Sample Designation	Annealing Temperature(°C)	Annealing Time(h)
Cu/Ni 1	400	168
Cu/Ni 2	500	72
Cu/Ni 3	600	24
Cu/Ni 4	700	5
Cu/Ni 5	800	0.75
Cu/Co-Mo 1	400	168
Cu/Co-Mo 2	500	72
Cu/Co-Mo 3	600	24
Cu/Co-Mo 4	700	5
Cu/Co-Mo 5	800	0.75
Cu/Co-P 1	400	168
Cu/Co-P 2	500	72
Cu/Co-P 3	600	24
Cu/Co-P 4	700	5
Cu/Co-P 5	800	0.75
Cu/Co-Mo-P 1	400	168
Cu/Co-Mo-P 2	500	72
Cu/Co-Mo-P 3	600	24
Cu/Co-Mo-P 4	700	5
Cu/Co-Mo-P 5	800	0.75

3.6.2 Copper/Cobalt-Molybdenum-Phosphorus (Barrier)/Nickel Systems

In order to evaluate the performance of cobalt-molybdenum-phosphorus being a diffusion barrier for copper, alloy layers of thickness 0.5μm and 1.0μm were electroplated respectively on the copper substrates using the best bath as described in Section 3.5, in which the same plating conditions and pretreatment procedure of the copper substrate were used. Electroplated samples were then activated and plated with 20μm bright nickel. Diffusion experiments of Cu/Co-Mo-P(barrier)/Ni systems were conducted for samples at temperatures ranging from 400°C to 800 °C. Concentration-distance profiles were obtained by EDS and the results were compared with the Cu/Ni system.

3.6.3 Copper/Barrier/Gold System

To evaluate the effectiveness of different electroposited coating as diffusion barrier for copper/gold interdiffusion, electroplated Ni, Co, Co-Mo, Co-P and Co-Mo-P of thickness 1μm were electroplated respectively on pretreated copper substrates. Gold coatings were then electroplated on the copper/barrier in a bath containing 15g/l potassium gold cyanide, 100g/l potassium citrate. The pH was adjusted to 5.2~5.5 by adding citric acid. The current density was kept within the range 0.1~0.15 A/dm^2 and the temperature was maintained at 40°C. Diffusion experiments of copper/barrier/gold system were conducted at 400 °C for 48 hr. Concentration-distance profiles were then obtained by EDS after annealing.

3.7 Determination of Internal Stress by Spiral Contractometer

Spiral contractmeter produced by YAMAMOTO-METKISHIKENKI Co. was used in study. The helix made of stainless steel was mounted onto the meter body. The spiral constant was found by the torsional angle for load of 10 g. Both the open side (tensile stress) and close side (compressive stress) were tested. The helix was pretreated and plated by the sample solution. The torsional angle was recorded and the thickness of the coating was found by weight different.

3.8 X-ray diffraction studies

A Philips X-ray diffractometer with a high intensity Cu tube was operated at 40kV and 35mA with the monochromated incident radiation of CuKα(λ=0.15406 nm) for measuring the lattice parameter at room temperature. The diffracted rays were detected with a Xe gas filled proportional detector; and a step-by-step technique was employed with steps of 0.05° from 35°~80°. XRD spectra were recorded in the Bragg-Brentano geometry the 2θ interval.

3.9 Corrosion Test

3.9.1 Anti-perspiration Test

The formulation of artificial perspiration is shown as follow:

Sodium Chloride	0.5%
Urea	0.1%
Lactic Acid	0.1%
pH	6.5 Adjusted by diluted Aqueous Ammonia

All reagents are analytical reagent grade (A.R.) and diluted by double deionized water. All glassware were soaked in 2 mol dm^{-3} nitric acid for one day before use and then rinsed with double deionized water. The Polarographic analyzer MODEL 394 with linear D.C. ramp was connected with electrode MODEL 303A SMDE Hanging mercury electrode for analyzing metal ions. The electrolyte used in the cell was 0.2 mol dm^{-3} potassium thiocyanate. The settings of polarographic analyzer and Hanging mercury electrode are shown as follow:

MODEL 303A SMDE
Hanging mercury electrode

DROP SIZE:	Large
MODE:	HDME

Polarographic analyzer
MODEL 394

SCAN RATE:	5 mV/ s
SCAN RANGE	1.5 V
SCAN DIRECTION:	POSITIVE
INITIAL POTENTIAL	-1.2 V
OPERATION MODE	DIFFERENTIAL PLUSE
DROP TIME	1 s
PURGE TIME	240 s
DEPOSITION TIME	105 s
EQUILIBRIUM TIME	15 s

The standard solutions of 2,4,6 and 8ppm cobalt were pipetted into the cell for electrolysis. The peak currents were recorded and calibration graph was obtained. The sample with known area was rinsed with double deionized water and dipped in artificial perspiration for sever days. The artificial perspiration was diluted in order that the result fitted into the calibration range. The concentration of cobalt ion in artificial perspiration was found as the standard solutions and the corrosion rate was determinated.

3.9.2 DC Polarization Measurements

DC polarization was carried out on selected cobalt-molybdenum and cobalt-molybdenum-phosphorus alloy of 1 cm^2 geometric area in the cell is shown in Fig.3.9.

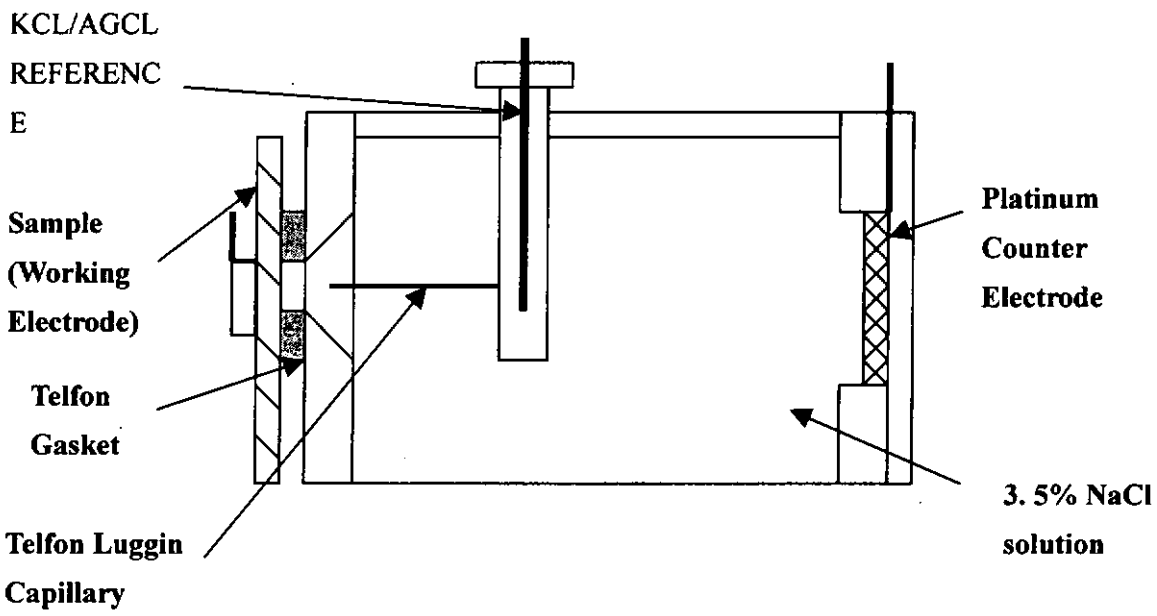

Fig. 3.9 Schematic Diagram of the Flat Cell used for Linear Polarization Measurements

The test cell consisted of a platinum counter electrode and a saturated KCl/AgCl reference electrode. The reference electrode is housed in a Luggin well, with a fixed Teflon Luggin capillary protruding from the bottom of the well. A Teflon gasket exposes a 1 cm^2 area of the working electrode to the cell solution. The Luggin capillary is positioned at the proximity to the center of the working electrode.

DC polarization studies were carried out using EG & G PARC Model 273 Potentiostat. The potential scans were taken place within ± 250mV of E_{corr} for each specimen with

a scan rate of the 0.166 mV/s. The resulting Tafel plots and potential versus current polarization plots for different sample were obtained. A Corrosion Measurement & Analysis Software(EG & G Model 352) was used to analyze the DC polarization measurement results.

Chapter 4 Results and Discussion on Plating Parameters

4.1 Cobalt-molybdenum Bath

4.1.1 Citrate Cobalt-Molybdenum Bath

4.1.1.1 Effect of Sodium molybdate concentration in plating bath on molybdenum contents in deposits

Sodium molybdate is a main ingredient of the baths that is the source of molybdenum. The formulations of the bath and operating conditions used are listed as below:

Bath solution

Cobalt(II) sulphate, $CoSO_4.7H_2O$	60g/l
Sodium molybdate $Na_2MoO_4.H_2O$	Varise, 5~40g/l
Citric acid, $C_6H_8O_7.H_2O$	180g/l
Aqueous ammonia NH_3	Adjust to suitable pH

Operating condition

Hull cell total current :	2A
pH:	3.0
Anode	Platinized titanium
Temperature	60°C

Table 4.1.1 and Figure 4.1.1 show the effect of the variations of concentrations of sodium molybdate on the wt% of the coating contents. Figure 4.1.2 shows the

appearance of panels and Figure 4.1.3 shows X-ray energy of the Co-Mo electrodeposit.

Table 4.1.1 The variation of sodium molybdate on the coating contents.

Na_2MoO_4 concentration (g/l)	Co (wt. %)	Mo (wt. %)
5	83.8	16.2
10	83.2	16.8
20	77.9	22.1
25	76.7	23.3
30	68.4	31.6

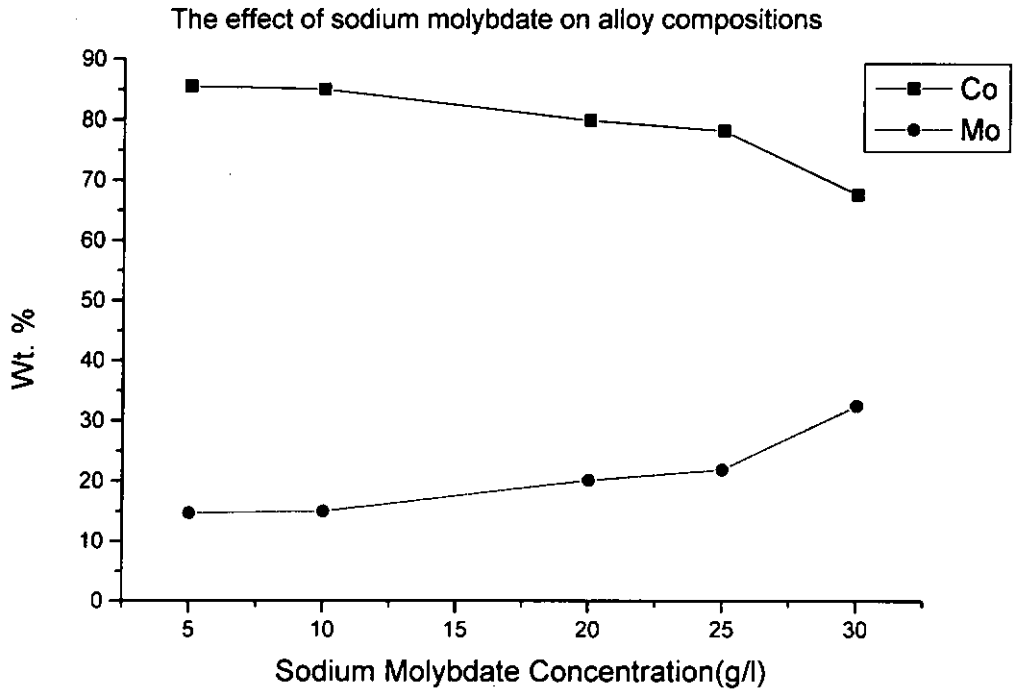

Figure 4.1.1 Effect of sodium molybdate bath concentration on alloy compositions

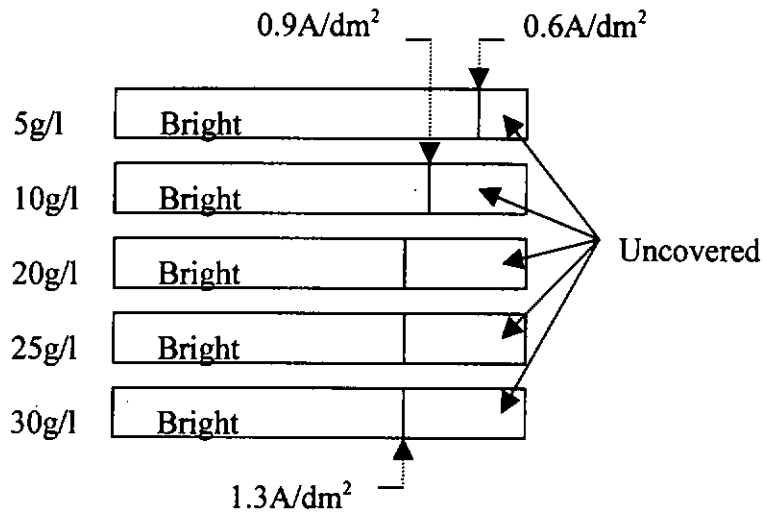

Fig. 4.1.2 The appearance of Hull cell panels in the test of bath sodium molybdate concentration

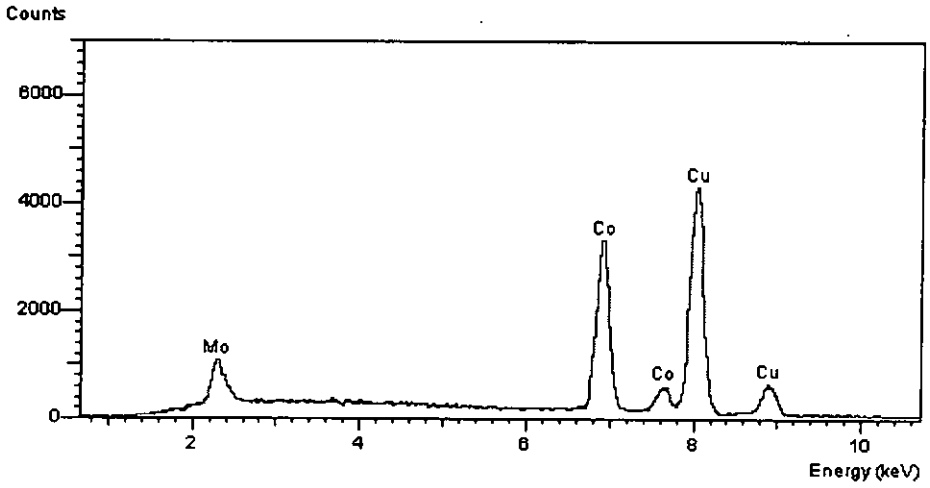

Fig 4.1.3 X-ray energy of the Co-Mo electrodeposit

All panels had a bright coating and the SEM micrograph is shown in Fig 4.1.4. However, as the sodium molybdate concentration increased, the plating power at low current density decreased. At the highest concentration in this test, the critical deposit current density was 1.3 A/dm^2.

As thee concentration of sodium molybdate was increase, the molybdenum in the coating increased. At 30g/l sodium molybdate, the highest molybdenum content (31.6%) in this experiment was obtained.

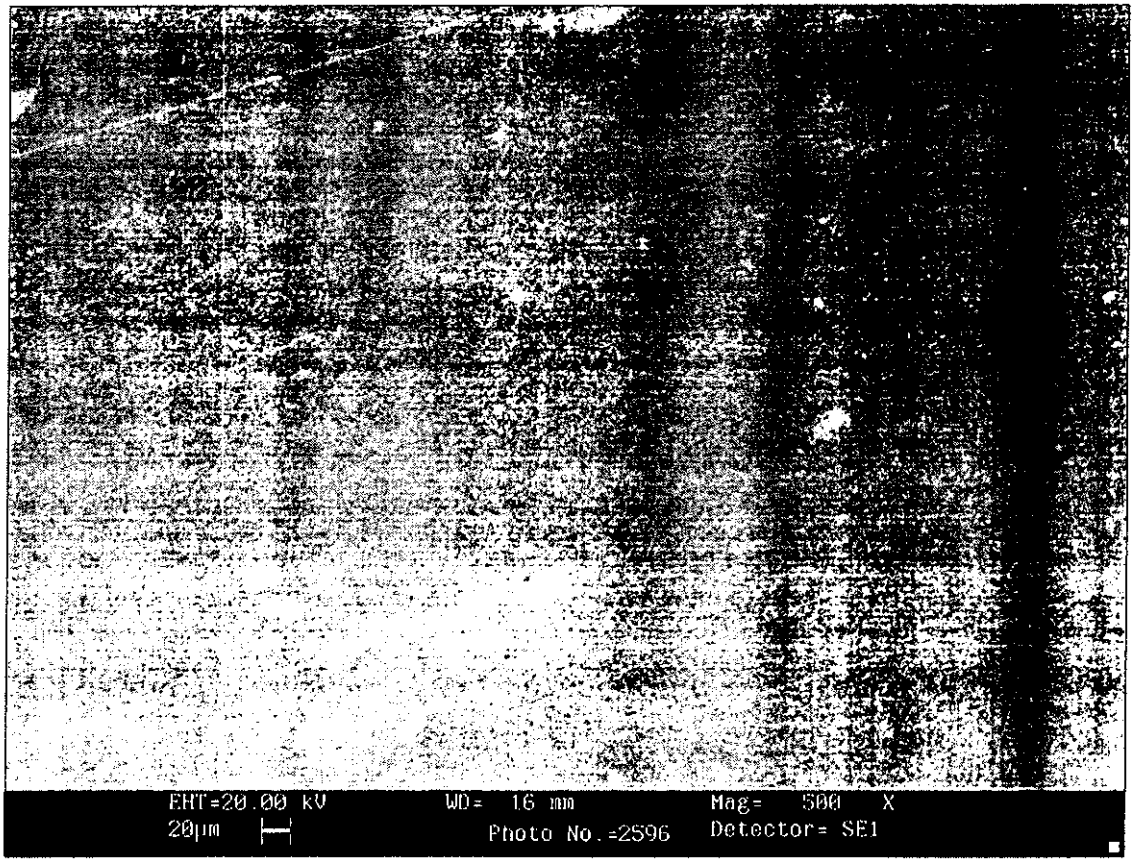

Figure 4.1.4 SEM micrograph of the surface of Co-Mo coating electrodeposited at $2A/dm^2$

4.1.2 Free Alkaline Cobalt-Molybdenum Bath

Figure 4.1.5 shows the effect of each factor affecting the weight percentage of molybdenum content in thecoating for free alkaline bath.

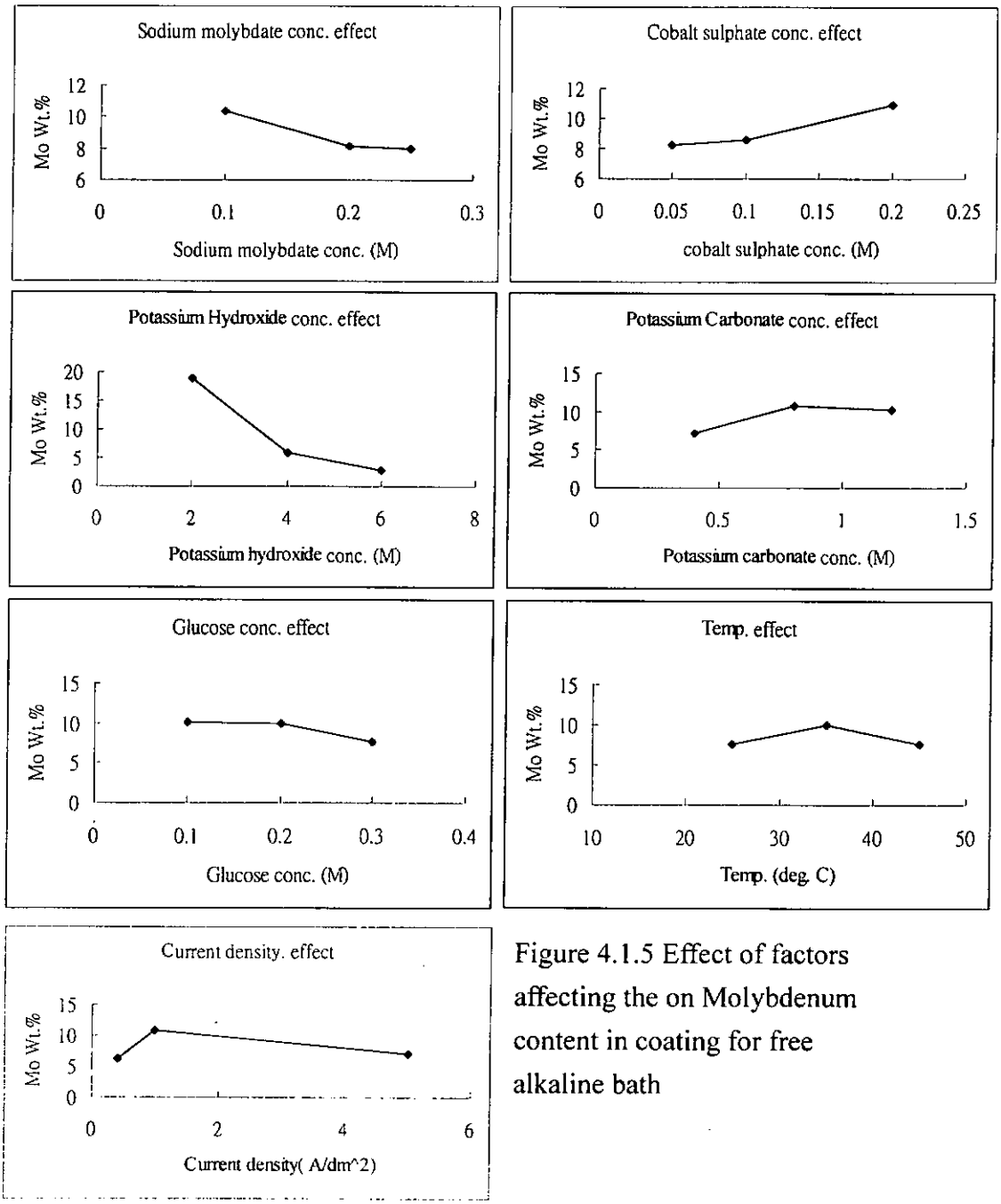

Figure 4.1.5 Effect of factors affecting the on Molybdenum content in coating for free alkaline bath

It shows that the most important factor affecting the molybdenum content is the concentration of potassium hydroxide in the plating bath. The lower the concentration

of potassium hydroxide, the higher the molybdenum content in the coating is obtained.

After eighteen experiments, the best combination of each factor for a bath and operating conditions is:

Cobalt(II) sulphate	0.2 M
Sodium molybdate	0.1 M
Potassium hydroxide	2.0 M
Potassium carbonate	0.8 M
Glucose	0.1 M
Current density	1.0 A dm^{-2}
Temperature	35°C

From the above operating conditions, a Co-Mo coating with 25.3wt% Mo was produced. All panels in the experiment could produce bright coatings. In comparison with the citrate Co-Mo bath, the covering power of the bath was better and could deposit even in very low current density. It may be due to the high conductivity of the bath solution. However, the bath solutions were not very stable and insoluble cobalt hydroxides easily were formed on the anode and in the solution.

4.2 Cobalt-Phosphorus Bath

4.2.1 Effect of Sodium hypophosphite concentration in the plating bath on phosphorus contents in the deposits

Sodium hypophosphite is a main ingredient of the baths that is the source of phosphorus. The formulations of the bath and operating condition used are list below:

Bath solution

Cobalt(II) sulphate, $CoSO_4.7H_2O$	60g/l
Sodium hypophosphite, $NaH_2PO_2.H_2O$	Varise, 5~30g/l
Citric acid, $C_6H_8O_7.H_2O$	180g/l
Aqueous ammonia NH_3	Adjust to suitable pH

Operating condition

Hull cell total current:	2A
pH:	3.0
Anode	Platinized titanium
Temperature	60°C

Table 4.2.1 and Figure 4.2.1 show the result on the variation of sodium molybdate on the molybdenum and phosphorus in the coating contents. Figure 4.2.2 shows the appearance of panels and Figure 4.2.3 show X-ray energy of the Co-P electrodeposit.

Table 4.2.1 Variation of sodium hypophosphite on the coating contents.

Na_2MoO_4 concentration (g/l)	Co (wt. %)	P (wt. %)
5	87.2	12.8
10	84.8	15.2
20	77.9	22.1
25	77.4	22.6
30	No Data since no coating formed	

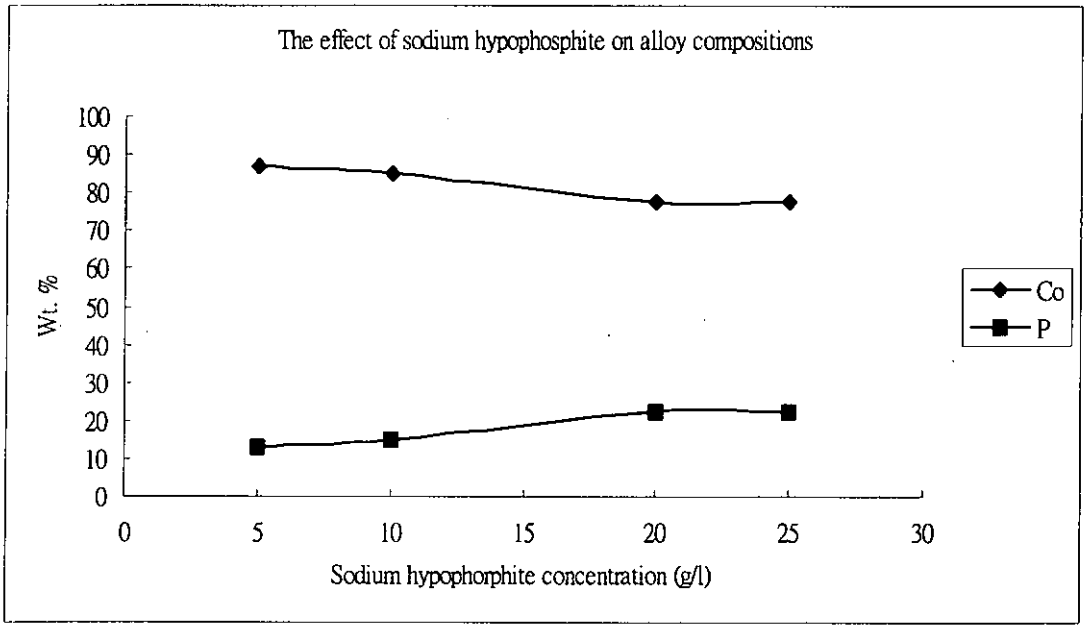

Figure 4.2.1 Effect of sodium hypophosphite bath concentration on alloy compositions

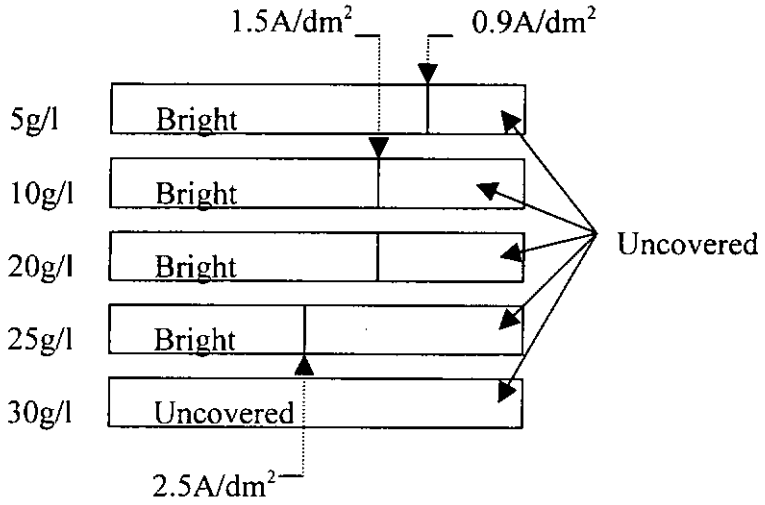

Fig. 4.2.2 The appearance of Hull cell panels in the test of bath conc. of NaH_2PO_2

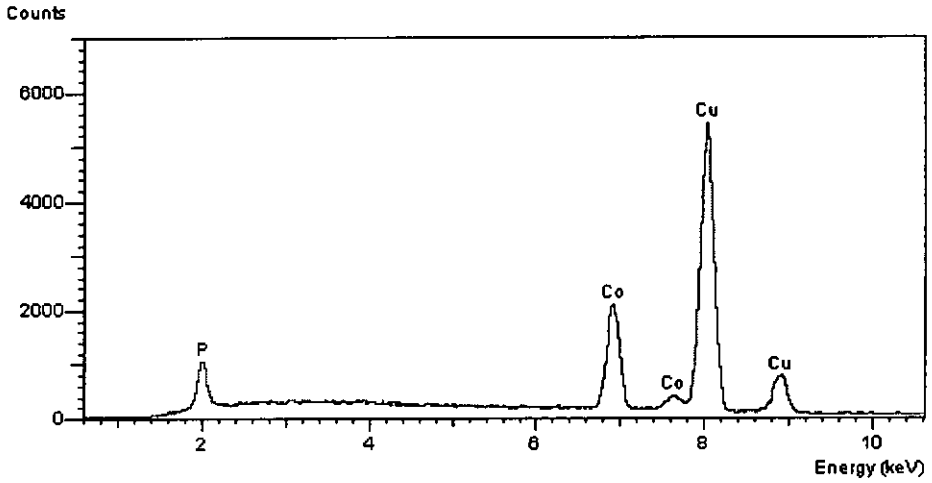

Fig 4.2.3 X-ray energy of the Co-P electrodeposit

All panels had a bright coating except the bath with 30g/l sodium hypophosphite. However, as the sodium hypophosphite concentration is increased, the plating power at low current density decreased. At the highest concentration in this test, the critical deposit current density was 2.5 A/dm^2.

As the concentration of sodium hypophosphite was increased, the phosphorus in the coating increased. At 25g/l sodium hypophosphite the highest phosphorus content (22.6%) in this experiment could be obtained.

4.3 Cobalt-Molybdenum-Phosphorus Bath

4.3.1 Effect of cobalt (II) sulphate concentration in the plating bath on molybdenum and phosphorus contents in the deposits

Cobalt (II) sulphate is the main ingredient of the baths which provide the cobalt(II) ions for plating.

The formulations of the bath and operating condition used are listed below:

Bath solution

Cobalt(II) sulphate, $CoSO_4.7H_2O$	Varies, 30~90g/l
Sodium molybdate $Na_2MoO_4.H_2O$	35g/l
Sodium hypophosphite, $NaH_2PO_2.H_2O$	20g/l
Citric acid, $C_6H_8O_7.H_2O$	180g/l
Aqueous ammonia NH_3	Adjust to suitable pH

Operating condition

Hull cell total current:	2A
pH:	3.0
Anode	Platinized titanium
Temperature	60°C

Table 4.3.1 and Figure 4.3.1 show the results of the variation of cobalt(II) sulfate on the wt % of molybdenum and phosphorus in the coating contents. Figure 4.3.2. shows the appearance of panels and Figure 4.3.3 shows X-ray energy of the Co-Mo-P

electrodeposit.

Table 4.3.1 Variation of cobalt(II) sulfate on the coating contents in Co-Mo-P bath

$CoSO_4$ concentration (g/l)	Co (wt. %)	Mo (wt. %)	P (wt. %)
30	62.9	12.5	24.6
45	68.3	10.2	21.5
60	72.0	8.0	20.1
75	76.1	6.5	17.4
90	82.3	5.1	15.6

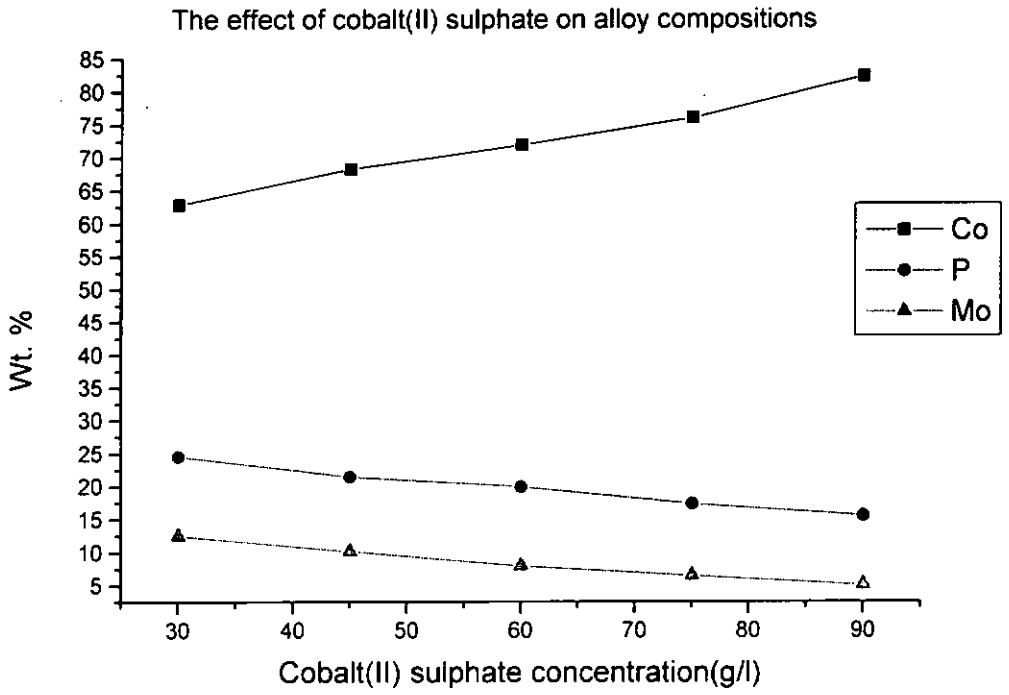

Fig. 4.3.1 Effect of bath cobalt(II) sulphate concentration on alloy compositions in Co-Mo-P bath

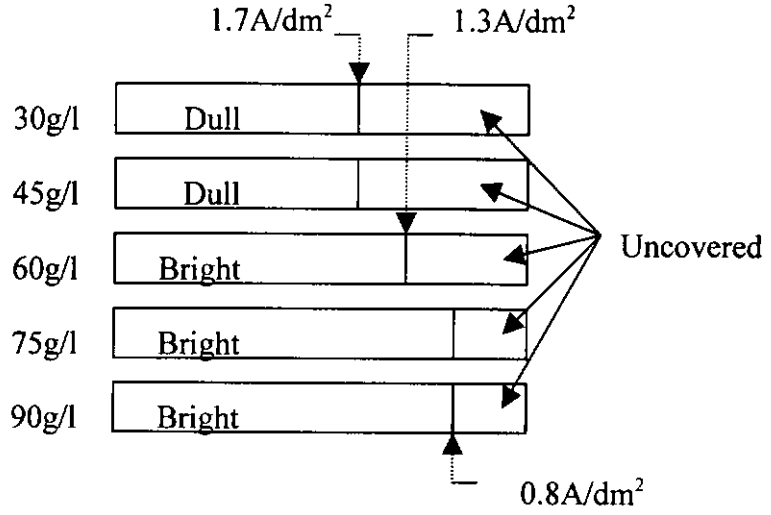

Fig. 4.3.2 The appearance of Hull cell panels in the test of bath cobalt(II) sulfate concentration in Co-Mo-P bath

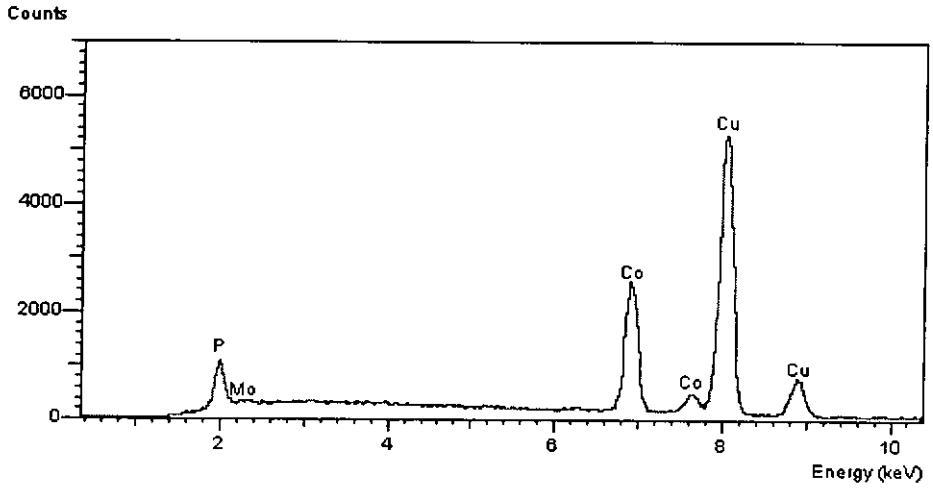

Fig 4.3.3 X-ray energy of the Co-Mo-P electrodeposit

It shows that as the concentration of cobalt(II) sulfate was increased, wt % of molybdenum and phosphorus contents decreased. In the lower concentration range of cobalt(II) sulfate (30~45g/l $CoSO_4$), the bath solution did not give a bright coating. Moreover, the higher concentration of cobalt(II) sulfate gave a wider current density

range for bright coating. To obtain a balance between high molybdenum-phosphorus contents and bright coating, the optimized concentration of cobalt(II) sulfate for bath was 60g/ml.

4.3.2 Effect of sodium molybdate concentration in the plating bath on molybdenum and phosphorus contents in the deposits

Sodium molybdate is another main ingredient of the baths that is the source of molybdenum.

The formulations of the bath and operating condition used are listed below:

Bath solution

Cobalt(II) sulphate, $CoSO_4.7H_2O$	60g/l
Sodium molybdate $Na_2MoO_4.H_2O$	Varies, 5~40g/l
Sodium hypophosphite, $NaH_2PO_2.H_2O$	20 g/l
Citric acid, $C_6H_8O_7.H_2O$	180g/l
Aqueous ammonia NH_3	Adjust to suitable pH

Operating condition

Hull cell total current :	2A
pH:	3.0
Anode	Platinized titanium
Temperature	60°C

Table 4.3.2 and Figure 4.3.4 show the results of the variation of sodium molybdate on the wt %molybdenum and phosphorus in the coating contents. Figure 4.3.5 shows the appearance of panels.

Table 4.3.2 Variation of sodium molybdate on the coating contents in Co-Mo-P bath.

Na_2MoO_4 concentration (g/l)	Co (wt. %)	Mo (wt. %)	P (wt. %)
10	73.8	5.2	21.0
20	72.0	7.2	20.8
30	71.6	7.9	20.5
35	72.0	8.0	20.0
40	64.4	15.0	20.6

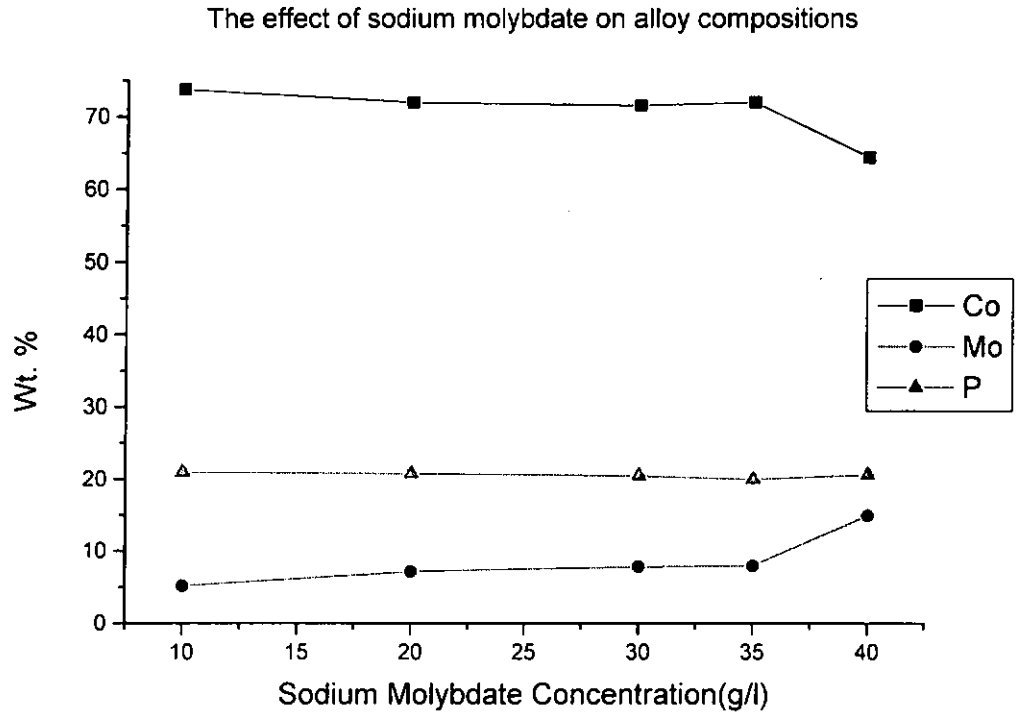

Figure 4.3.4 Effect of sodium molybdate bath concentration on alloy compositions in Co-Mo-P

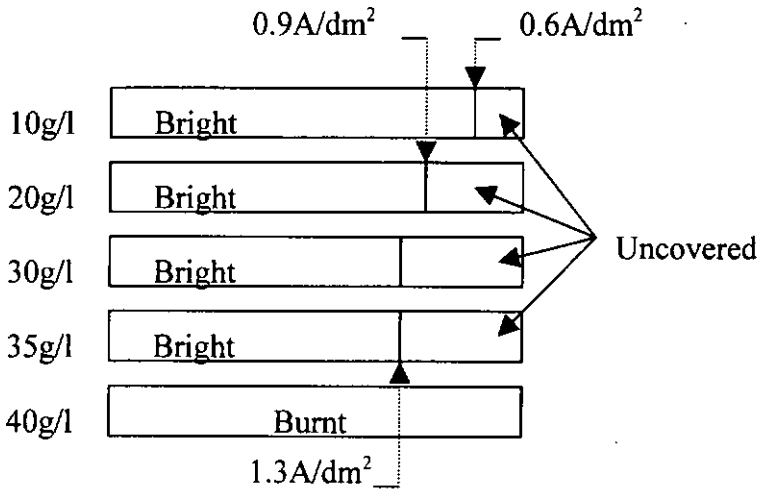

Fig. 4.3.5 The appearance of Hull cell panels in the test of bath sodium molybdate concentration in Co-Mo-P bath

As the concentration of sodium molybdate was increased, the wt % of molybdenum in the coating increased. At 35g/l sodium molybdate, the highest molybdenym content with a bright appearance was obtained. If molybdate concentration in bath was further increase, a burnt coating was obtained.

4.3.3 Effect of sodium hypophosphite concentration in the plating bath on molybdenum and phosphorus contents in the deposits

Sodium hypophosphite is ingredient of the baths, which is the source of phosphorus.

The formulations of the bath and operating condition used are listed as below:

Bath solution

Cobalt(II) sulphate, $CoSO_4.7H_2O$	60 g/l
Sodium molybdate $Na_2MoO_4.H_2O$	35 g/l
Sodium hypophosphite, $NaH_2PO_2.H_2O$	Varies, 5~40 g/l
Citric acid, $C_6H_8O_7.H_2O$	180 g/l
Aqueous ammonia NH_3	Adjust to suitable pH

Operating condition

Hull cell total current :	2A
pH:	3.0
Anode	Platinizied titanium
Temperature	60°C

Table 4.3.3 and Figure 4.3.6 show the result of the variation of sodium hypophosphite on the wt % of the molybdenum and phosphorus in the coating contents. Figure 4.3.7 shows the appearance of panels.

Table 4.3.3 Variation of sodium hypophosphite on the coating contents.

NaH_2PO_2 concentration (g/l)	Co (wt. %)	Mo (wt. %)	P (wt. %)
5	76.8	11.2	12.0
10	74.8	10.0	15.2
20	72.0	8.0	20.0
30	71.3	7.2	21.5
40	No Data since no coating form		

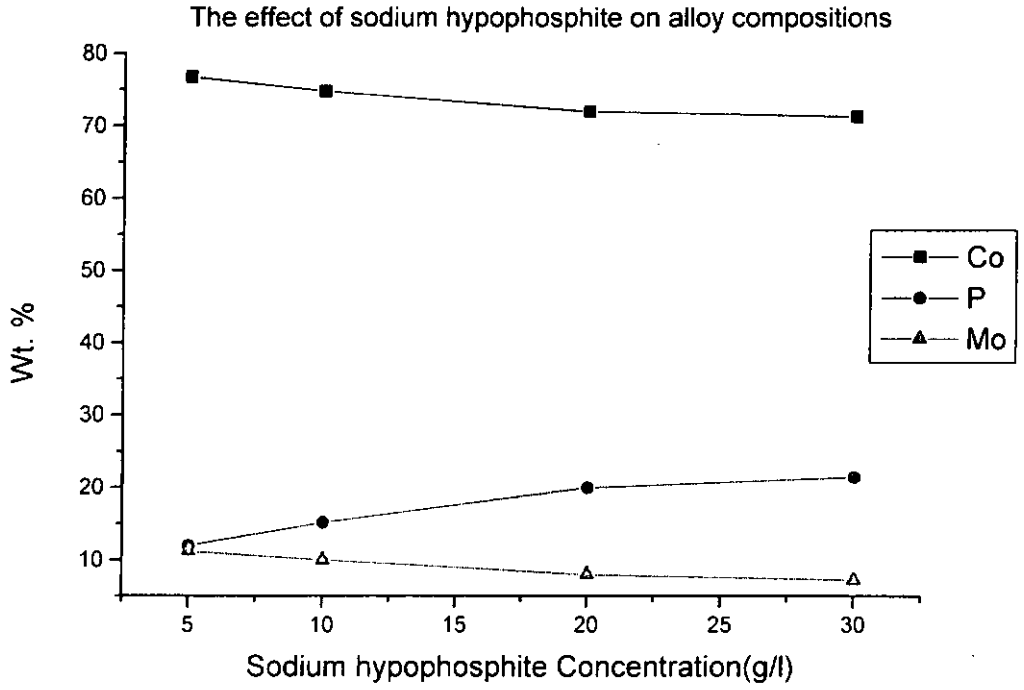

Figure 4.3.6 Effect of bath sodium hypophosphite concentration on alloy compositions

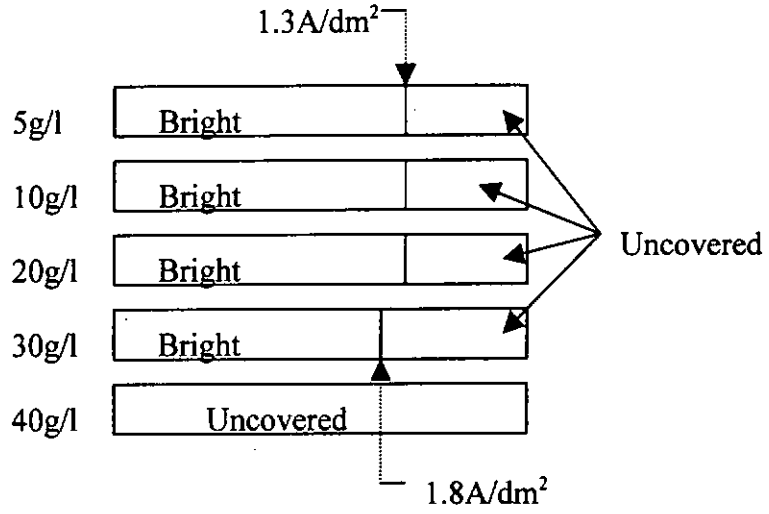

Fig. 4.3.7 The appearance of Hull cell panels in the test of bath sodium hypophosphite concentration in Co-Mo-P bath

The sodium hypophosphite supplies the $H_2PO_2^-$ ion as phosphorus in the coating:

$$H_3PO_2 + H^+ + e^- \rightarrow P + 2H_2O$$

The reaction shows, when the concentration of $H_2PO_2^-$ was increased, the phosphorus content increased. However, it was impossible to increase the concentration higher than 30g/l. When the sodium hypophosphite concentration was 40g/l, no deposition was found.

4.3.4 Effect of citric acid concentration in the plating bath on molybdenum and phosphorus contents in the deposits

Citric acid is a complexing agent in the bath. It complexes with cobalt(II) ion and prevents the precipitation of insoluble cobalt salts.

The formulations of the bath and operating condition used are listed as below:

Bath solution

Cobalt(II) sulphate, $CoSO_4.7H_2O$	60g/l
Sodium molybdate $Na_2MoO_4.H_2O$	35g/l
Sodium hypophosphite, $NaH_2PO_2.H_2O$	20 g/l
Citric acid, $C_6H_8O_7.H_2O$	Varies, 30~180g/l
Aqueous ammonia NH_3	Adjust to suitable pH

Operating condition

Hull cell total current :	2A
pH:	3.0
Anode	Platinized titanium
Temperature	60°C

Table 4.3.4 and Figure 4.3.8 show the results of the variation of citric acid on the wt % molybdenum and phosphorus in the coating contents. Figure 4.3.9 shows the appearance of panels.

Table 4.3.4 Variation of citric acid on the coating contents in Co-Mo-P bath.

Citric acid concentration (g/l)	Co (wt. %)	Mo (wt. %)	P (wt. %)
30	40.0	55.0	5.0
60	42.8	50.0	7.2
120	76.0	12.0	12.0
160	72.0	10.0	18.0
180	72.0	8.0	20.0

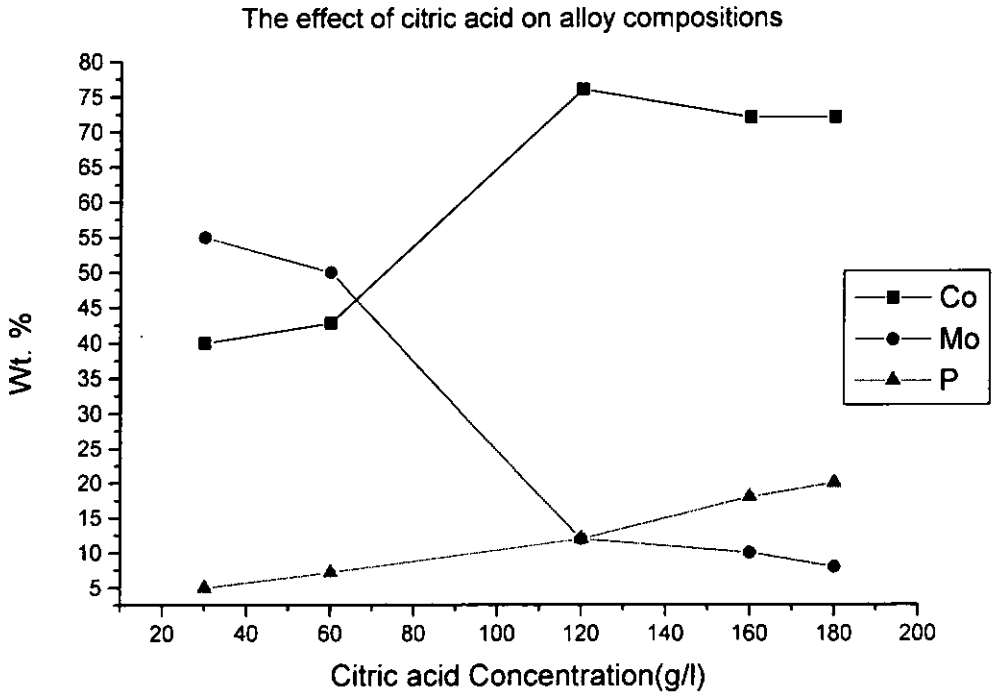

Figure 4.3.8 Effect of bath citric acid concentration on alloy compositions in Co-Mo-P Bath

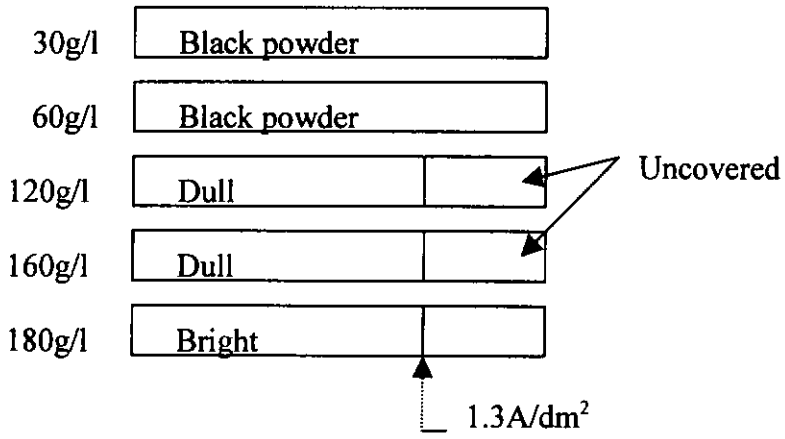

Fig. 4.3.9 The appearance of Hull cell panels in the test of bath citric acid concentration in Co-Mo-P bath

As the concentration of citric acid was increased, the amount of ammonia for adjusts pH increased. This mean that the concentration of ammonia was also increased. Both citric acid and ammonia are the complexing agent for cobalt. The amount of complex is formed between cobalt and citric acid increases with higher citric acid concentration. At lower citric acid concentration range, coatings of high molybdenum content and low cobalt content were deposited. It is believed that the reduction of phosphorus requires the cobalt surface for catalysis.

4.3.5 Effect of pH concentration in the plating bath on molybdenum and phosphorus contents in the deposits

The formulations of the bath and operating condition used are listed as below:

Bath solution

Cobalt(II) sulphate, $CoSO_4.7H_2O$	60g/l
Sodium molybdate $Na_2MoO_4.H_2O$	35g/l
Sodium hypophosphite, $NaH_2PO_2.H_2O$	20 g/l
Citric acid, $C_6H_8O_7.H_2O$	180g/l
Aqueous ammonia NH_3	Adjust to suitable pH

Operating condition

Hull cell total current :	2A
pH:	Varies, 2.0~4.0
Anode	Platinized titanium
Temperature	60°C

Table 4.3.5 and Figure 4.3.10 show the results of the variation of bath pH on the wt % of molybdenum and phosphorus in the coating contents. Figure 4.3.11 shows the appearance of the panels.

Table 4.3.5 Variation of bath pH on the coating contents in Co-Mo-P bath.

Bath pH	Co (wt. %)	Mo (wt. %)	P (wt. %)
2.0	59.3	18.2	22.5
2.5	68.2	10.2	21.6
3.0	72.0	8.0	20.0
3.5	76.8	5.2	18.0
4.0	No Data since no coating form		

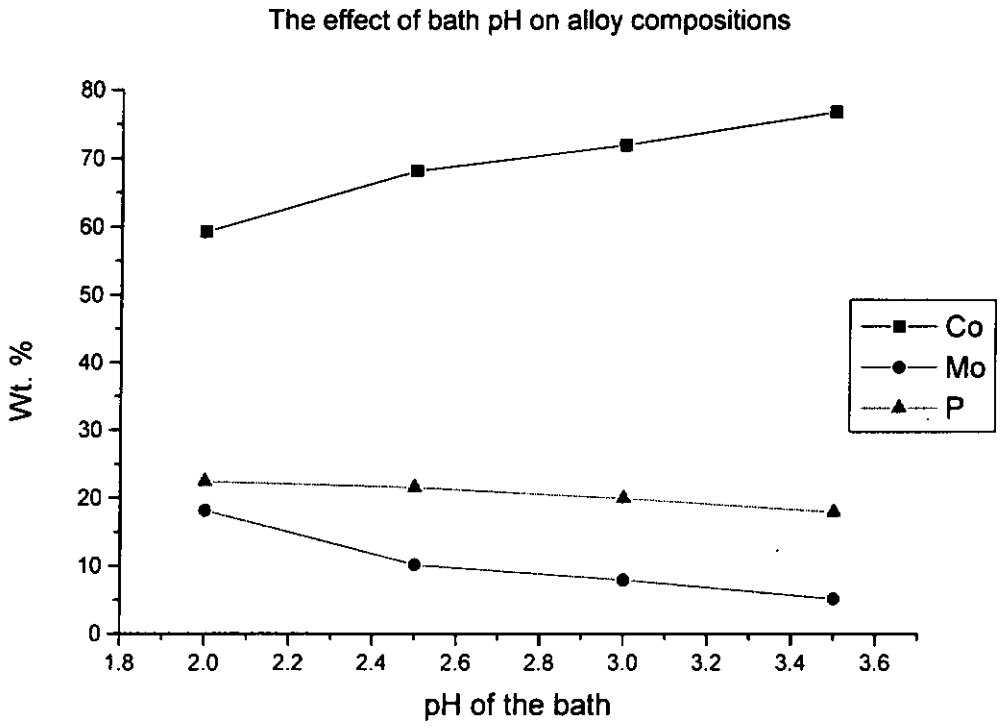

Figure 4.3.10 Effect of bath pH on alloy compositions in Co-Mo-P bath

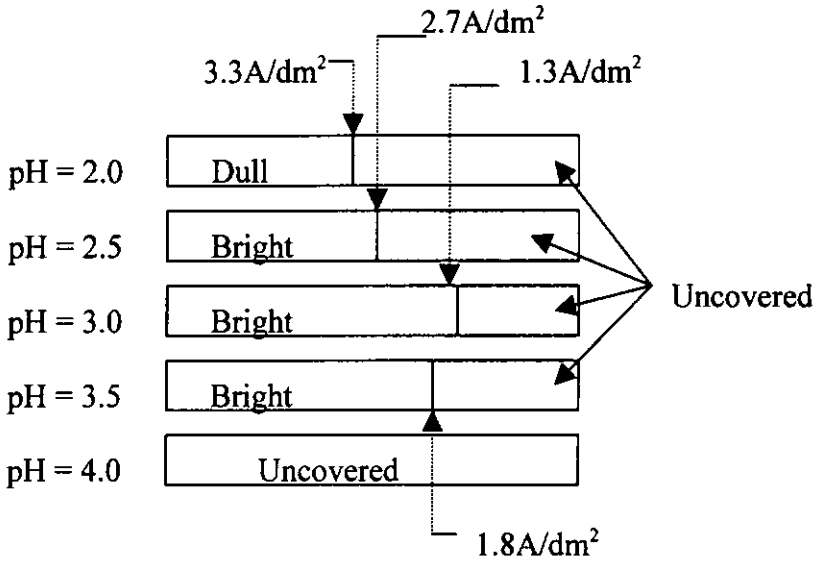

Fig. 4.3.11 The appearance of Hull cell panels in the test of bath pH in Co-Mo-P bath

At bath pH = 3.0, a wider current density range for bright coating was obtained. The phosphorus content was increased as the pH decreased.

$$H_3PO_2 + H^+ + e^- \rightarrow P + 2H_2O$$

The reaction shows, when the concentration of H^+ increases (pH decrease), the phosphorus contents increase. At bath pH = 4.0, it was find that there was no deposition.

Chapter 5 Results and Discussion on Coating Properties

5.1 Diffusion Experiments

5.1.1 Copper/Barrier Systems

5.1.1.1 Copper/Nickel Systems

Figure 5.1.1 to 5.1.5 show the concentration-distance profiles at the diffusion zone of Cu/Ni couples at 400° to 800°C heat treatment temperatures respectively. The corresponding chemical interdiffusion coefficients of the Cu/Ni couples are listed in Table 5.1.1.

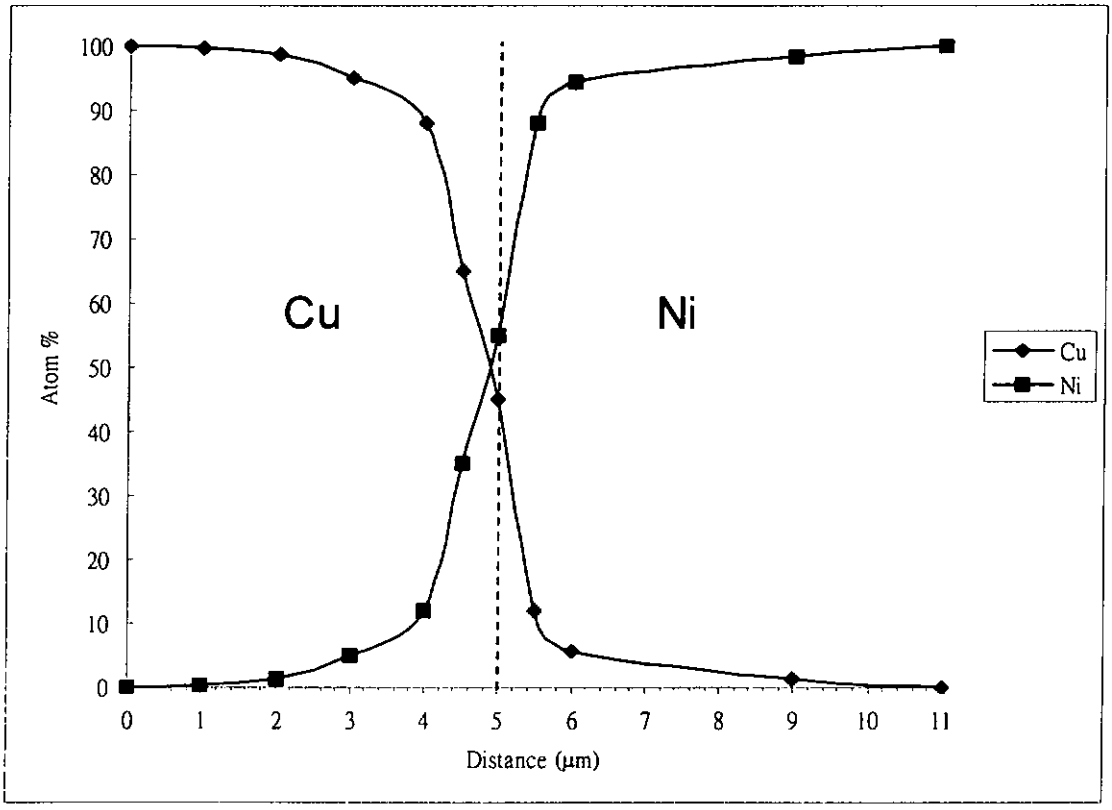

Fig 5.1.1 Concentration- Distance Profile of Cu/Ni couple after heat treatment at 400°C for 168h.

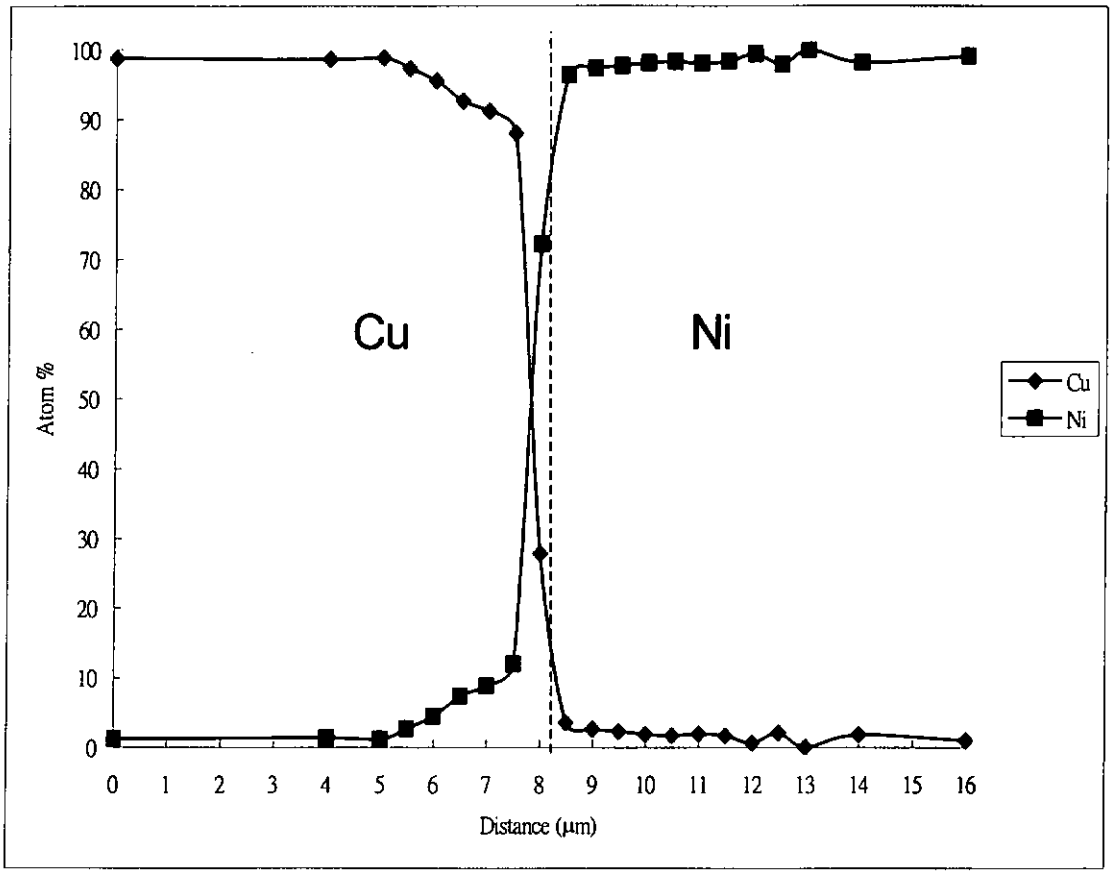

Fig 5.1.2 Concentration- Distance Profile of Cu/Ni couple after heat treatment at 500°C for 72h.

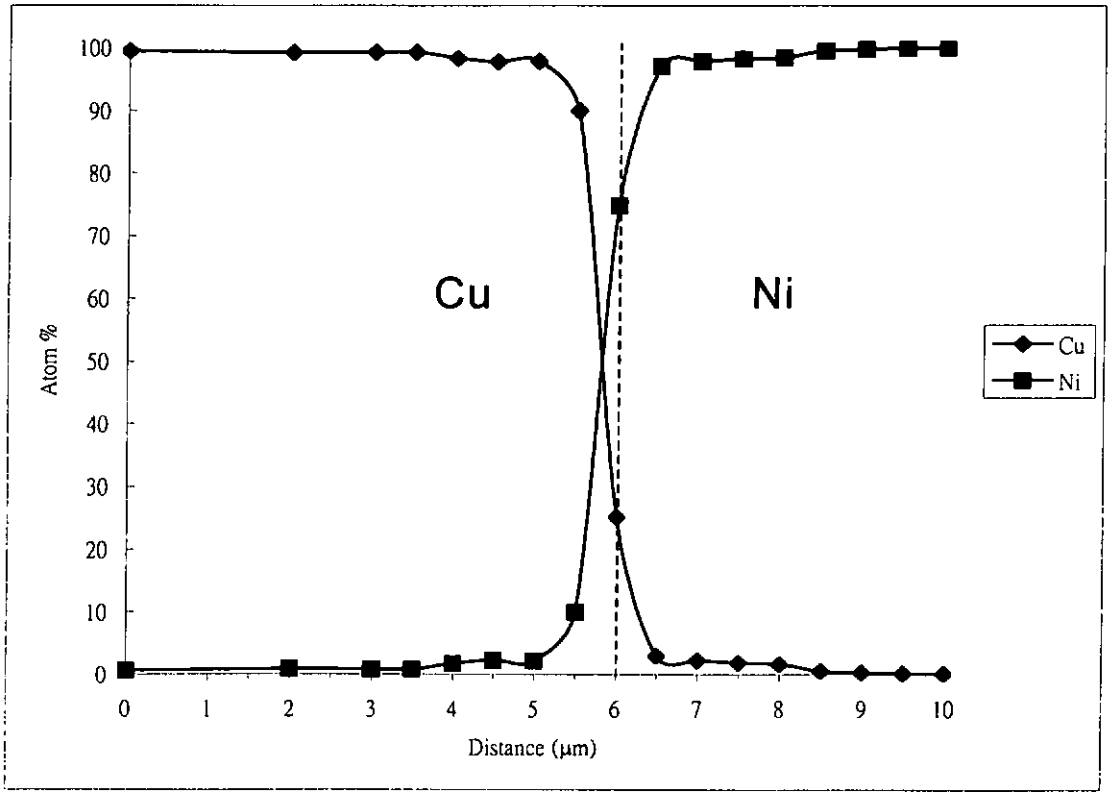

Fig 5.1.3 Concentration- Distance Profile of Cu/Ni couple after heat treatment at 600°C for 24h.

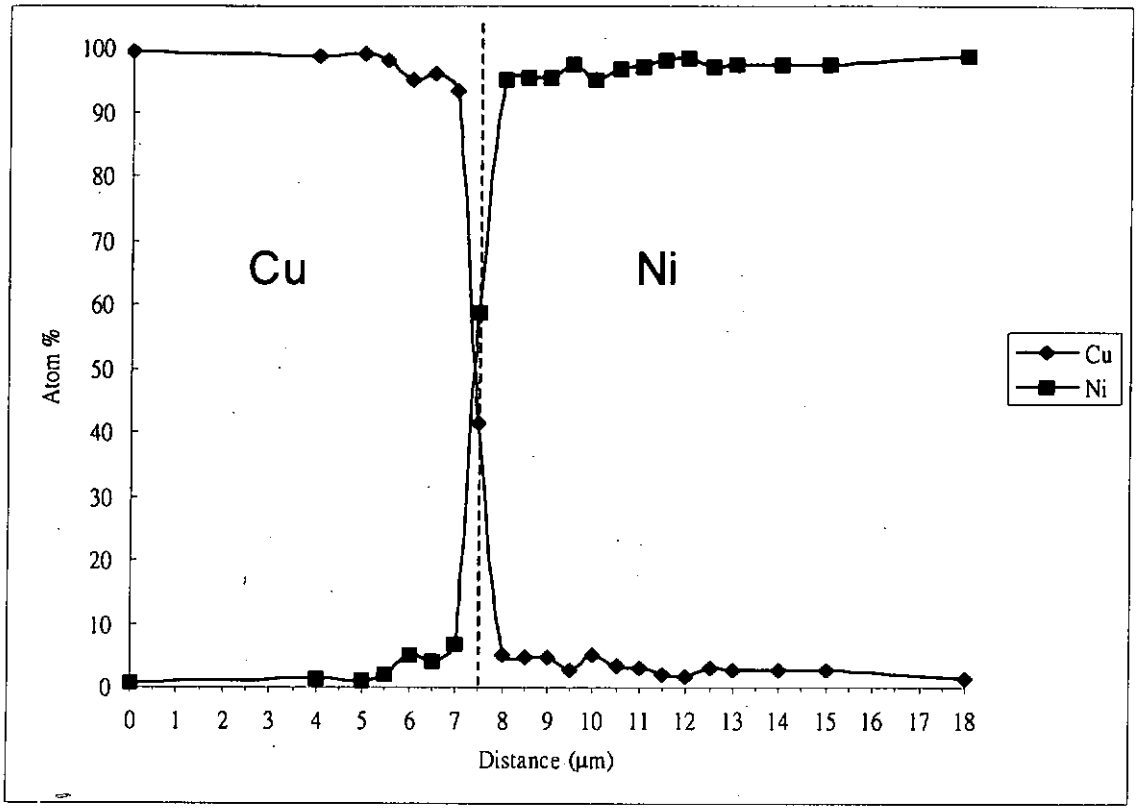

Fig 5.1.4 Concentration- Distance Profile of Cu/Ni couple after heat treatment at 700°C for 3h.

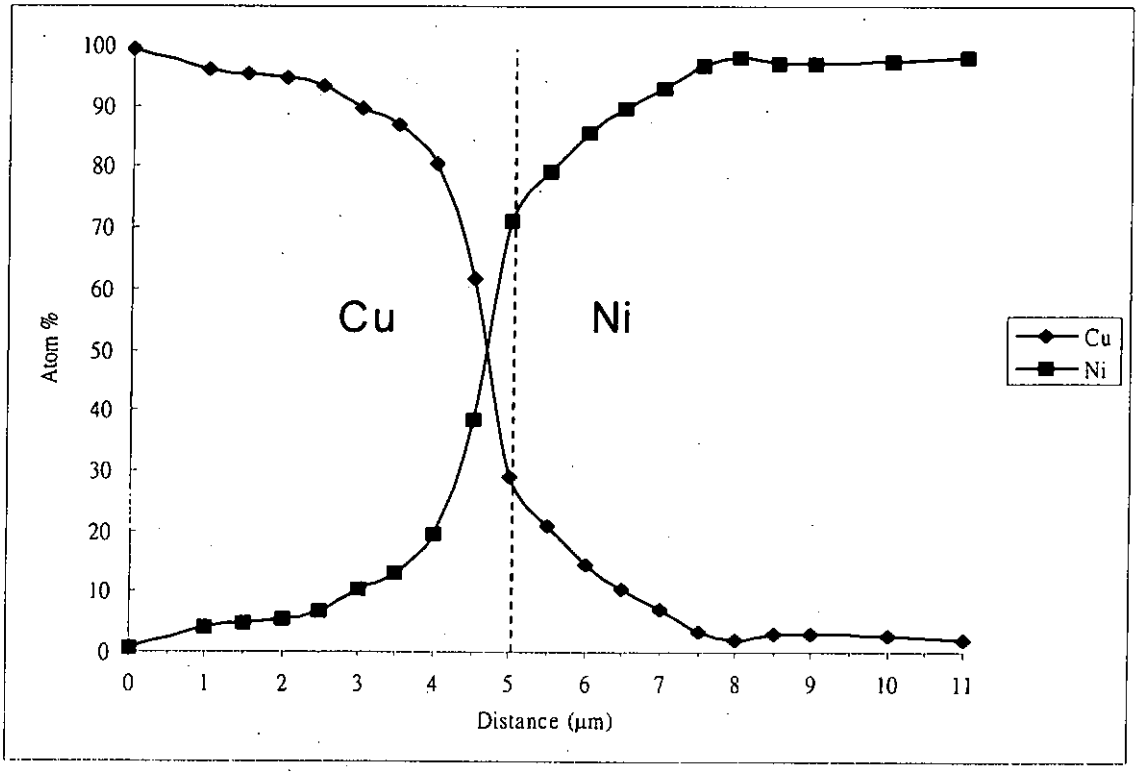

Fig 5.1.5 Concentration- Distance Profile of Cu/Ni couple after heat treatment at 800°C for 0.75h.

Table 5.1.1 Chemical Interdiffusion Coefficients of Cu/Ni Couples at Different Temperature and copper concentration calculated by Boltzmann-Matano Method

Annealing Temp (°C)	Annealing Time (h)	D (cm^2/s)			
		20% Cu	40% Cu	60% Cu	80% Cu
400	168	7.17×10^{-15}	9.66×10^{-15}	1.24×10^{-14}	9.66×10^{-15}
500	72	9.52×10^{-14}	7.65×10^{-14}	6.01×10^{-14}	7.65×10^{-14}
600	24	1.36×10^{-13}	1.51×10^{-13}	2.04×10^{-13}	2.97×10^{-13}
700	5	1.57×10^{-13}	2.07×10^{-13}	3.47×10^{-13}	8.22×10^{-13}
800	0.75	8.04×10^{-12}	7.52×10^{-12}	8.95×10^{-12}	7.52×10^{-12}

Since the chemical diffusion coefficient is a function of concentration, its dependence on temperature must be represented by a family of curves. Curves $\log_{10} D$ Vs. 1000/T for concentration of 20% to 80% copper are plotted in Figures 5.1.6 through 5.1.9, respectively.

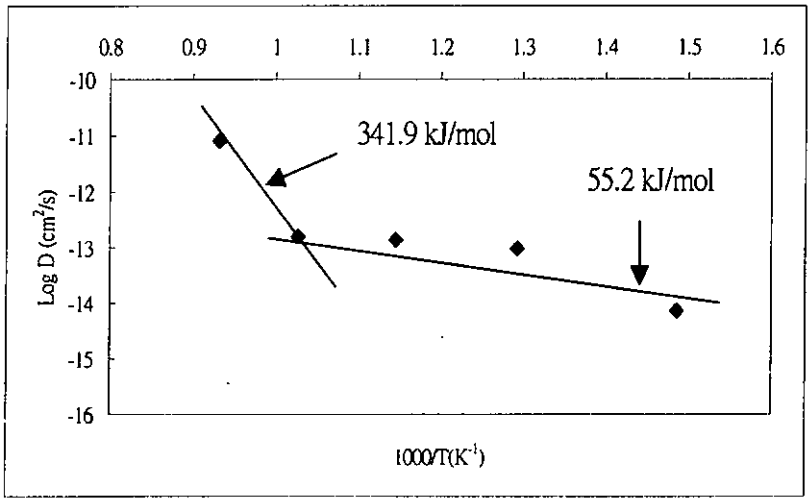

Fig. 5.1.6 The Arrhenius plot of diffusivities at 20% copper in Cu/Ni system

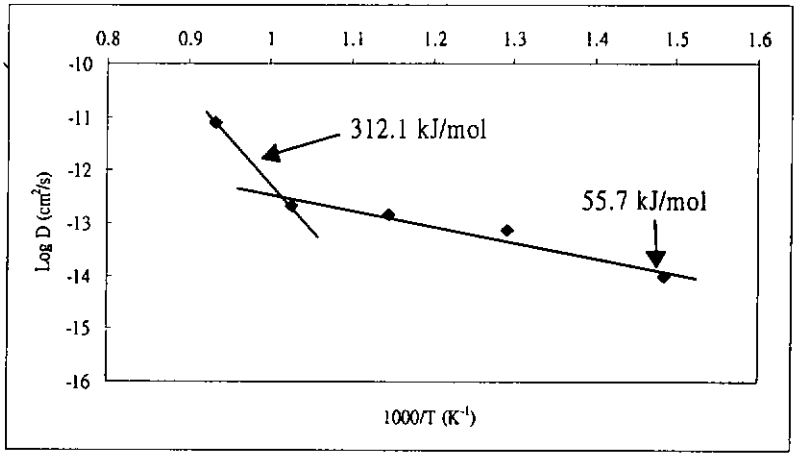

Fig. 5.1.7 The Arrhenius plot of diffusivities at 40% copper in Cu/Ni system

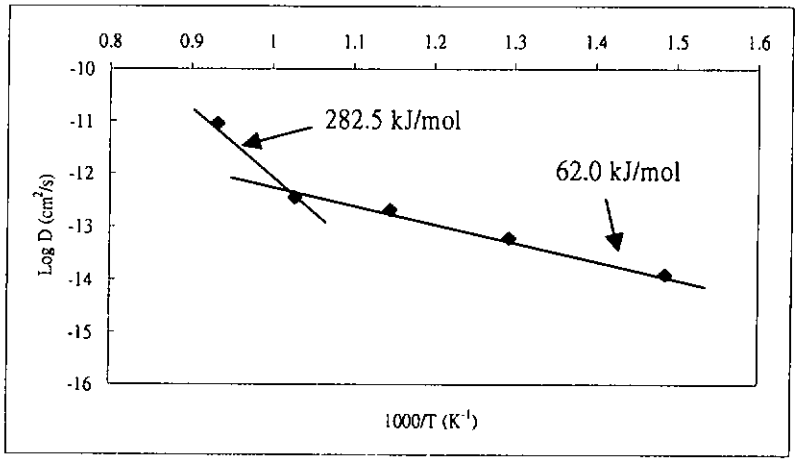

Fig. 5.1.8 The Arrhenius plot of diffusivities at 60% copper in Cu/Ni system

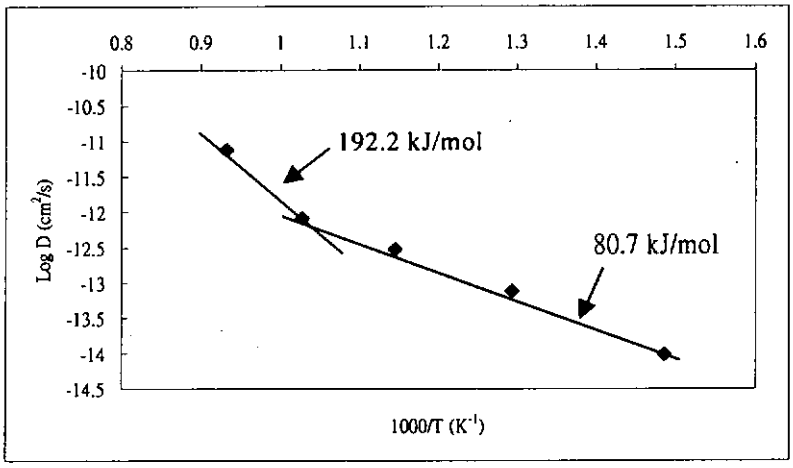

Fig. 5.1.9 The Arrhenius plot of diffusivities at 80% copper in Cu/Ni system

Diffusion along the defect paths has a lesser temperature dependence than the lattice diffusion and usually becomes dominant at low temperatures. At higher temperature, volume diffusion is predominant. For all the four concentrations, the general shapes of the curves are identical. The data conform to an Arrhenius equation $D = D_0 \exp(-Q/RT)$, where D_0 is the frequency factor, Q is apparent activation energy for diffusion and R is gas constant 8.32 J mol^{-1} K^{-1}. In the mid temperature range of 400°C to 700°C all data points fall above the curve extrapolated from the higher temperature, thus indicating that a low temperature diffusion mechanism predominates.

Apparent activation energies for diffusion were calculated in Figures 5.1.12 through 5.1.15. In the high temperature range, the value of Q decreases from 341.9 to 192.2 kJ mol^{-1} as the copper concentration increases from 20 to 80%. In the mid

temperature range, the value of Q is seen to be approximately 20% that of Q at the high temperature.

5.1.1.2 Copper/Cobalt-Molybdenum Systems

Diffusion experiments were carried out on Cu/Co-15 atom %Mo couples. Figure 5.1.10 to 5.1.14 show concentration-distance profiles at the diffusion zone of heat-treated Cu/Co-Mo couples at 400° C to 800° C respectively. The chemical interdiffusion coefficient D was found to be a function of concentration. The corresponding chemical interdiffusion coefficients of the Cu/Ni couples are listed in Table 5.1.2.

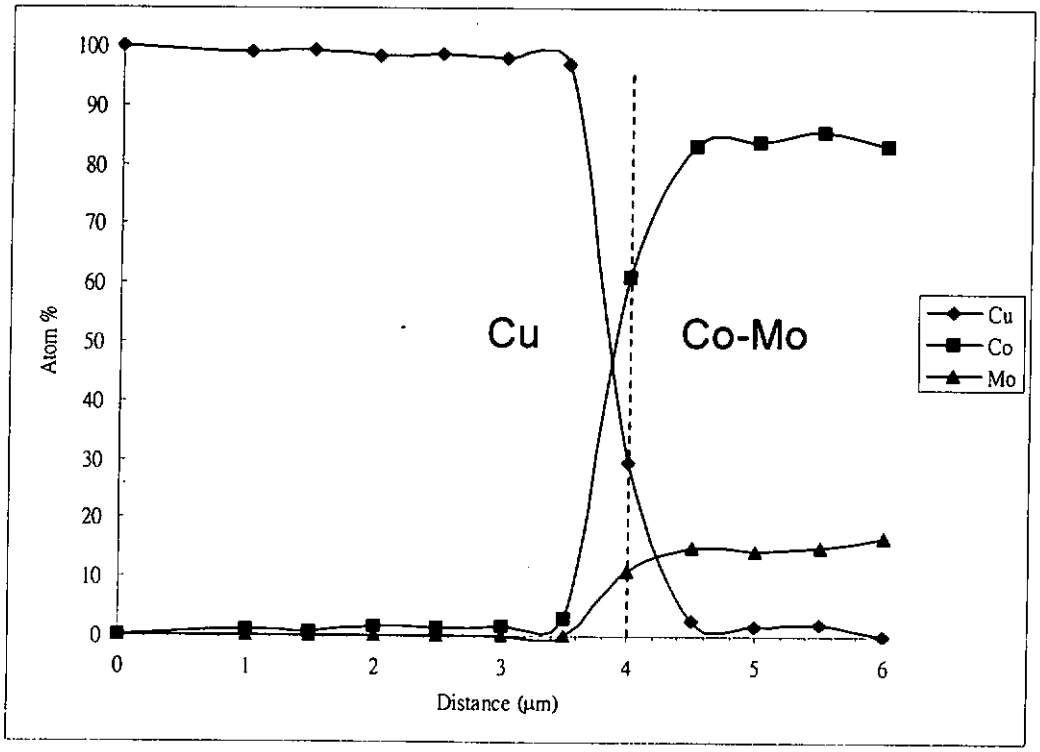

Fig 5.1.10 Concentration- Distance Profile of Cu/Co-Mo couple after heat treatment at 400°C for 168h.

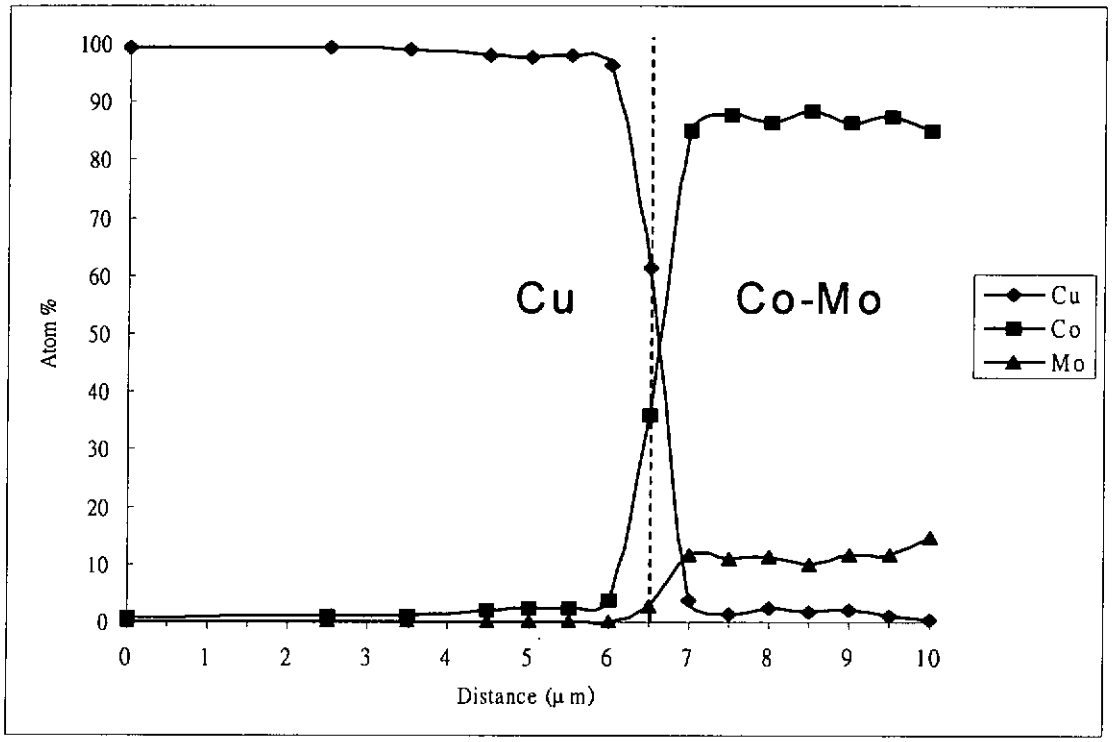

Fig 5.1.11 Concentration- Distance Profile of Cu/Co-Mo couple after heat treatment at 500°C for 72h.

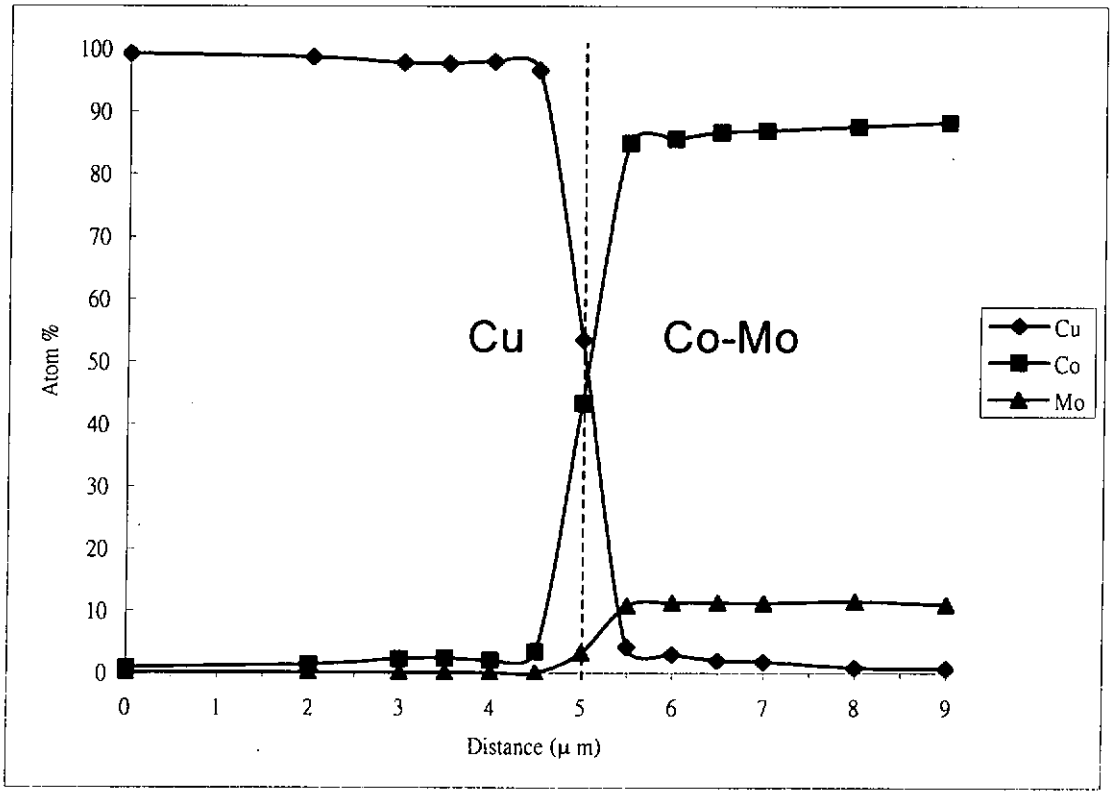

Fig 5.1.12 Concentration- Distance Profile of Cu/Co-Mo couple after heat treatment at 600°C for 24h.

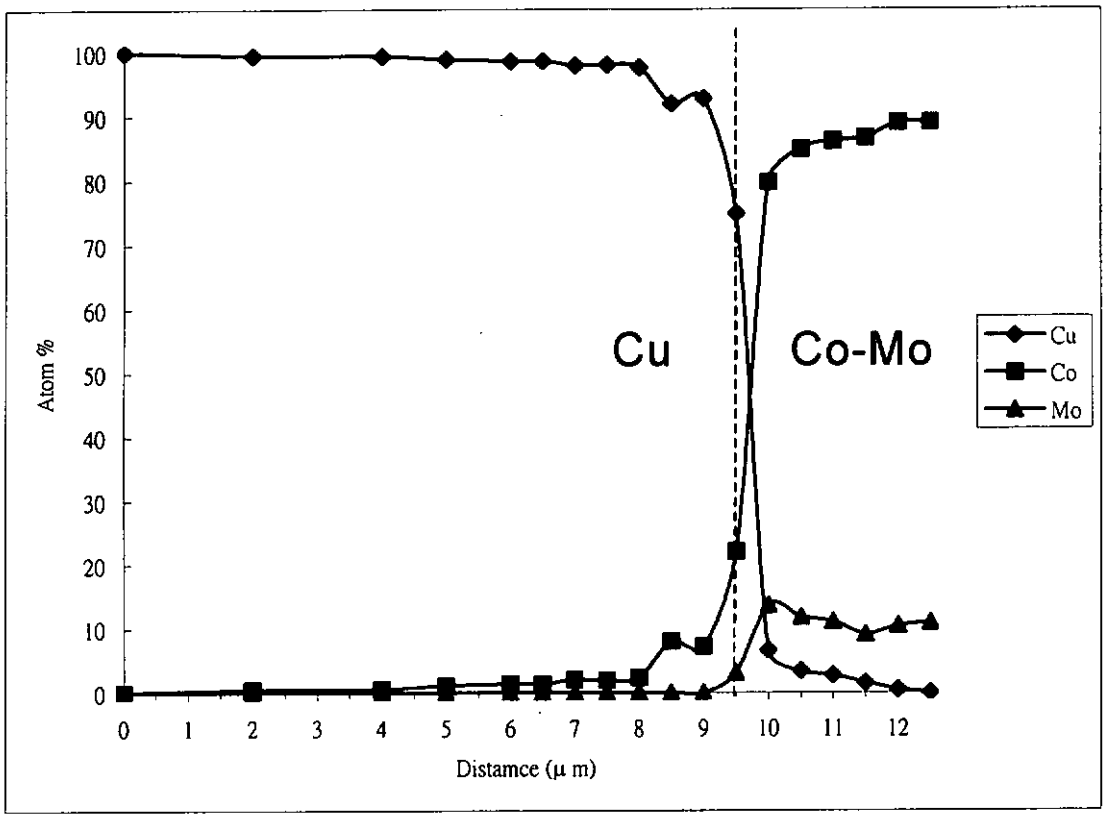

Fig 5.1.13 Concentration- Distance Profile of Cu/Co-Mo couple after heat treatment at 700°C for 5h.

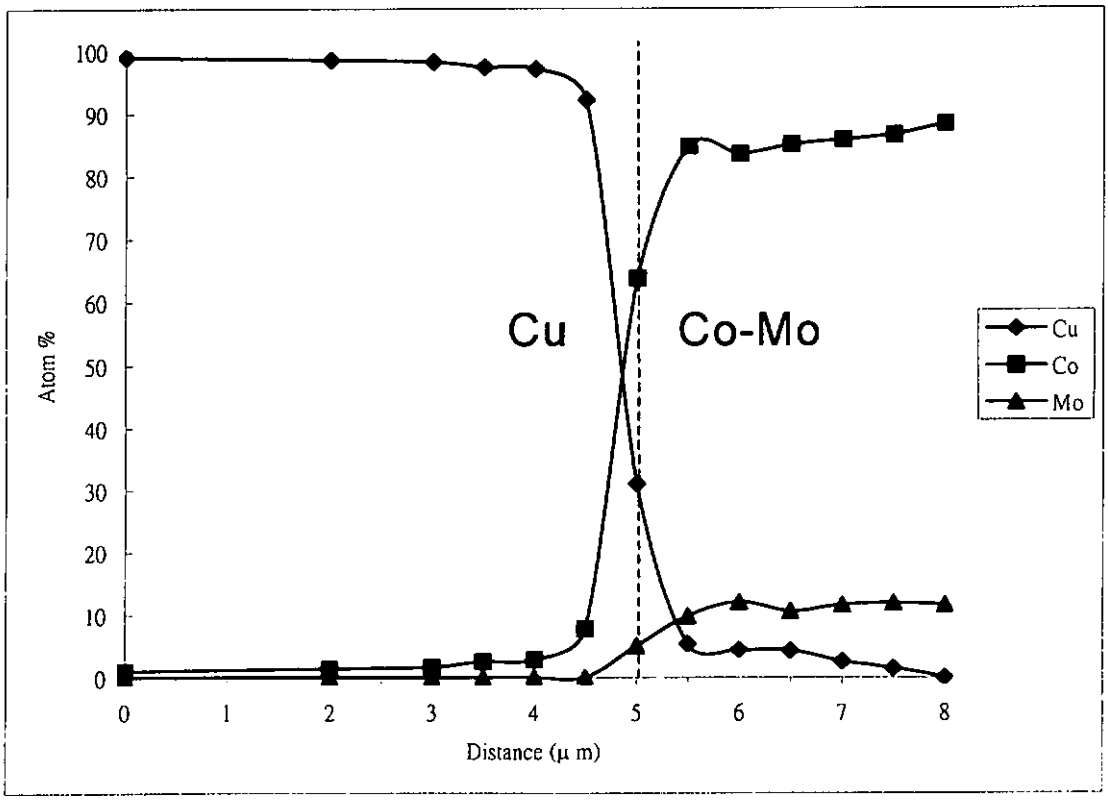

Fig 5.1.14 Concentration- Distance Profile of Cu/Co-Mo couple after heat treatment at 800°C for 0.75h.

Table 5.1.2 Chemical Interdiffusion Coefficients of Cu/Co-Mo Couples at Different Temperature and copper concentration calculated by Boltzmann-Matano Method

Annealing Temp (°C)	Annealing Time (h)	D (cm^2/s)			
		20% Cu	40% Cu	60% Cu	80% Cu
400	168	5.690×10^{-16}	5.980×10^{-16}	6.680×10^{-16}	1.254×10^{-15}
500	72	1.834×10^{-15}	2.313×10^{-15}	2.734×10^{-15}	4.884×10^{-15}
600	24	7.743×10^{-15}	7.178×10^{-15}	7.561×10^{-15}	9.119×10^{-15}
700	5	4.194×10^{-14}	3.669×10^{-14}	3.907×10^{-14}	1.104×10^{-13}
800	0.75	1.376×10^{-11}	1.385×10^{-11}	1.768×10^{-11}	3.385×10^{-11}

A curve of log D as a function of concentration for each of the temperatures investigated is plotted in Fig. 5.1.15.

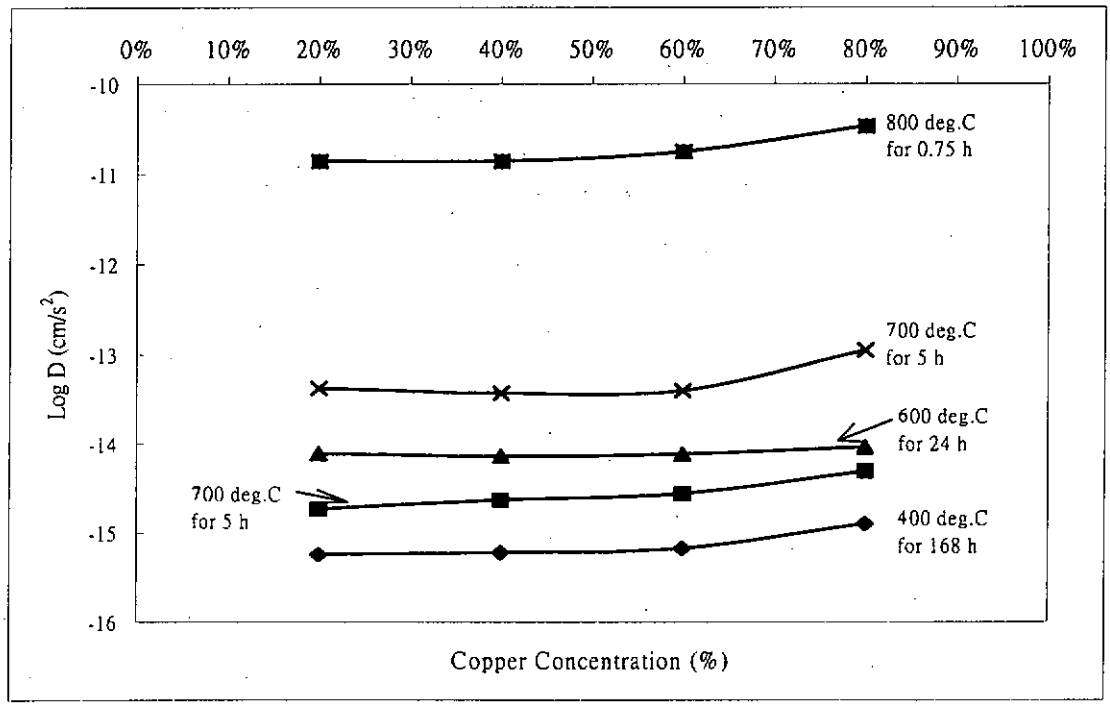

Fig 5.1.15 Variation of D with Copper Concentration for Different Heat Treatment Conditions in Cu/Co-Mo couple

Similar to the Cu/Ni system, the Curves of $\log_{10}$ D Vs. 1/T for concentration of 20% to 80% copper are plotted in Figures 5.1.16 through 5.1.19, respectively.

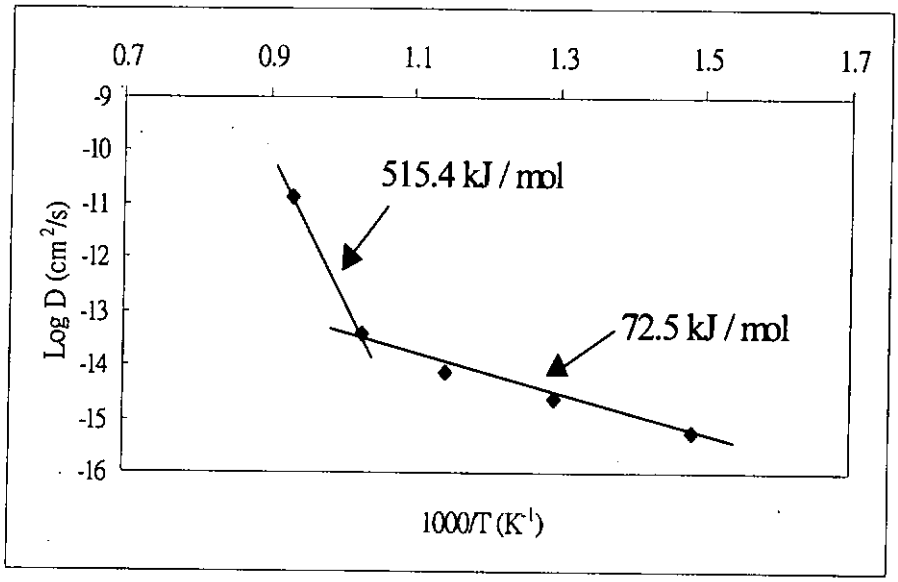

Fig. 5.1.16 The Arrhenius plot of diffusivities at 20% copper in Cu/Co-Mo system

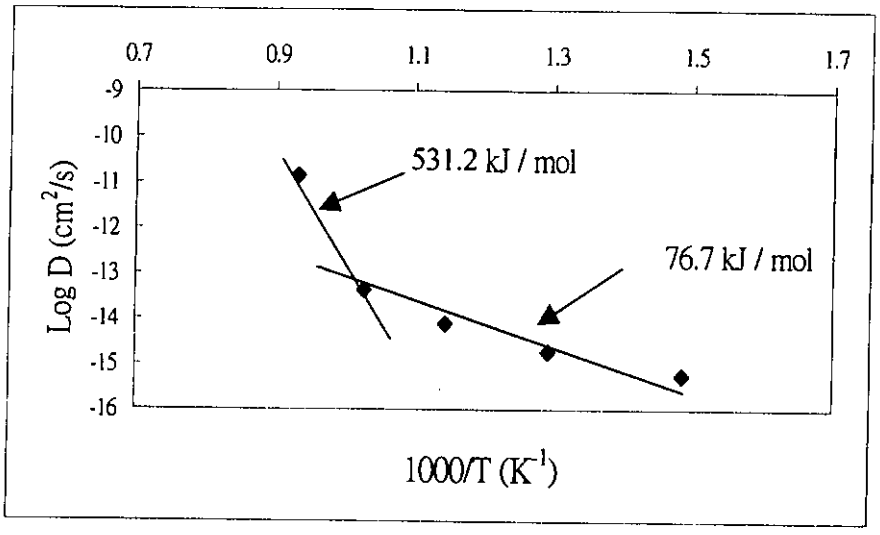

Fig. 5.1.17 The Arrhenius plot of diffusivities at 40% copper in Cu/Co-Mo system

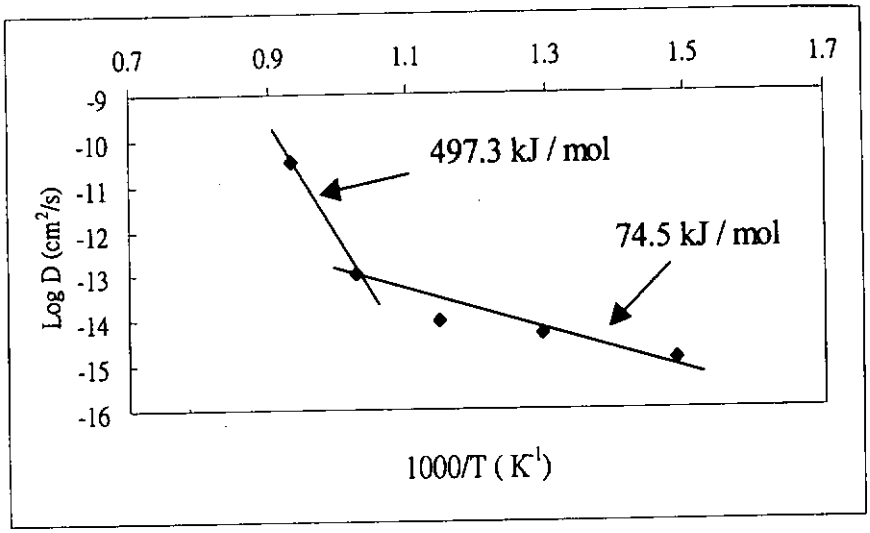

Fig. 5.1.18 The Arrhenius plot of diffusivities at 60% copper in Cu/Co-Mo system

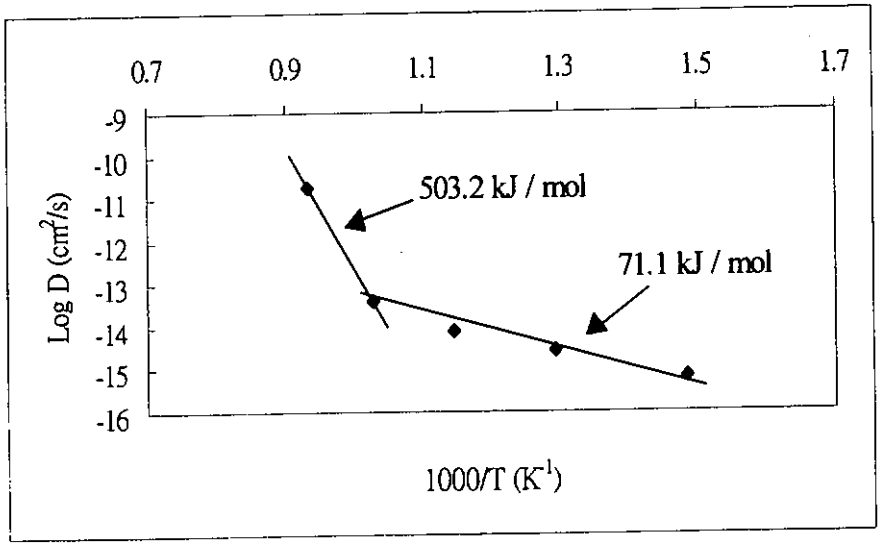

Fig. 5.1.19 The Arrhenius plot of diffusivities at 80% copper in Cu/Co-Mo system

The general shapes of the curves are identical and similar to the Cu/Ni system. Apparent activation energies for diffusion were calculated in Figures 5.1.16 through 5.1.19. In the mid temperature range, the value of Q is seen to be approximately 15% that of Q at the high temperature.

5.1.1.3 Copper/Cobalt-Phosphorus Systems

Diffusion experiments were carried out on Cu/Co-13 (atom%) P couples. Figure 5.1.20 to 5.1.24 show concentration-distance profiles at the diffusion zone of heat-treated Cu/Co-P couples at 400°C to 800° C respectively. The chemical interdiffusion coefficient D was found to be function of concentration and are listed in Table 5.1.3.

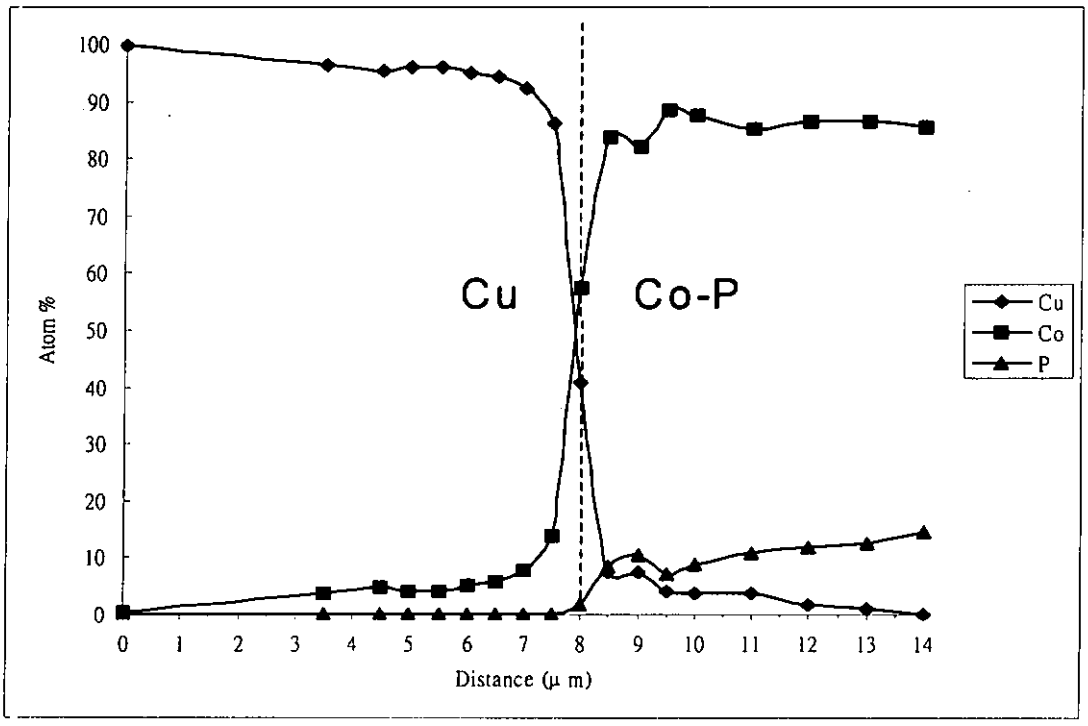

Fig 5.1.20 Concentration- Distance Profile of Cu/Co-P couple after heat treatment at 400°C for 168h.

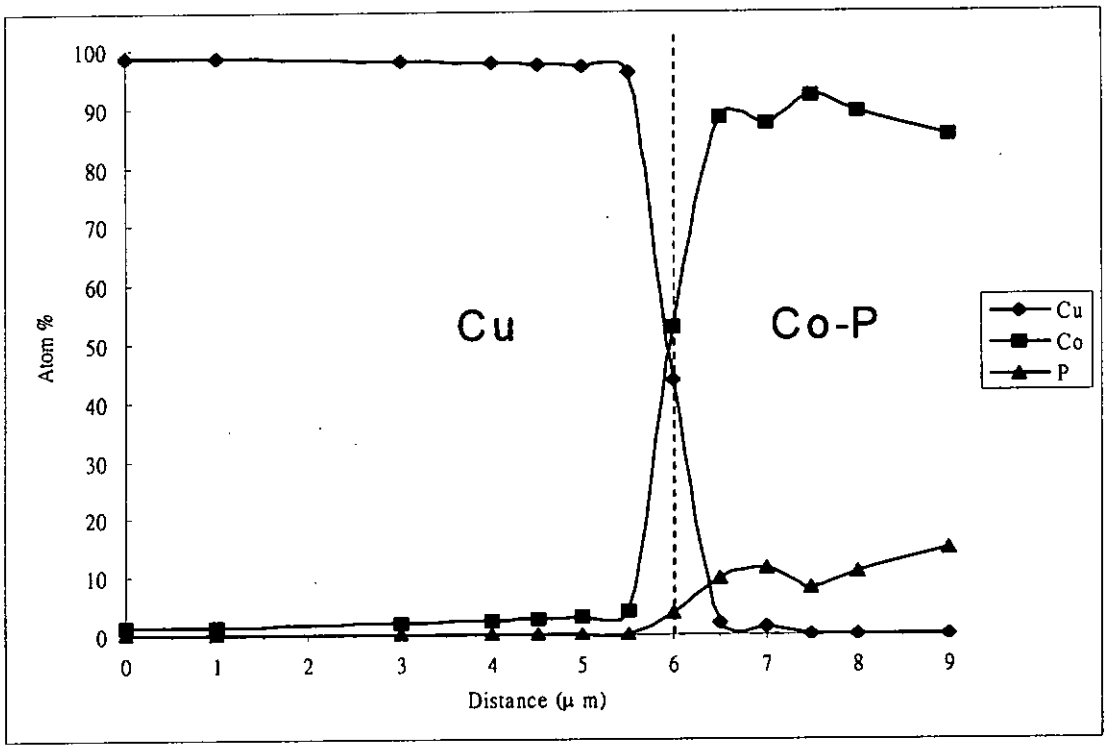

Fig 5.1.21 Concentration- Distance Profile of Cu/Co-P couple after heat treatment at 500°C for 72h.

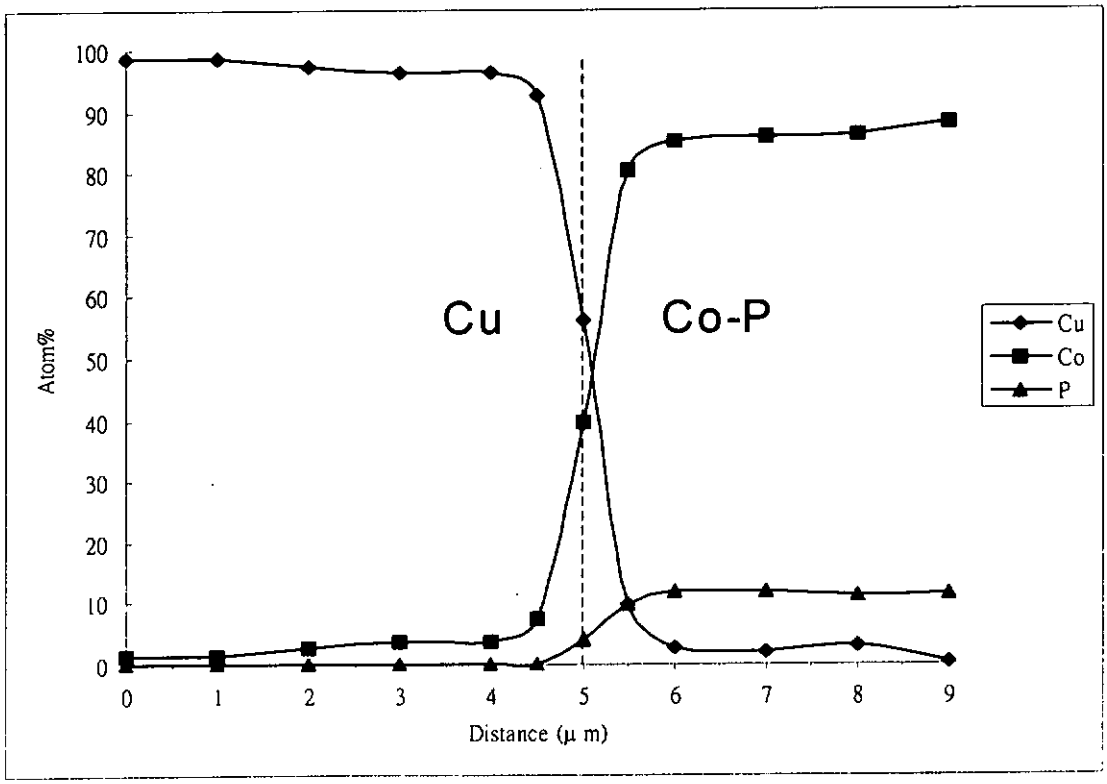

Fig 5.1.22 Concentration- Distance Profile of Cu/Co-P couple after heat treatment at 600°C for 24h.

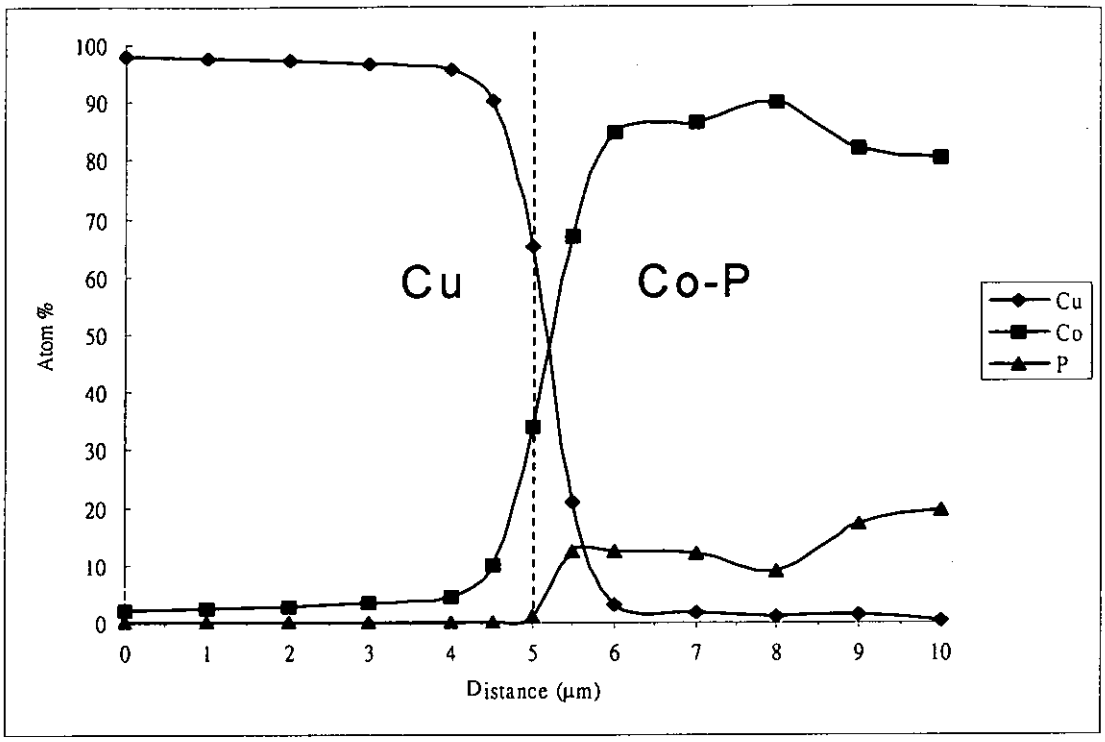

Fig 5.1.23 Concentration- Distance Profile of Cu/Co-P couple after heat treatment at 700°C for 5h.

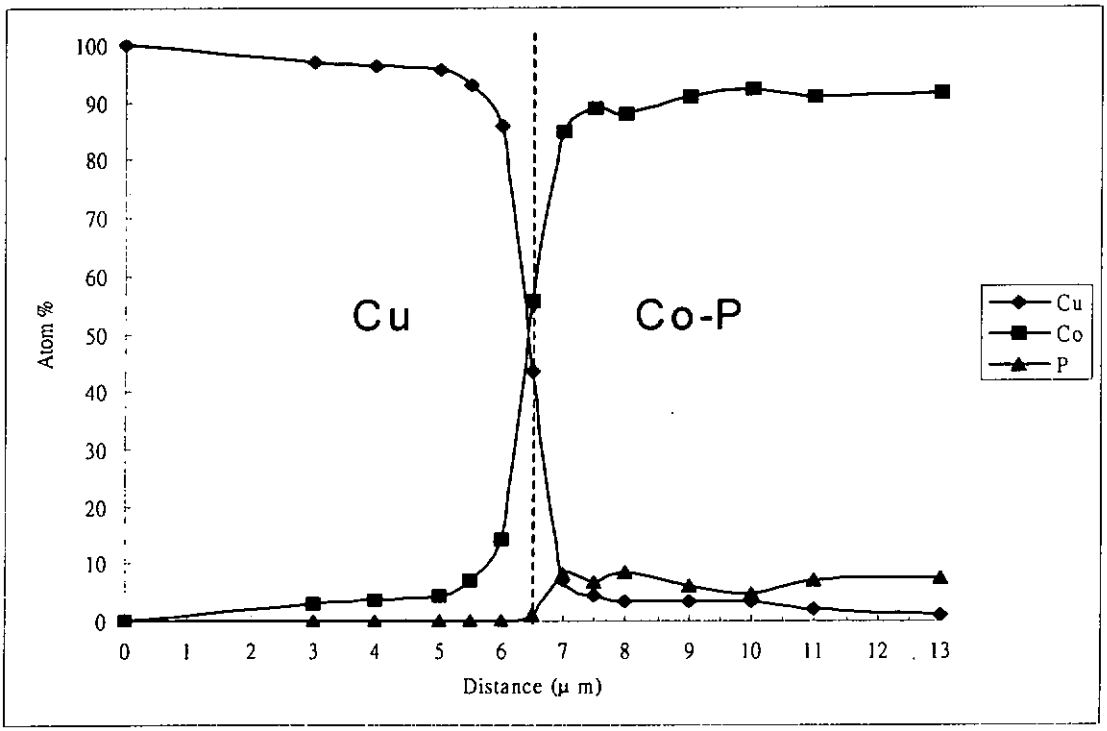

Fig 5.1.24 Concentration- Distance Profile of Cu/Co-P couple after heat treatment at 800°C for 0.75h.

Table 5.1.3 Chemical Interdiffusion Coefficients of Cu/Co-P Couples at Different Temperature and copper concentration calculated by Boltzmann-Matano Method

Annealing Temp (°C)	Annealing Time (h)	D (cm^2/s)			
		20% Cu	40% Cu	60% Cu	80% Cu
400	168	3.301×10^{-15}	3.347×10^{-15}	4.153×10^{-15}	6.854×10^{-15}
500	72	1.105×10^{-15}	1.597×10^{-15}	2.734×10^{-15}	4.210×10^{-15}
600	24	1.186×10^{-14}	1.193×10^{-14}	2.025×10^{-14}	3.799×10^{-14}
700	5	7.869×10^{-14}	9.338×10^{-14}	1.201×10^{-13}	1.908×10^{-13}
800	0.75	7.101×10^{-13}	8.510×10^{-13}	7.242×10^{-13}	1.042×10^{-12}

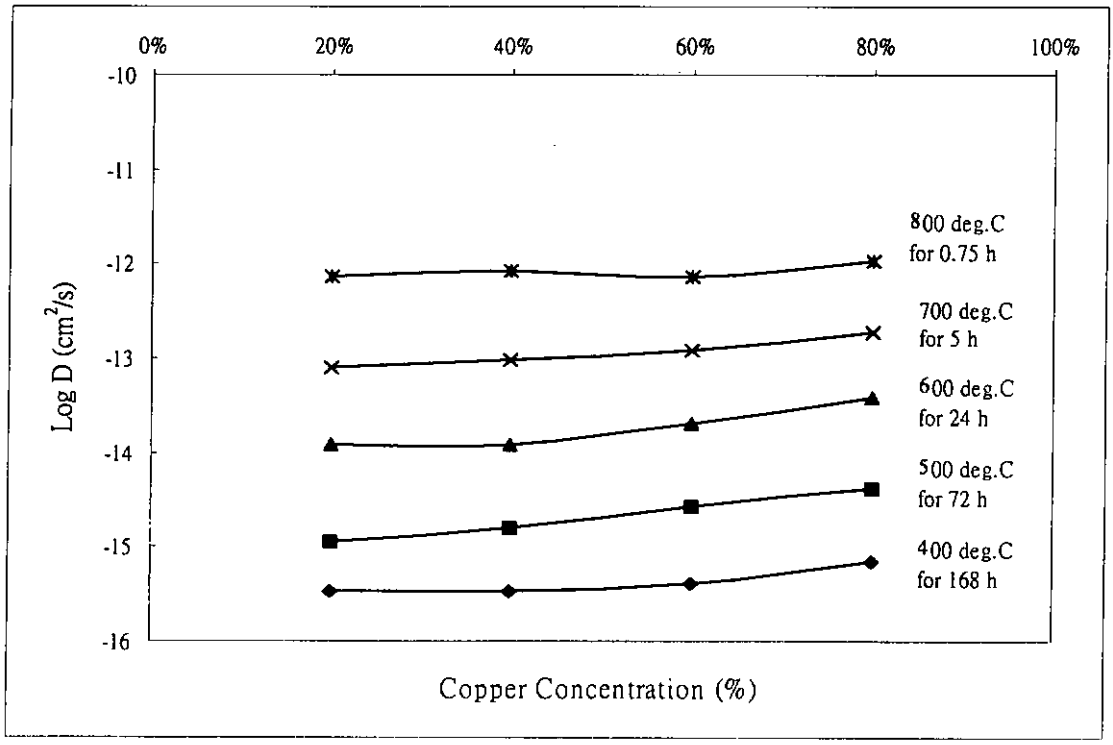

Fig 5.1.25 Variation of D with Copper Concentration for Different Heat Treatment Conditions in Cu/Co-P couple

The log D as a function of concentration for each of the temperatures investigated is plotted in Fig. 5.1.25. The Arrhenius plot of diffusivities for concentration of 20% to

80% copper are plotted in Figures 5.1.26 through 5.1.29, respectively.

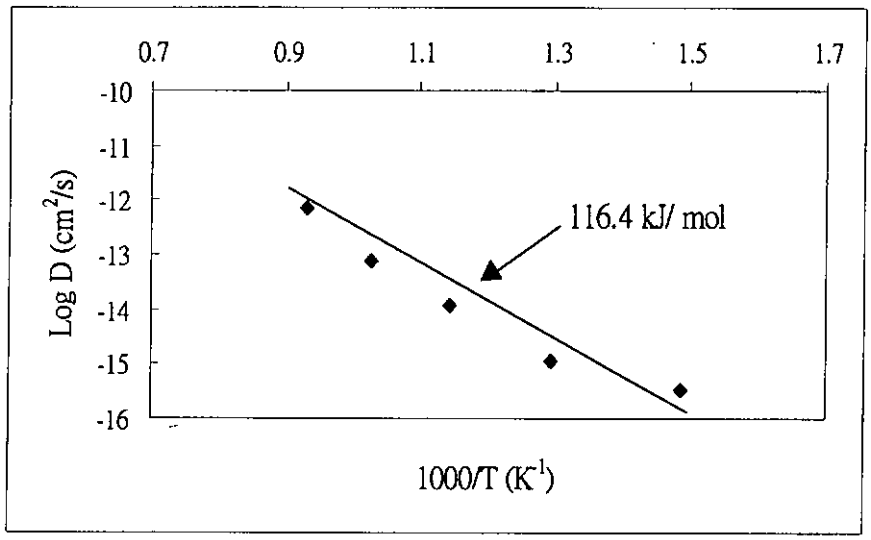

Fig.5.1.26 The Arrhenius plot of diffusivities at 20% copper in Cu/Co-P system

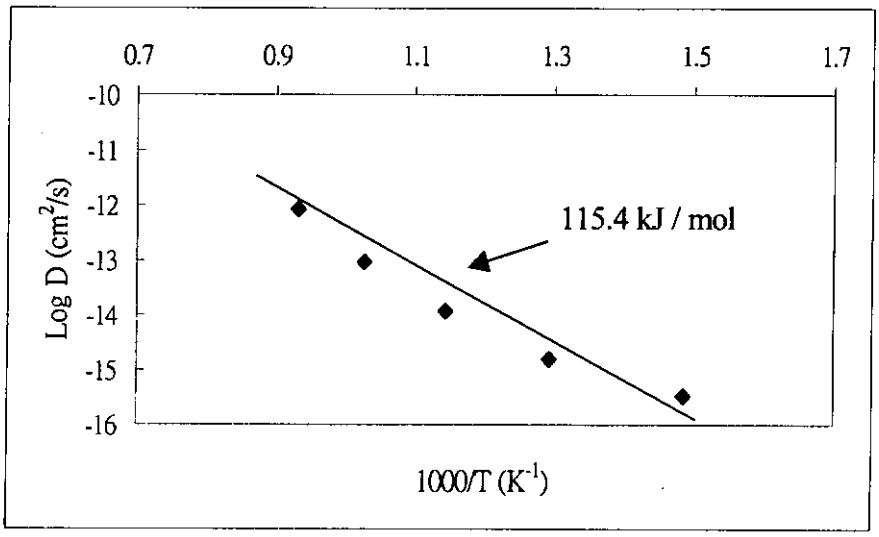

Fig.5.1.27 The Arrhenius plot of diffusivities at 40% copper in Cu/Co-P system

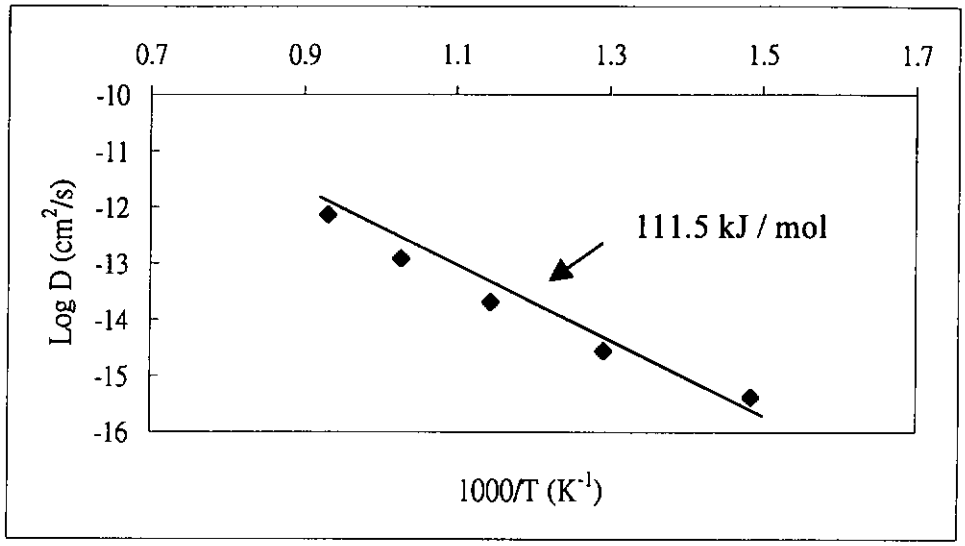

Fig.5.1.28 The Arrhenius plot of diffusivities at 60% copper in Cu/Co-P system

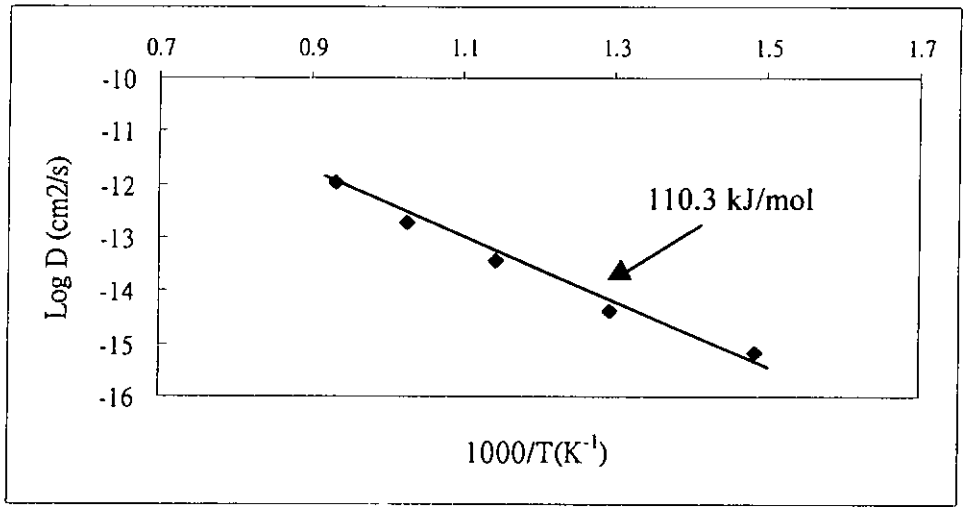

Fig.5.1.29 The Arrhenius plot of diffusivities at 80% copper in Cu/Co-P system

Unlike the Cu/Ni and Cu/Co-Mo systems, the Arrhenius plots of Cu/Co-P system show no transition region in the temperature range studied. The apparent activation energies for diffusion Q decreases from 116.4 kJ/mol to 110.3 kJ/mol as the copper concentration increases from 20% to 80%.

5.1.1.4 Copper/Cobalt-Molybdenum-Phosphorus Systems

The cobalt-molybdenum-phosphorus alloy coatings with 6 atom% Mo and 20 atom% P were plated on copper. Diffusion experiments were carried at temperature ranging from 400°C to 800° C. Concentration-distance profiles at the diffusion zone were obtained. Figure 5.1.30 to 5.1.34 shows concentration-distance profilesthe of heat-treated Cu/Co-Mo-P couples and chemical interdiffusion coefficients of each sample are listed in Table 5.1.4.

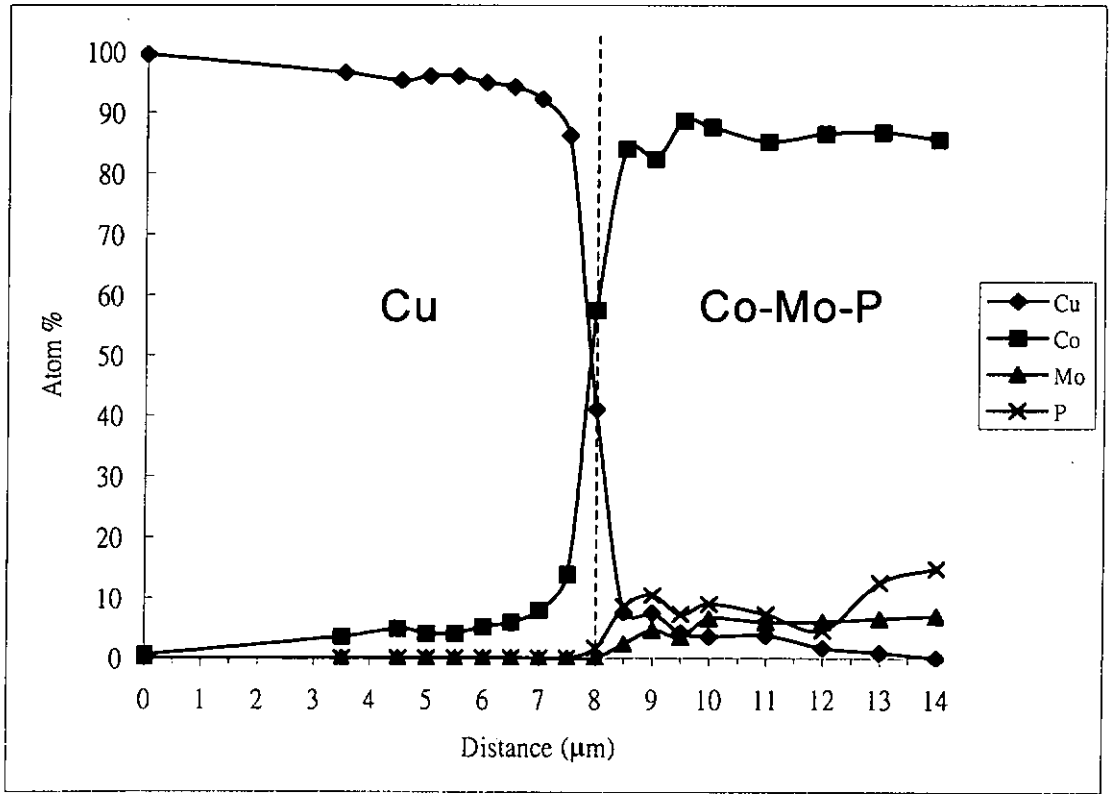

Fig 5.1.30 Concentration- Distance Profile of Cu/Co-Mo-P couple after heat treatment at 400°C for 168h.

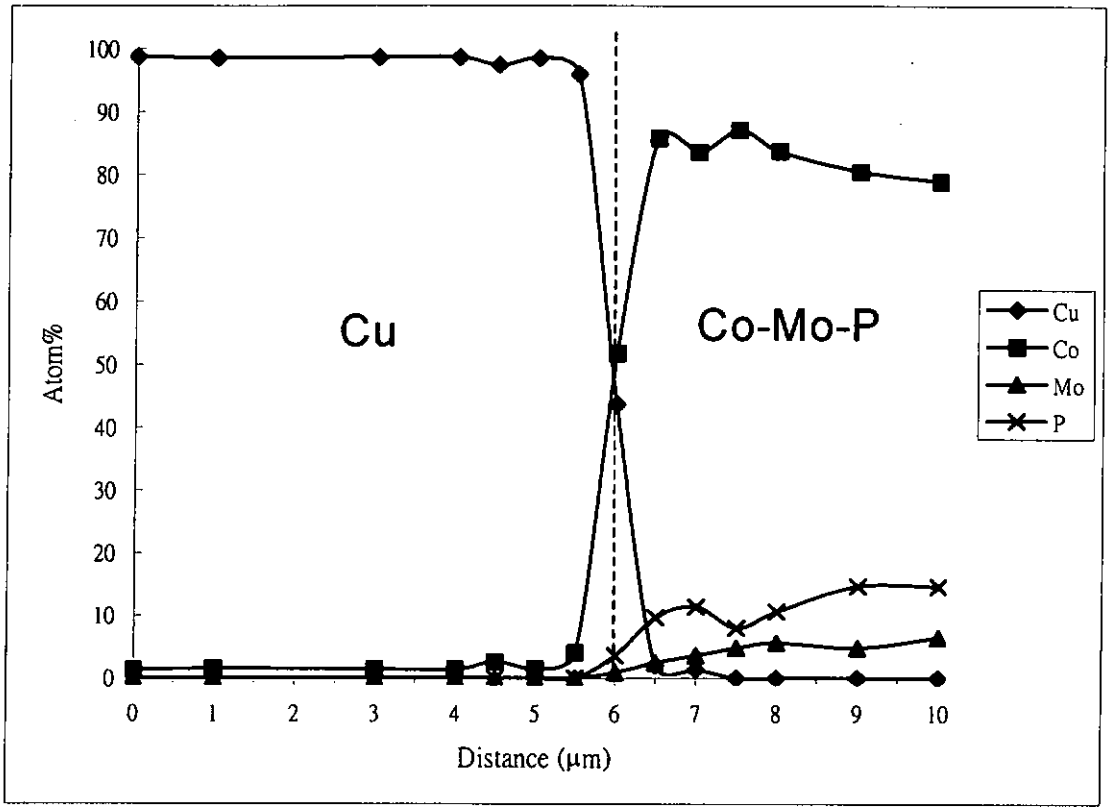

Fig 5.1.31 Concentration- Distance Profile of Cu/Co-Mo-P couple after heat treatment at 500°C for 72h.

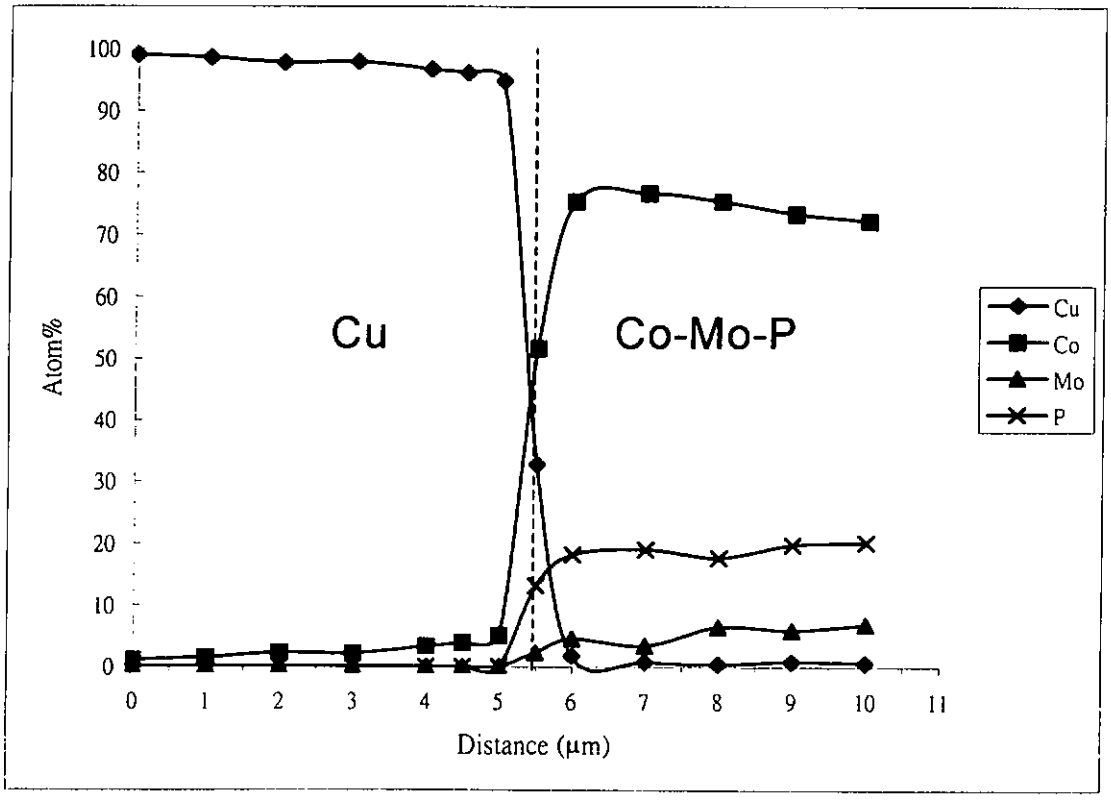

Fig 5.1.32 Concentration- Distance Profile of Cu/Co-Mo-P couple after heat treatment at 600°C for 24h.

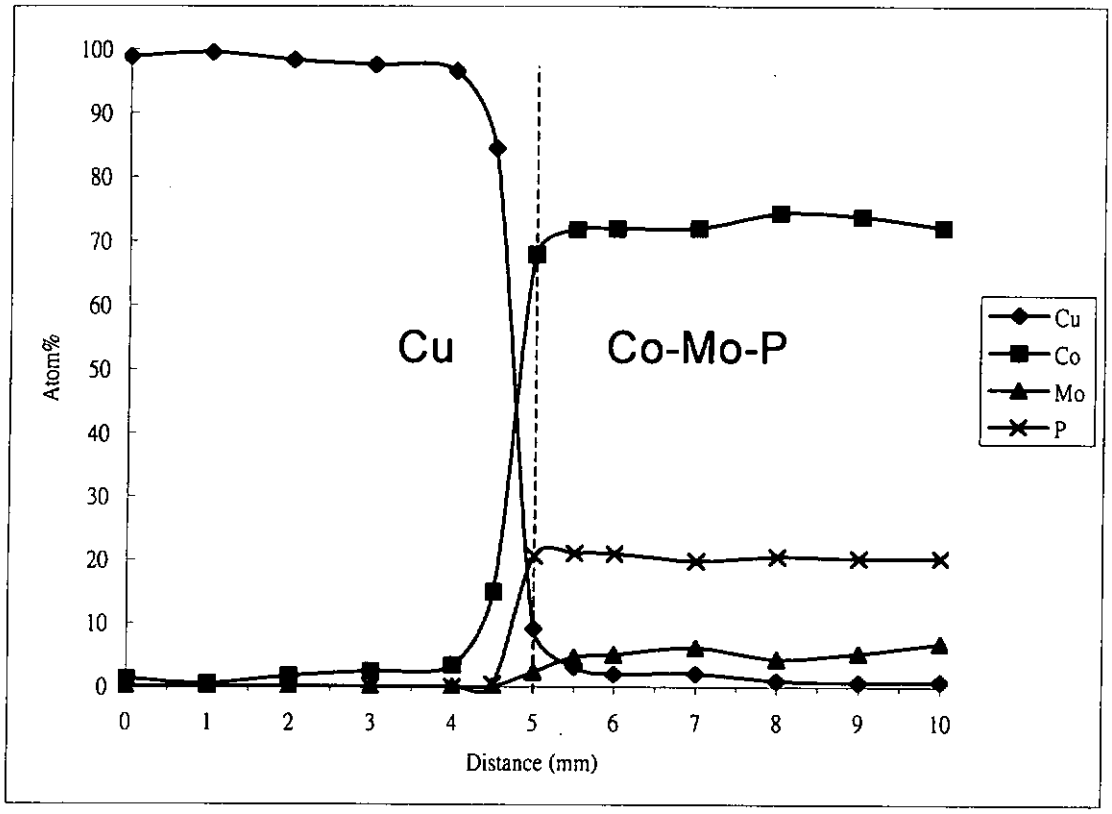

Fig 5.1.33 Concentration- Distance Profile of Cu/Co-Mo-P couple after heat treatment at 700°C for 5h.

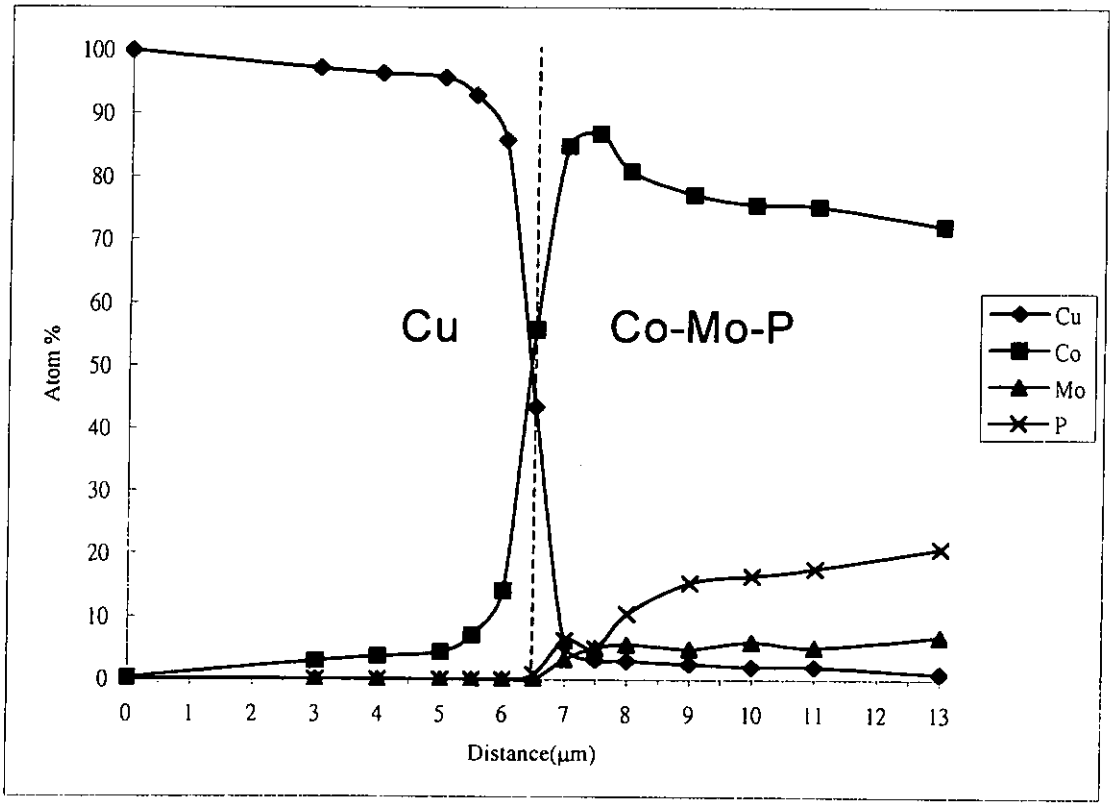

Fig 5.1.34 Concentration- Distance Profile of Cu/Co-Mo-P couple after heat treatment at 800°C for 0.75h.

Table 5.1.4 Chemical Interdiffusion Coefficients of Cu/Co-Mo-P Couples at Different Temperature and copper concentration calculated by Boltzmann-Matano Method

Annealing Temp (°C)	Annealing Time (h)	D (cm^2/s)			
		20% Cu	40% Cu	60% Cu	80% Cu
400	168	2.561×10^{-15}	2.994×10^{-15}	3.917×10^{-15}	6.014×10^{-15}
500	72	1.095×10^{-15}	1.395×10^{-15}	2.561×10^{-15}	4.102×10^{-15}
600	24	3.617×10^{-15}	7.219×10^{-15}	1.058×10^{-14}	1.765×10^{-14}
700	5	3.629×10^{-14}	3.100×10^{-14}	3.257×10^{-14}	4.354×10^{-14}
800	0.75	6.892×10^{-13}	8.021×10^{-13}	8.954×10^{-13}	9.540×10^{-13}

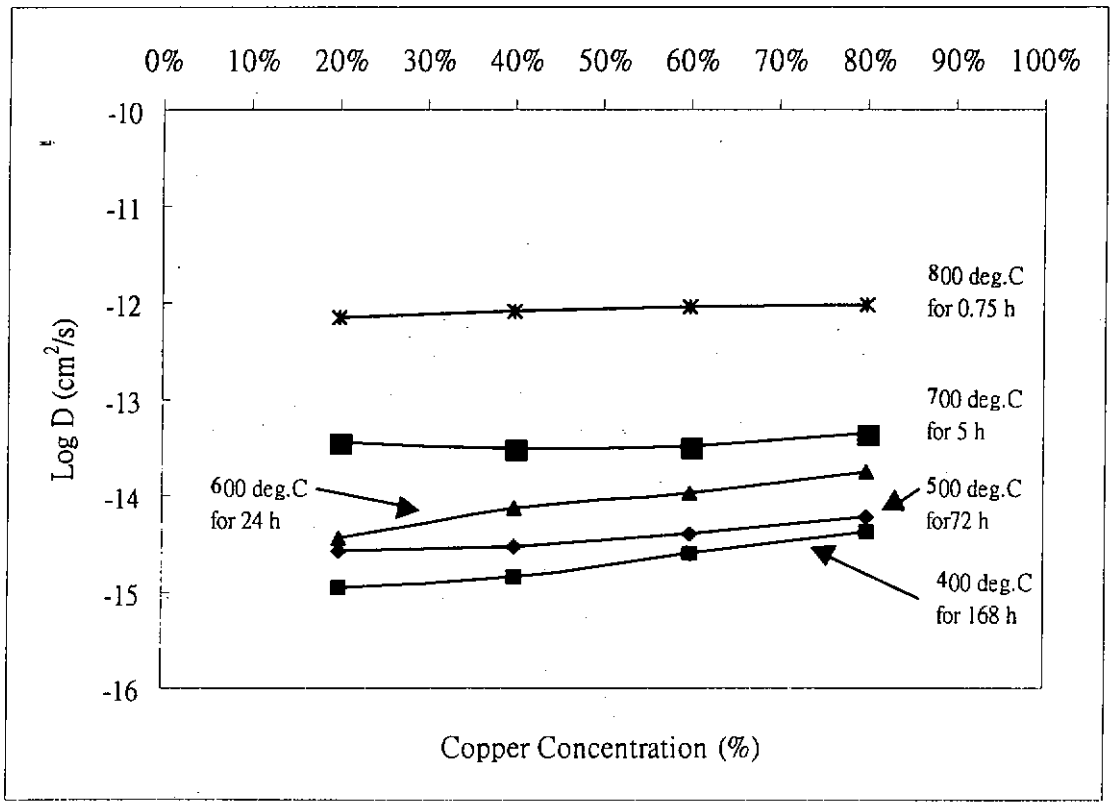

Fig 5.1.35 Variation of D with Copper Concentration for Different Heat Treatment Conditions in Cu/Co-Mo-P couple

The curves of log D as a function of concentration for each of the temperatures investigated is plotted in Fig. 5.1.35. The Arrhenius plot of diffusivities for are plotted in Figures 5.1.36 through 5.1.39, respectively.

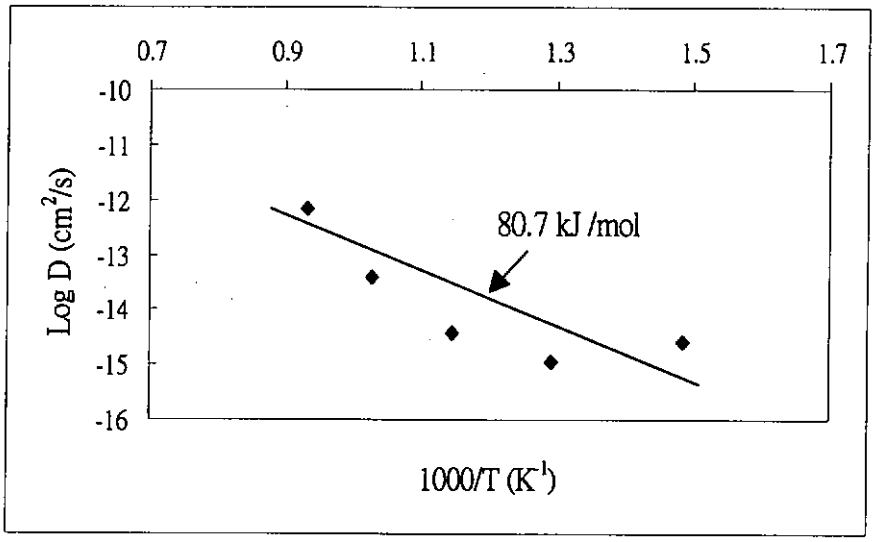

Fig. 5.1.36 The Arrhenius plot of diffusivities at 20% copper in Cu/Co-Mo-P system

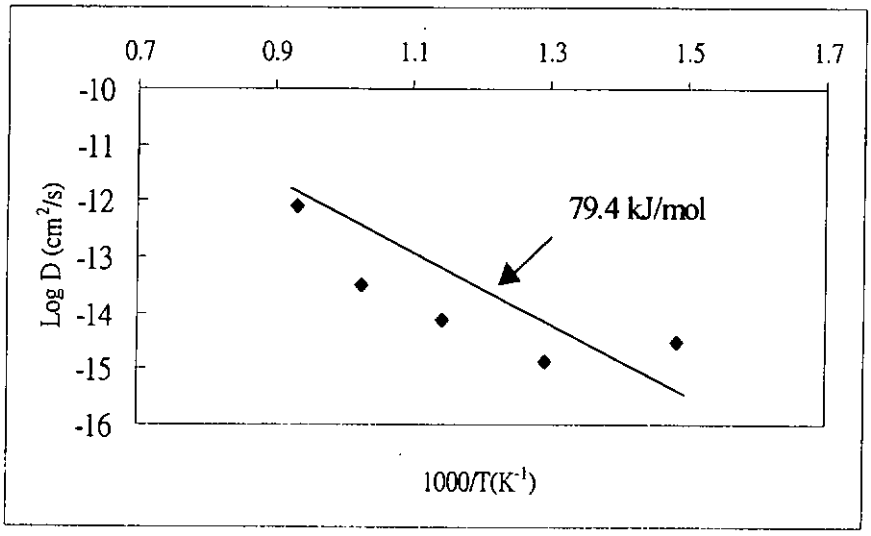

Fig. 5.1.37 The Arrhenius plot of diffusivities at 40% copper in Cu/Co-Mo-P system

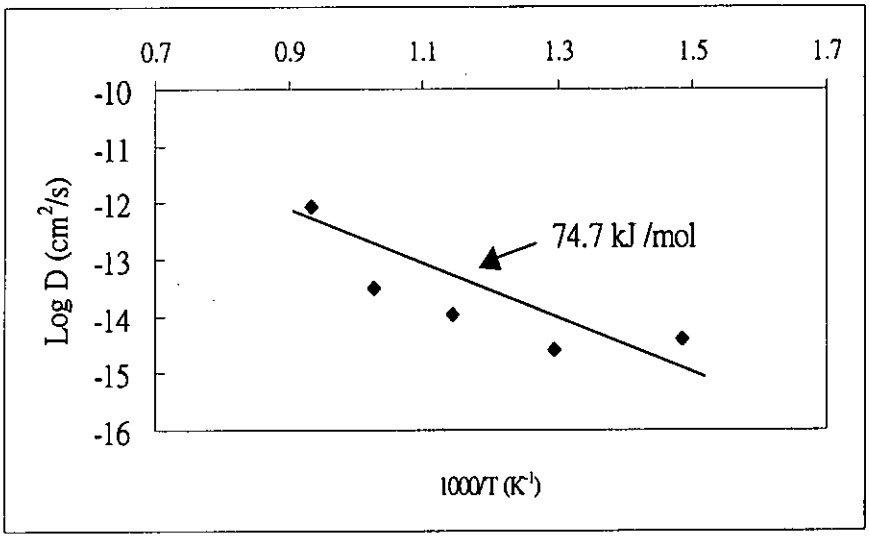

Fig. 5.1.38 The Arrhenius plot of diffusivities at 60% copper in Cu/Co-Mo-P system

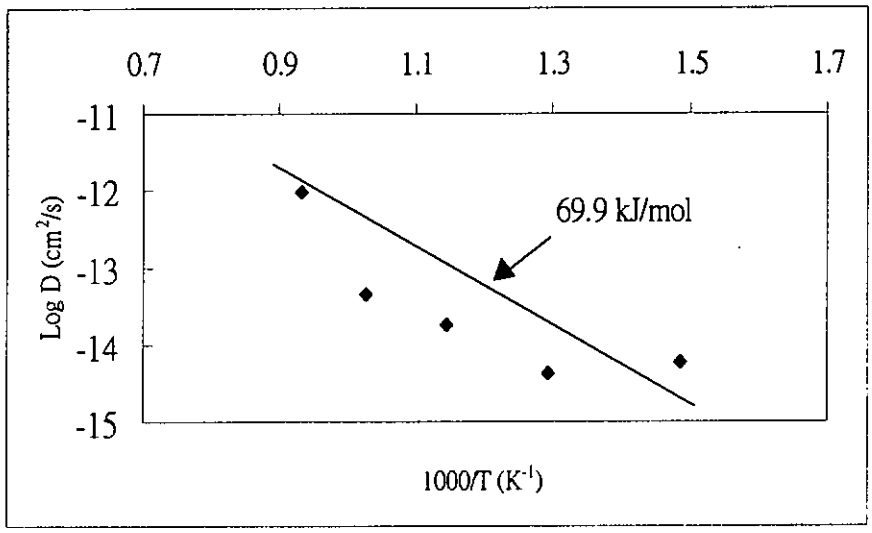

Fig. 5.1.39 The Arrhenius plot of diffusivities at 80% copper in Cu/Co-Mo-P system

The curves are similar to the Cu/Co-P system that shows no transition region in the temperature range studied. Apparent activation energies for diffusion were calculated in Figures 5.1.36 through 5.1.39 and vary from 87.7 kJ/mol to 69.9 kJ/mol.

5.1.1.5 Comments on the Diffusion Experiments of Copper/Barrier Systems

To compare the copper diffusion barrier property of the barrier, the term interdiffusion coefficient D can be used as a parameter. At low temperature range (400°C -500°C), the interdiffusion coefficients for Cu/Co-P couples have the same order of magnitude as the Cu/Co-Mo couples. The D of Cu/Ni couples are nearly higher than those cobalt base alloy systems by one order of magnitude at 400°C. At mid temperature range (600°C -700°C), the interdiffusion coefficients for Cu/Co-Mo couples have the same order of magnitude as the Cu/Co-Mo-P couples. The Cu/Ni systems show the highest values of interdiffusion coefficients of four systems.

At high temperature (800°C), it is interesting to note that the gives the interdiffusion coefficients of the Cu/Co-Mo system is higher than those systems by one of order magnitude.

From the results of Arrhenius plot of these systems, the diffusion mechanisms may be indicated. For the system of Cu/Ni and Cu/Co-Mo, a transition region can be observed. Polycrystalline metals usually show this result [13]. Figure 5.1.40 shows the Arrhenius plot of Cu/Co-Mo system of all temperature and copper concentration studied.

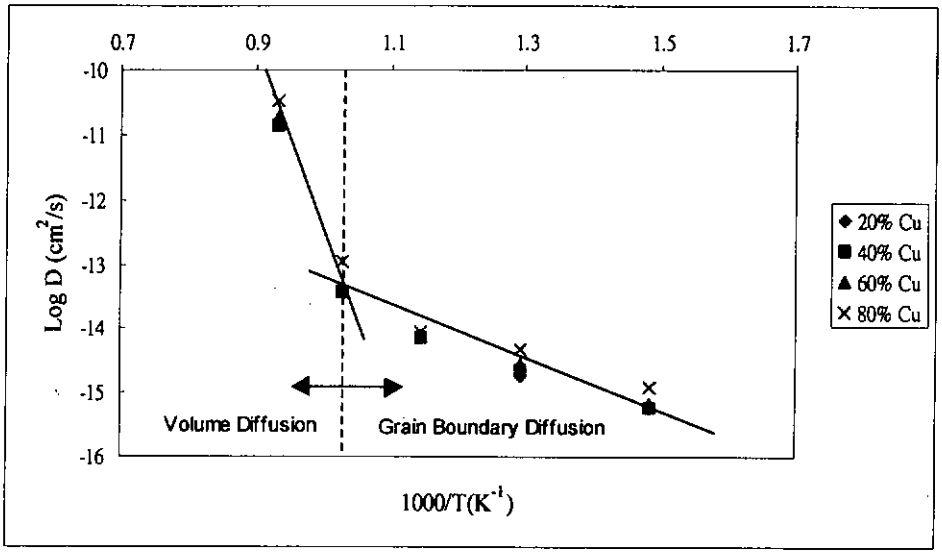

Figure 5.1.40. The Arrhenius plot of diffusivities in Cu/Co-Mo system

A summary of comparisons among Ni, Co-Mo, Co-P and Co-Mo-P for their diffusion barrier property based on the interdiffusion coefficients in the Cu/Barrier is is given in Table 5.1.5.

Table 5.1.5 A summary of comparison of the diffusion barrier property of Ni, Co-Mo ,Co-P and Co-Mo-P

Temperature	Ability for withstanding Copper Diffusion (In ascending order)
400°C	Ni < Co-Mo-P < Co-P ≈ Co-Mo
500°C	Ni < Co-Mo ≈ Co-P ≈ Co-Mo-P
600 ~ 700°C	Ni < Co-P < Co-Mo ≈ Co-Mo-P
800°C	Co-Mo < Ni < Co-Mo-P ≈ Co-P

5.2 Copper/Cobalt-Molybdenum-Phosphorus (Barrier)/Nickel Systems

To evaluate the diffusion barrier property of cobalt-molybdenum-phosphorus, interdiffusion of a Cu/Co-Mo-P (barrier)/Ni were studied. The samples of thickness 0.5μm and 1 μm were heat treated at temperature ranging 400°C to 800°C. Figure 5.2 show the Copper Concentration- Distance Profile of Cu/Co-Mo-P/Ni couple after heat treatment at 800°C for 0.75h.

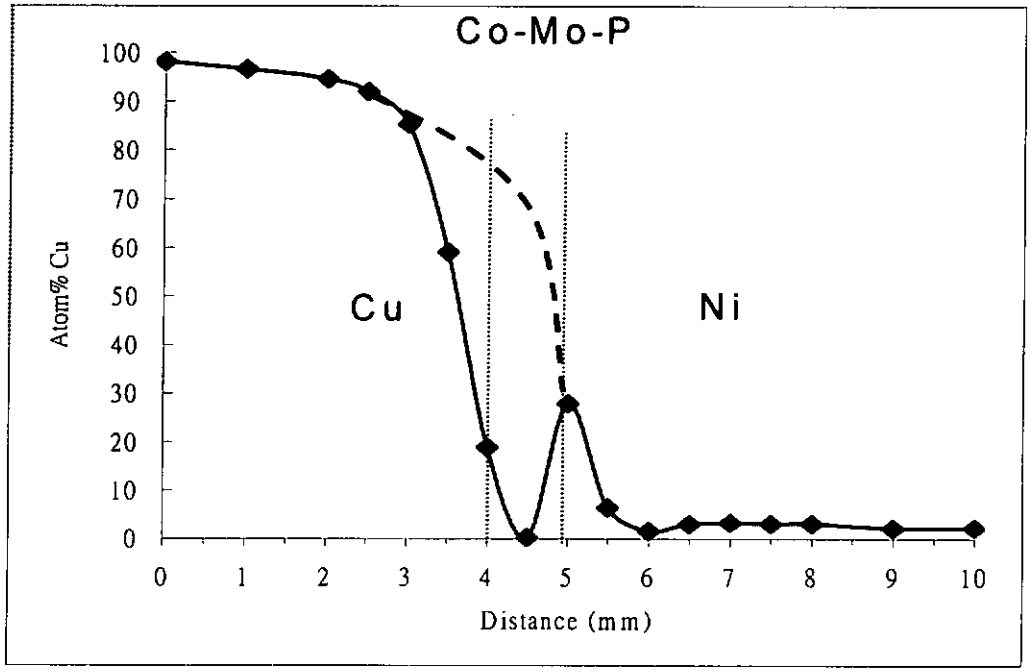

Figures 5.2 The Copper Concentration-Distance Profile of Cu/Co-Mo-P/Ni couple after heat treatment at 800°C for 0.75h; apparent D is determined by joining the discontinued points of the Cu concentration profile.

Because of the mutual insolubility between copper and cobalt, very little amount of copper was detected by EDS scan in the Co-Mo-P coatings. The performance of cobalt and nickel as a diffusion barrier was determined by a semi-quantitative method.

By joining the two discontinued points of copper concentration on both sides of the barrier can help determinate the apparent interdiffusion coefficient between Cu/Barrier/Ni. Then Cu concentration profiles were calculated by using Boltzmann-Matano Method.

Table 5.2.1 Apparent interdiffusion coefficients at 20% Cu of Cu/Ni for Cu/Co-Mo-P(Barrier)/Ni system and interdiffusion coefficients at 20% Cu of Cu/Ni after heat treatment at different temperatures.

Annealing Temp (°C)	Annealing Time (h)	D (cm^2/s)		
		Ni (No Barrier)	Ni (0.5 μm Barrier)	Ni (1 μm Barrier)
400	168	7.17×10^{-15}	2.84×10^{-15}	1.11×10^{-15}
500	72	9.52×10^{-14}	9.29×10^{-15}	6.74×10^{-15}
600	24	1.51×10^{-13}	2.53×10^{-13}	2.09×10^{-13}
700	5	1.57×10^{-13}	1.36×10^{-13}	1.08×10^{-13}
800	0.75	8.04×10^{-12}	3.14×10^{-12}	1.62×10^{-12}

Table 5.2.2 Apparent interdiffusion coefficients at 40% Cu of Cu/Ni for Cu/Co-Mo-P(Barrier)/Ni system and interdiffusion coefficients at 40% Cu of Cu/Ni after heat treatment at different temperatures.

Annealing Temp (°C)	Annealing Time (h)	D (cm^2/s)		
		Ni (No Barrier)	Ni (0.5 μm Barrier)	Ni (1 μm Barrier)
400	168	9.66×10^{-15}	2.30×10^{-15}	1.82×10^{-15}
500	72	7.65×10^{-14}	1.02×10^{-14}	1.00×10^{-14}
600	24	1.51×10^{-13}	6.69×10^{-13}	2.885×10^{-13}
700	5	2.07×10^{-13}	1.51×10^{-13}	1.595×10^{-13}
800	0.75	7.52×10^{-12}	3.28×10^{-12}	1.572×10^{-12}

Table 5.2.3 Apparent interdiffusion coefficients at 60% Cu of Cu/Ni for Cu/Co-Mo-P(Barrier)/Ni system and interdiffusion coefficients at 60% Cu of Cu/Ni after heat treatment at different temperatures.

Annealing Temp (°C)	Annealing Time (h)	D (cm^2/s)		
		Ni (No Barrier)	Ni (0.5 μm Barrier)	Ni (1 μm Barrier)
400	168	1.235×10^{-14}	2.673×10^{-15}	2.079×10^{-15}
500	72	6.012×10^{-14}	1.619×10^{-14}	1.320×10^{-14}
600	24	1.569×10^{-13}	9.162×10^{-14}	5.157×10^{-14}
700	5	2.042×10^{-13}	1.972×10^{-13}	1.355×10^{-13}
800	0.75	8.954×10^{-12}	3.348×10^{-12}	1.708×10^{-12}

Table5.2.4 Apparent interdiffusion coefficients at 80% Cu of Cu/Ni for Cu/Co-Mo-P(Barrier)/Ni system and interdiffusion coefficients at 80% Cu of Cu/Ni after heat treatment at different temperatures.

Annealing Temp (°C)	Annealing Time (h)	D (cm^2/s)		
		Ni (No Barrier)	Ni (0.5 μm Barrier)	Ni (1 μm Barrier)
400	168	9.658×10^{-15}	4.450×10^{-15}	1.991×10^{-15}
500	72	7.652×10^{-14}	4.092×10^{-14}	2.911×10^{-14}
600	24	8.219×10^{-14}	2.674×10^{-14}	2.416×10^{-14}
700	5	2.972×10^{-13}	1.358×10^{-13}	1.060×10^{-13}
800	0.75	7.521×10^{-12}	3.456×10^{-12}	2.135×10^{-12}

The apparent interdiffusion coefficient between copper and nickel would be lowered if barrier had delayed interdiffusion between copper and nickel. Conversely, the apparent interdiffusion coefficient between copper and nickel would be increased if the copper atoms diffuse into the barrier layer with higher rate than that diffusing into nickel. The interdiffusion coefficients of Cu/Ni system and apparent

interdiffusion coefficients of Cu/Co-Mo-P/Ni systems are shown in Table 5.2.1 to 5.2.4 respectively. These values are useful for evaluation of the barrier property of Co-Mo-P alloy deposition. Results of the diffusion experiments show that apparent interdiffusion coefficients of Cu/Co-Mo-P/Ni system are about two(0.5μm) to four(1μm) times smaller than Cu/Ni systems. This shows that the Co-Mo-P is an effective barrier for copper penetration.

5.3 Copper/Barrier/Gold System

To evaluate the effectiveness of different barrier coating, a data treatment method suggested by Marx *et al* [52] was used. To measure the extent of diffusion of the copper into the gold layer upon heat treatment, a "copper penetration" was arbitrarily defined as the distance on the copper concentration profile from the mid-plane of the barrier coating the 10 atomic percent copper composition plane, as shown in Fig 5.3.1. To be an effective barrier, diffusion of the barrier material itself to either the copper substrates or gold coating should be small. To measure the extent of diffusion of the barrier material into the gold coating upon heat treatment, a "barrier coating penetration" was also defined as the distance on the barrier materials concentration profile from the central of the barrier coating to the 10 atomic percent of that barrier material. The electroplated Ni, Co, Co-Mo, Co-P and Co-Mo-P of thickness 1μm were electroplated respectively on pretreated copper substrates. Gold coatings were

then electroplated on the copper/barrier and diffusion experiments of copper/barrier/gold system were conducted at 400 °C for 48 hr. Concentration-distance profiles were then obtained by EDS after annealing. Figures 5.3.2 to 5.3.7 show the Concentration-Distance profile of different systems after heat treatment at 400°C for 48h. Table 5.3 shows the value of "copper penetration" and "barrier coating penetration" of those barrier coatings.

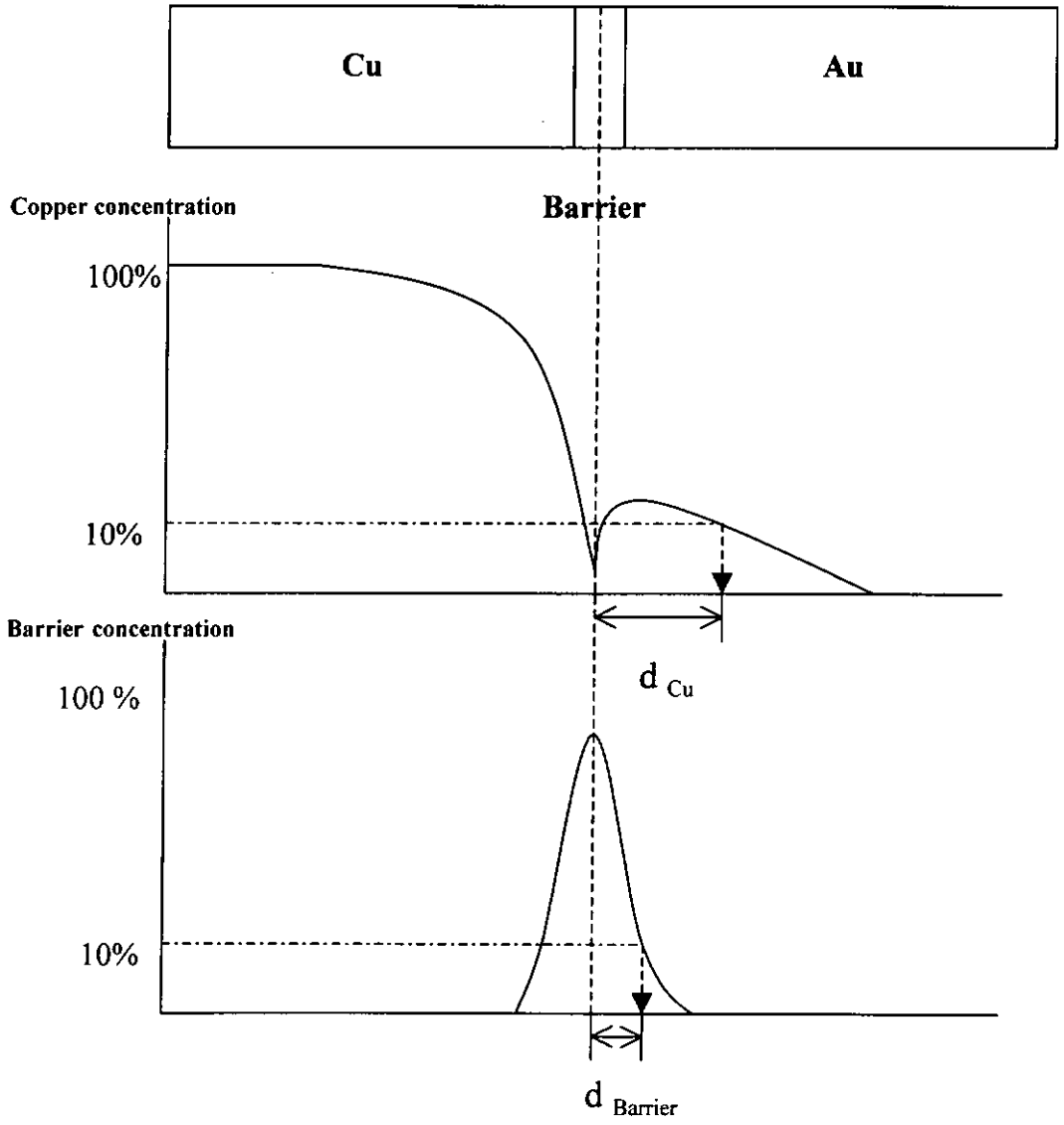

Fig 5.3.1 The concentration-distance profile of Cu in the barrier and gold coatings yield information on the effectiveness of the barrier studied.

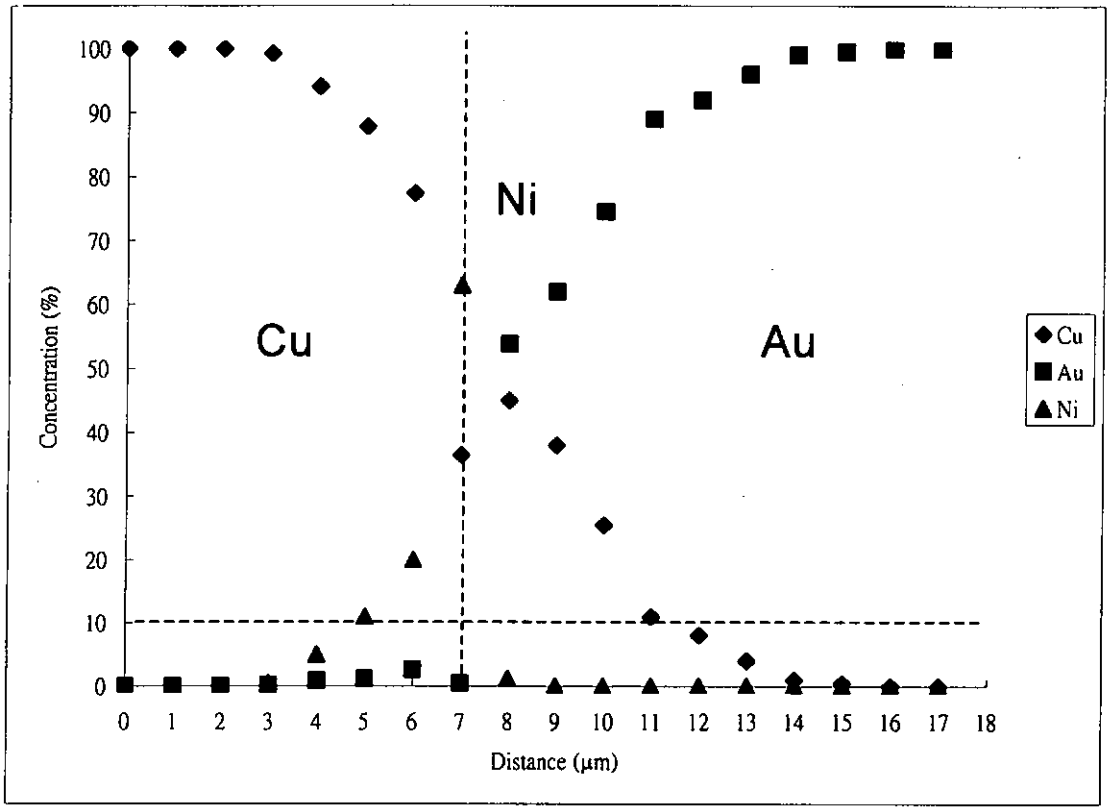

Fig 5.3.2 Concentration- Distance Profile of Cu/Ni/Au system after heat treatment at 400°C for 48h.

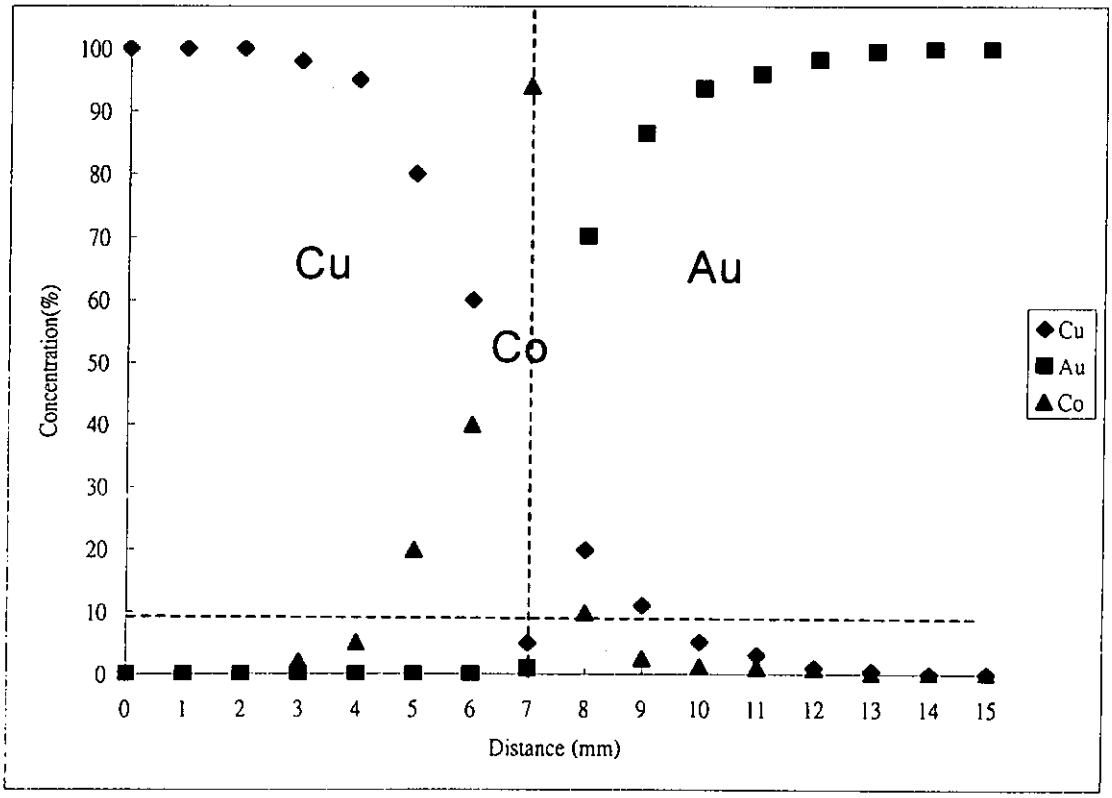

Fig 5.3.3 Concentration- Distance Profile of Cu/Co/Au system after heat treatment at 400°C for 48h.

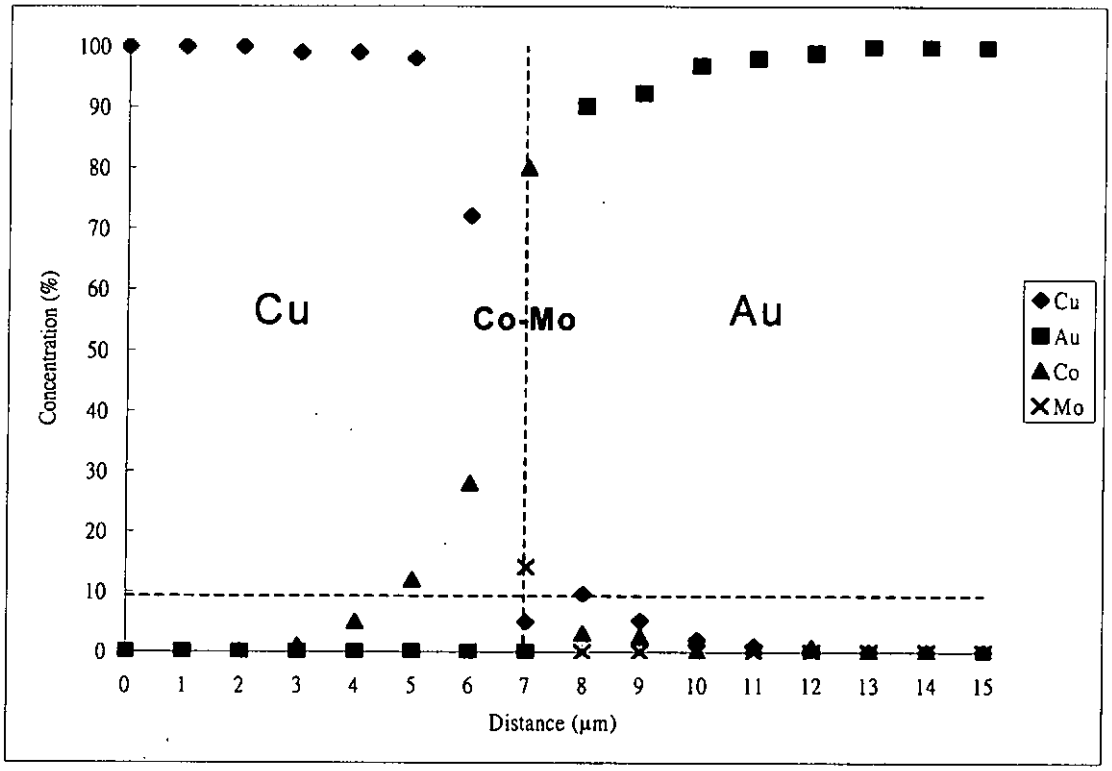

Fig 5.3.4 Concentration- Distance Profile of Cu/Co-Mo/Au system after heat treatment at 400°C for 48h.

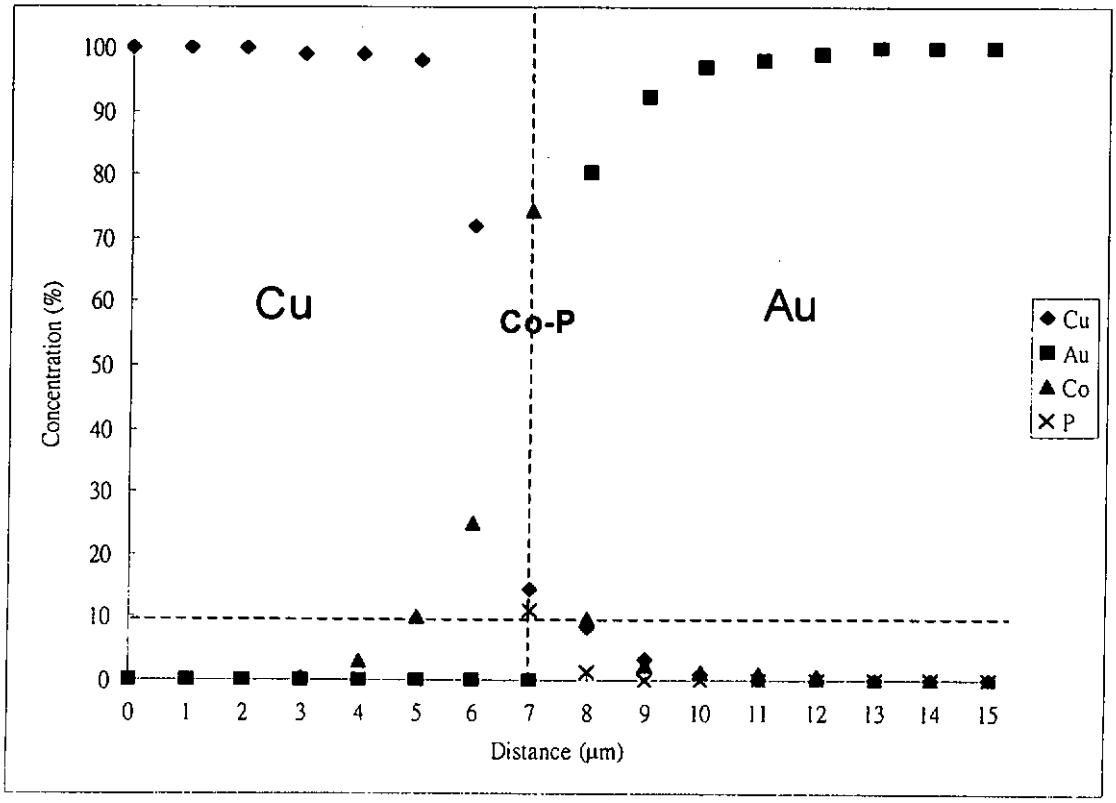

Fig 5.3.5 Concentration- Distance Profile of Cu/Co-P/Au system after heat treatment at 400°C for 48h.

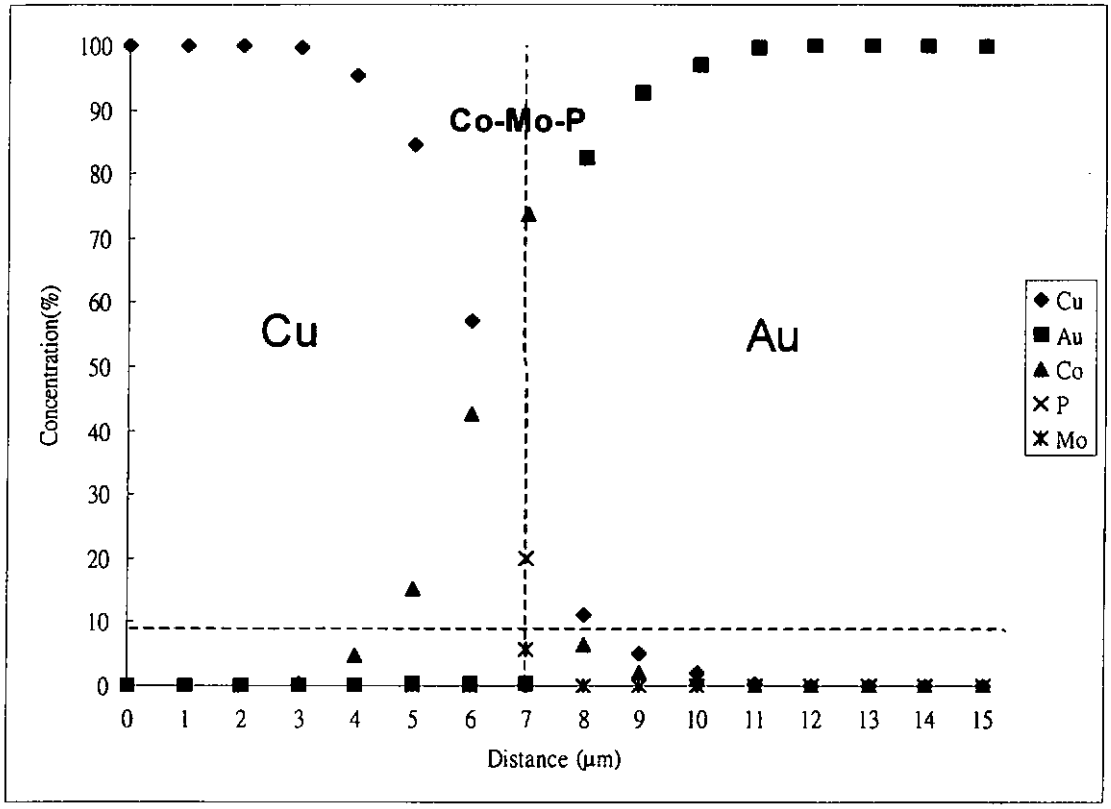

Fig 5.3.6 Concentration- Distance Profile of Cu/Co-Mo-P/Au system after heat treatment at 400°C for 48h.

Table 5.3 Penetration values of different Cu/barrier/Au specimens.

Barrier	Thickness(μm)	Copper penetration(μm)	Barrier coating penetration(μm)
Ni	1	4	ND*
Co	1	2	1
Co-Mo	1	1	ND*
Co-P	1	1	1
Co-Mo-P	1	1	ND*

*ND: No diffusion

Co-Mo and Co-Mo-P barrier plated specimens as shown in Table 5.3, show the best performance among the other barrier. Both barriers of 1 μm decrease copper penetration in diffusion heat treatment at 400°C for 48 hours to less than 1 μm. The thermal stability of Co-Mo and Co-Mo-P at 400°C is also good such that negligible

diffusion of coating to gold layers were observed.

Co and Co-P coatings show fair performance as a diffusion barrier for copper diffusion. With Co barrier thickness of 1 μm, values of copper penetration are 2 μm and 1 μm respectively. The thermal stability of Co and Co-P are not as good as Co-Mo and Co-Mo-P since the barrier coating penetrations were observed. The cobalt barrier penetration to gold is about 1 μm. The results show that nickel barrier is not as effective as cobalt.

5.4 Internal Stress Studies

The internal stress of the cobalt, cobalt-molybdenum (form citrate bath), cobalt-phosphorus and cobalt-molybdenum-phosphorus were determined and listed in Table 5.4

Table 5.4 The internal stress of the Co, Co-Mo (form citrate bath), Co-P & Co-Mo-P

Coating	Alloy Composition	Internal Stress*
Co(from citrate bath)	-	+6.2~8.7
Co-Mo	68.4% Co, 31.6% Mo	+6.1~8.9
Co-P	78% Co, 22% P	+10.6~12.7
Co-Mo-P	72% Co, 8% Mo, 20% P	+11.4~15.5

* Positive Internal Stress means tensile stress.

The results of study show that tensile stresses exist in cobalt and cobalt base alloy. Internal stress increases when the molybdenum or phosphorus is introduced. The effect of phosphorus is more predominat than molybdenum. The internal stress is related to the adsorption of atomic hydrogen. The atomic hydrogen plays a role of reducing agent in reduction of phosphorus. Therefore, the coating may also absorb the atomic hydrogen and the internal stress increases.

5.5 X-ray Diffraction Studies

The bright coating Co-Mo with the highest molybdenum content from each type bath were selected for XRD determination. The coating with 31.6%(wt.%) Mo from citrate bath and the coating with 25.3%(wt.%) Mo from free alkaline bath were selected. The Co-Mo-P coating with 8.0% Mo and 20.0% P was also selected.

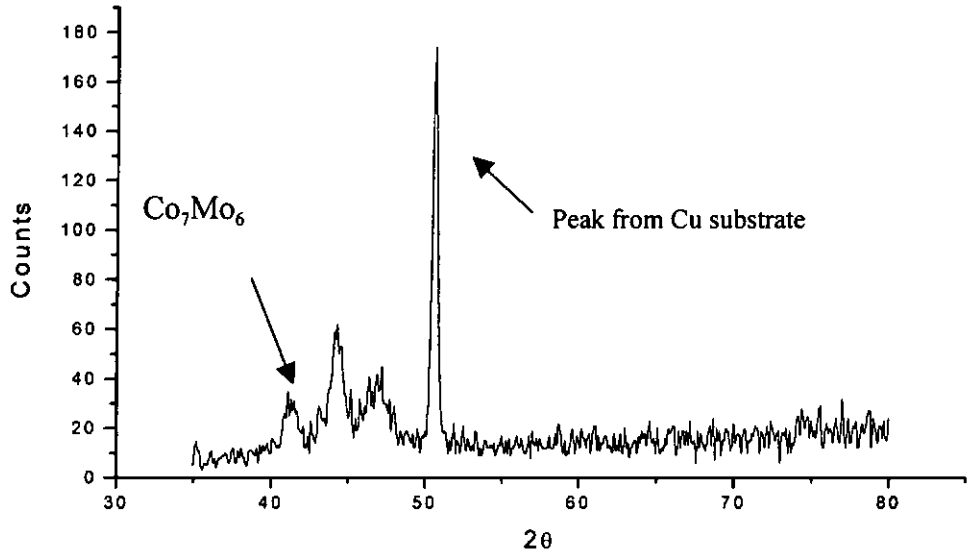

Figure 5.5.1 XRD spectrum of Co-Mo coating with 31.6% Mo from citrate bath.

Figure 5.5.1 shows the X-ray diffraction pattern of the Co-Mo with 31.6% Mo electrodeposit plated from a citrate bath. Co_7Mo_6 [52] is indicated in XRD spectrum.

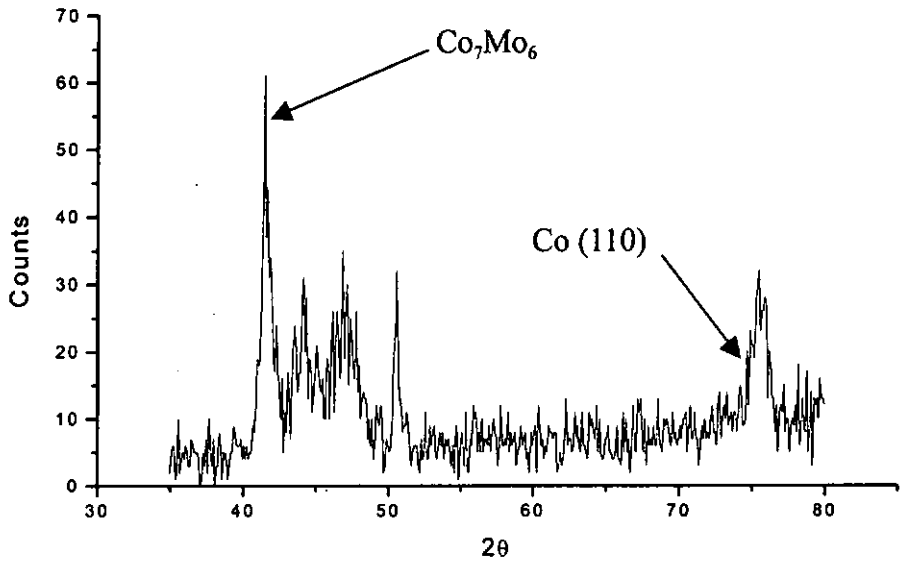

Figure 5.5.2 XRD spectrum of Co-Mo coating with 25.3% Mo from free alkaline bath.

Figure 5.5.2 shows the X-ray diffraction pattern of the Co-Mo with 25.3 wt.% Mo electrodeposit plated from a free alkaline bath. Co_7Mo_6 [53] is indicated in XRD spectrum. The Co(110) plane also can be indicated in spectrum. These show that the cobalt-molybdenum intermetallic compound and cobalt metal co-exist in the coating. However, an amorphous Co-Mo coating seems could not be obtained.

The Co-22 wt% P electrodeposit and Co- 8 wt% Mo-20 wt% P give a similar diffraction pattern. Figure 5.5.3 shows the X-ray diffraction pattern of the Co-Mo-P with 8.0 wt% Mo and 20 wt% P electrodeposit plated from citrate. Typical diffraction pattern for amorphous alloys were observed.

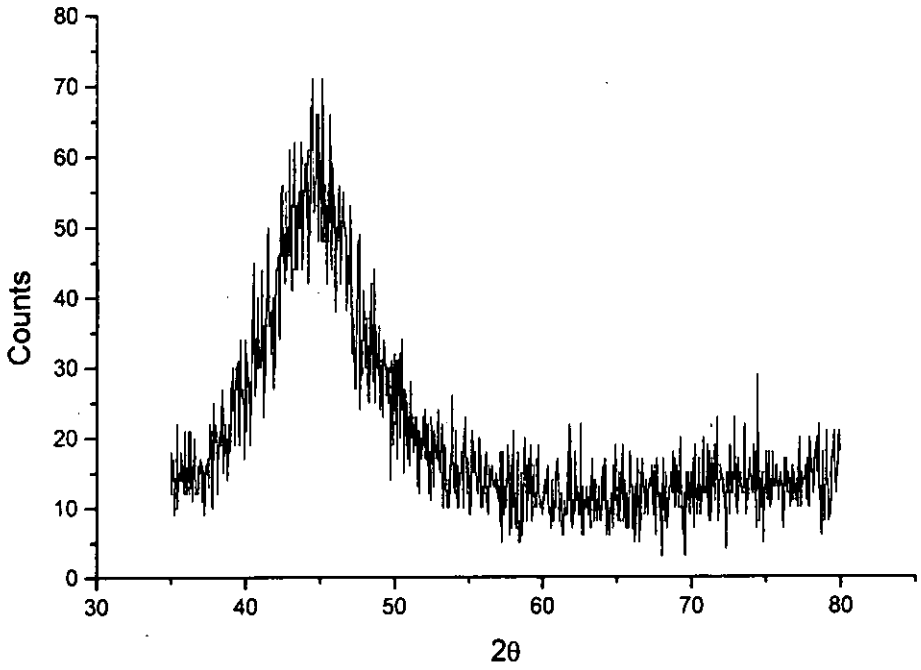

Figure 5.5.3 XRD spectrum of Co-Mo-P coating with 8.0% Mo and 20% P from citrate bath

Pao Yue-kong Library
PolyU • Hong Kong

5.6 Corrosion Test

5.6.1 Anti-perspiration Test

The corrosion rates of cobalt, cobalt-molybdenum, cobalt-phosphorus, cobalt-molybdenum-phosphorus coating in artificial perspiration are listed in Table 5.6.1.

Table 5.6.1. The corrosion rate of coatings in artificial perspiration

Sample	Alloy Composition	Corrosion rate (mg Co/ cm^2 week)
Cobalt	-	7.38
Cobalt-Molybdenum (from free alkaline bath)	74.7% Co, 25.3% Mo	6.21
Cobalt-Molybdenum (from citrate bath)	68.4% Co, 31.6% Mo	0.755
Cobalt-Phosphorus (from citrate bath)	78% Co, 22% P	0.721
Cobalt-Molybdenum-Phosphorus (from citrate bath)	72% Co, 8% Mo, 20% P	0.356

The cobalt-molybdenum alloy from free alkaline bath is not as good as that from citrate bath and the corrosion rate is similar to pure cobalt. Cobalt alloyed with molybdenum and phosphorus enhances corrosion resistance. The results show that it is about 10 times enhancement in cobalt alloyed with molybdenum and 8 times enhancement in cobalt alloyed with phosphorus. It is about 20 times enhancement in cobalt alloyed with both molybdenum and phosphorus. In the above investigation, the corrosion property of cobalt was changed dramatically in artificial perspiration after alloying with molybdenum and phosphorus. Molybdenum is known to increase anti-

corrosion property in metal alloying. The oxides of molybdenum develop a very good passive coating to prevent corrosion. Alloys such as 316 stainless steel containing 2-3% molybdenum can enhance corrosion resistance.

Amorphous metal alloys are more resist to corrosion due to absence of crystal defect. From the X-ray Diffraction studies, both cobalt-molybdenum and cobalt-molybdenum-phosphorus electrodeposits are amorphous. The synergistic effect of molybdenum and phosphorus show about 2 times enhancement in corrosion resistance in artificial perspiration.

5.6.2 DC Polarization Data

Bright coating of Co-Mo with the highest molybdenum content from each type of bath were selected for corrosion determination. Figures 5.6.1 to 5.6.3 illustrate the potentiodynamic measurement obtained with the cobalt-molybdenum and cobalt-molybdenum-phosphorus electrodeposits. Figure 5.6.1 shows the Tafel plots measured on the cobalt-molybdenum from citrate bath which contains 31.6%(w/w) molybdenum.

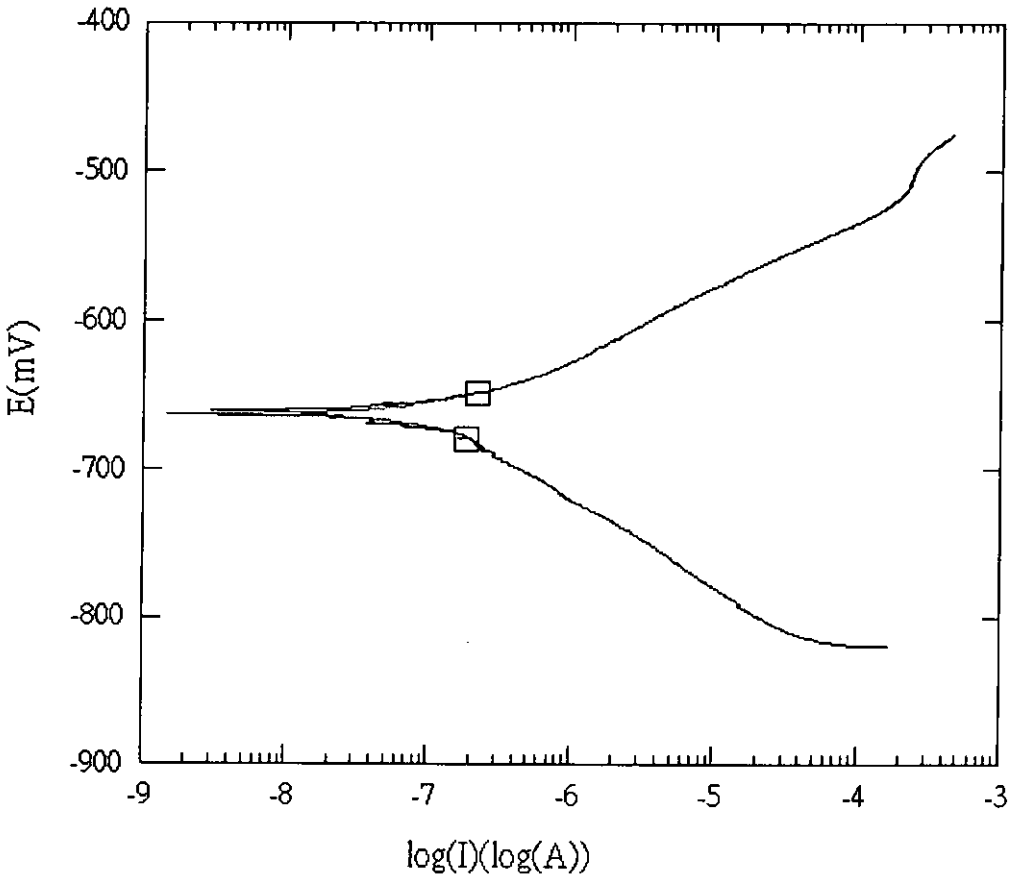

Figure 5.6.1 A potential scan of the Co-Mo electrodeposit from citrate bath

Figure 5.6.2 shows the Tafel plots measured on the cobalt-molybdenum from free alkaline bath which contains 25.6%(w/w) molybdenum.

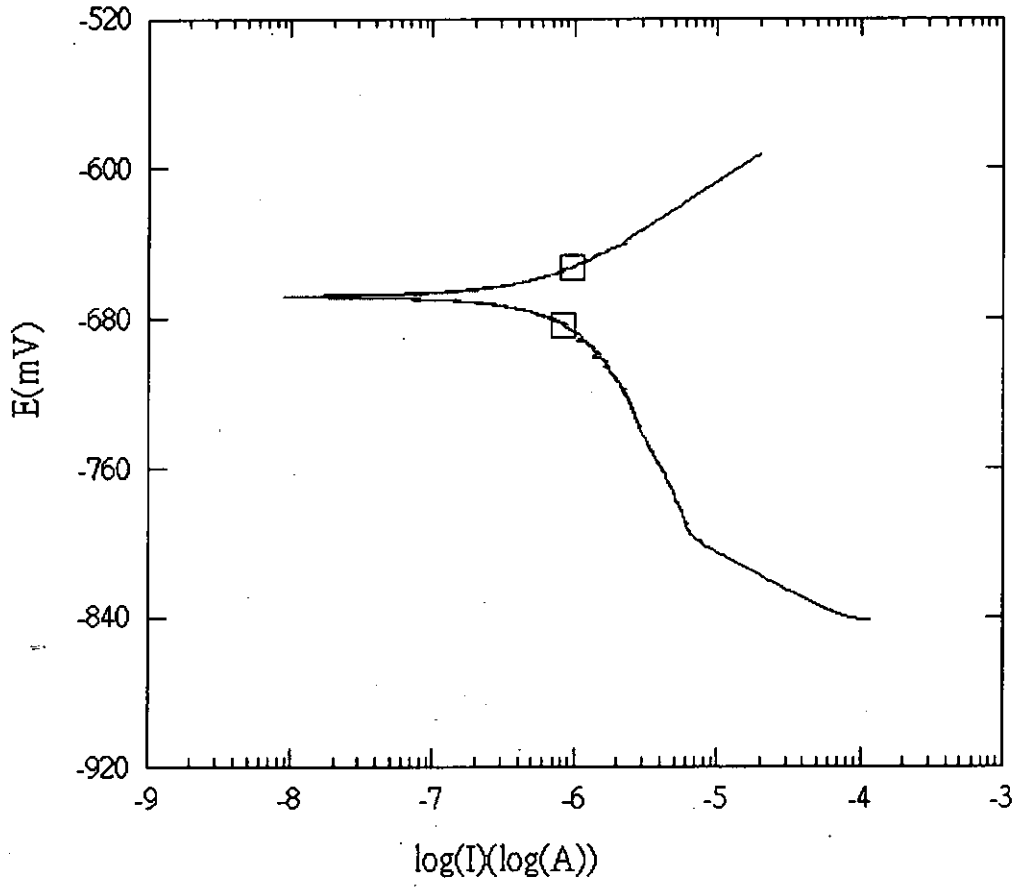

Figure 5.6.2 A potential scan of the Co-Mo electrodeposit from free alkaline bath

Figure 5.6.3 shows the Tafel plots measured on the cobalt-molybdenum-phosphorus from citrate bath which contains 8.0%(w/w) molybdenum and 20.0%(w/w) phosphorus. The resulting values for corrosion potential (E_{corr}) and corrosion current density (I_{corr}) are given in Table 4.5.

Table 5.6.2 The E_{corr} and I_{corr} for different electrodeposits.

Specimen	Composition	E_{corr} (mV)	I_{corr} (nA/cm^2)
Co-Mo (citrate bath)	Co-68.4%, Mo-31.6%	-663.5	262.9
Co-Mo (free alkaline bath)	Co-74.4%, Mo-25.6%	-668.3	1241.0
Co-Mo-P	Co-72%, Mo-8%, P-20%	-346.7	240.3

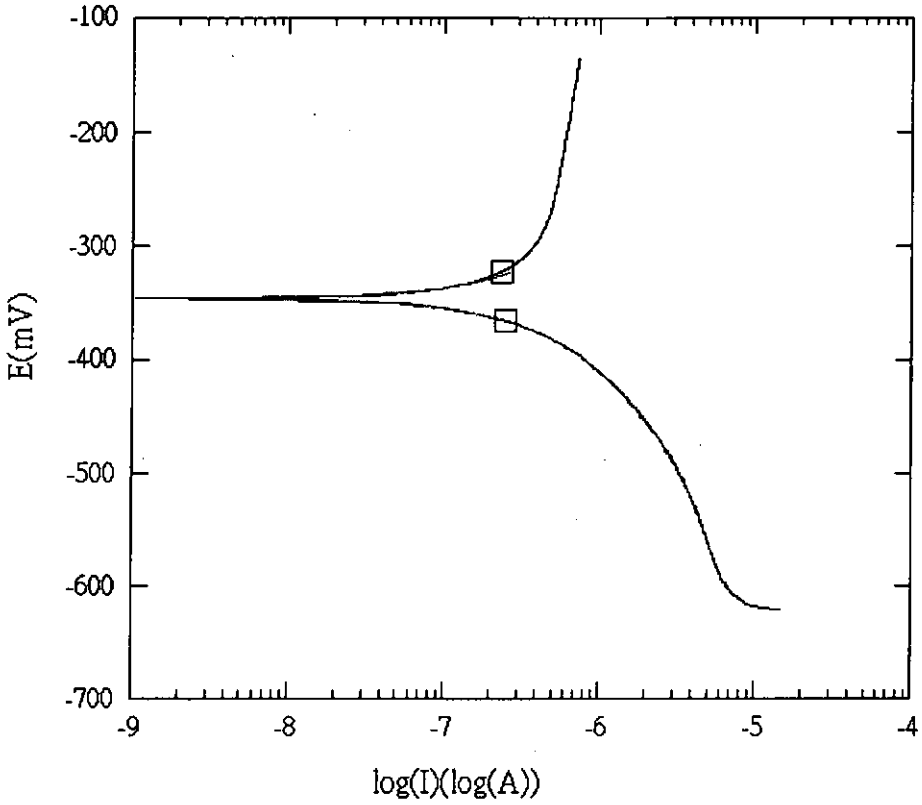

Figure 5.6.3 A potential scan of the Co-Mo-P electrodeposit from citrate bath

The data shows that the Co-Mo coating from the free alkaline bath is the most active coating in 3.5% sodium chloride which has the most negative E_{corr} (-668.3mV) and the largest I_{corr} (1241.0 nA) among different electrodeposits. There is only small difference in terms of E_{corr} between Co-Mo coatings from citrate bath and free alkaline bath. For the Co-Mo-P coating, which is an amorphous coating, with the most positive E_{corr} (-346.7mV) and the smallest I_{corr} (240.3 nA) among different electrodeposits.

Chapter 6 Conclusions

6.1 General Comments

The electroplating conditions for cobalt-molybdenum, cobalt-phosphorus and cobalt-molybdenum-phosphorus alloy coatings were studied. Citrate was used as the main complexing agent for all the plating baths. The free alkaline bath of cobalt-molybdenum also was studied. The covering power of the free alkaline baths of Co-Mo alloy is very good. However, the coatings formed did not exhibit as high corrosion resistance as those coatings obtained from the citrate bath. The citrate cobalt-molybdenum-phosphorus bath was formed by combining the citrate Co-Mo and citrate Co-P bath. The deposit obtained contains 8% molybdenum and 20% phosphorus. From this study, tensile stresses exist in all cobalt and cobalt base alloy coatings.

An attempt was made to evaluate the diffusion properties of different Ni, Co-Mo, Co-P and Co-Mo-P electrodeposited coatings. The interdiffusion coefficients of copper/barrier were determinated by concentration-profiling and calculated Boltzmann-Matano method. In general, it was found that the interdiffusion coefficients for nickel is higher than that of the cobalt base alloys. The results have indicated that thebarrier propety of these alloys are as effective and economical substitutes for nickel. Most data for the systems involved in this study deal with

temperature from 400°C to 800°C. Diffusion barrier properties of nickel and cobalt-molybdenum show substantial changes in high temperature range. For example, the temperature range of 700 –800 °C indicates a transition between the higher and lower diffusion mechanisms for copper/cobalt-molybdenum. This observation implies that the effectiveness of a diffusion barrier coating depends on the working temperatures required.

6.2 Main Findings

1. Cobalt-molybdenum alloy coatings can be obtained from a citrate bath containing cobalt sulfate and sodium molybdate. The maximum content of molybdenum inside the coating is 31.6% (weight %). The molybdenum content will increase as the concentration of sodium molybdate in bath solution increase. The coating formed is not an amorphous coating. The coating has better corrosion resistance than that of the Co-Mo alloy from the free alkaline bath.
2. The free alkaline baths for depositing cobalt-molybdenum have very good covering power (The ability for plating in very low current density). The maximum content of molybdenum of coating is 25.3% (weight %). The corrosion resistance is not as good as that of the coating that from the citrate bath and just slightly better than that of pure cobalt in the anti-perspiration test.

3. It is possible to obtain cobalt-phosphorus alloy coatings by using a citrate bath containing cobalt sulfate and sodium hypophoshite. For suitable plating conditions, the coatings formed are bright and with 22.1 weight % of phosphorus.
4. The citrate bath for plating cobalt-molybdenum and cobalt-phosphorus alloy can be combined to obtain cobalt-molybdenum-phosphorus plating bath. The plating bath can produce a bright alloy with 8% Mo and 20% P (weight %). The coating is amorphous and has 20 times improvement in anti-perspiration as compared with pure cobalt.
5. The cobalt base alloy coatings show better diffusion barrier property than that of nickel. Higher interdiffusion coefficients were observed for nickel than that of cobalt base alloys. However, the Co-Mo coating becomes poor in terms barrier property when the temperature is above 700°C.
6. From the Arrhenius plots of Cu/Ni and Cu/Co-Mo system, a transition region of changing diffusion mechanism is shown. The Cu/Co-P and Cu/Co-Mo-P systems did not show such transition region.
7. Diffusion barrier capability for different electrodeposited barrier coatings for Cu/Au interdiffusion at 400°C can be ranked in ascending order as Ni, Co, Co-P, Co-Mo, Co-Mo-P.
8. All electrodeposited cobalt alloy coatings studied are have tensile stress. The

introduction of phosphorus and molybdenum in the coating increases the stress.

6.3 Suggestions for Future Work

The objectives of the project are to investigate the electroplating methods for plating cobalt-molybdenum, cobalt-phosphorus and cobalt-molybdenum-phosphorus alloy coatings. The diffusion behavior and some coating properties were also studied. In order to get more information of the electrodeoposition and diffusion barrier mechanism, the author hopes that the following suggestions can help achieve better understanding for the deposition process and diffusion mechanism.

1. It is believed that the amorphous coatings are very good barriers since no grain boundary for the path of diffusion flux. Both Co-Mo-P and Co-P coatings are amorphous but they may recrystallize on heat treatment. The XRD spectra of different temperatures annealed Co-Mo-P and Co-P coatings can show the thermal stability in terms of resistance to recrystallization.
2. The studies of cathode polarization curve of the citrate baths are useful to find out know the mechanisms of the deposition process. This is helpful to improve the bath condition to obtain a better coating and improve the performance of bath.
3. The insoluble anodes are used in all citrate baths. However, the anodic oxidation of citrate may harm the bath solution. A study of preventing oxidization of the citrate at theanode is useful for prolonging the bath life. The possible methods

suggested are using new anode materials or ion-exchange membranes.

4. The internal stress can harm the coatings. A study on the effect of additives on internal stress may be useful. Some common additives such as saccharin may be used for reducing the internal stress.

References

1. Beck, R. P., Metalloberflache, 1993, **47**, 20.

2. Common Position (EC) No. 12/94, *Official Journal of the European Communities*, No.C137/60-64, 19 May (1994).

3. Ng, W.Y., Yeung, L.K., Chow, K.M. and Wong, T.T., *Electroplating and Finishing*, 1996, **15**, 14.

4. Lim, J. K., Russo, J.S. and Antonier, E., *Plat. Surf. Finish.*, 1996, **83**(3), 64.

5. Green, R.V. and Sargent, J.F., *Trans. Inst. Metal Finish.*, 1997, **75**(3), B51

6. Nishizawa, T. and Ishada, T. in "*Handbook of Binary Phase Diagrams*", Vol. 2, Moffalt, W.G. (Ed.), Genium Pub. Cop., Schenectady, NY, 1984.

7. Chow, K. M., *Thesis*, The Hong Kong Polytechnic University (1997).

8. Basketter, D.A., Barnes, E.G. and Allenly, C.F. "*Do Transition Metals in Household and Personal Product Play a Role in Allergic Contact Dermatitis*" in "*The Environmental Treat to the Skin*" , Marks, R and Plewig, G(ed.), Martin Dunity, London, **1992**.

9. 渡邊 徹, *アモルファスめっき法とその應用*, p. 60, 日刊工業新聞社, (1990).

10. Briggs, J.Z. and Schultze, H.W., *Plating* **46**, 1370-1376 (1959)

11. Safranek, W. H. and Vaaler, L. E. *Plating* **46**, 133-143 (1959)

12. Brenner, Abner, *Electrodeposition of Alloy, Principles and Practice*, Vol. II , p.

459, Academic Press,(1963)

13. Owen, E.L., "Interdiffusion", *Properties of Electrodeposits: Their Measurement and Significance*, Sard, R., Leidheiser, H., Jr., and Ogburn, F., Editors, The Electrochemical Society (1975).

14. Pinnel, M.R., "Diffusion related Behavior of Gold in Thin Film Systems", *Gold Bulletin,* **12**, No.2, 62(April 1979).

15. Antler, M., Plating **57**, 615(1970)

16. Giannuzzl, L.A., Hyres II J. W., Pickering, H.W., Bitler W.R., *Final Report, American Electroplaters' Society Project* no. 67, 1989.

17. Fairhurst, S., H.P.A. Illing, *Toxicol. Rev.* 19(1987) 204.

18. Coogan, T.P., Latta, D.M., Snow, E.T., Costa, M., *Crit. Rev. Toxicol.* **19**(4) (1989) 341.

19. 青谷 薫, *合金めっき I – Au 合金めっき I*, p. 123, 槙書店, (1999).

20. 曾華梁 等, *電鍍工藝手冊*, p.282, 機械工業出版社, (1989)

21. Brenner, Abner, *Electrodeposition of Alloy, Principles and Practice*, Vol. II , p.414, Academic Press,(1963)

22. Ng, W. Y. and Cheung, K. L., Electroplating and Finishing, 1998, **17**, 11

23. Ng, W. Y., Yeung, L.Y., Chow, K. M. and Wong, T. T., Electroplating and Finishing, 1996, **15**, 14

24. Price, W. P. and Brown, O. W.. Trans. Electrochem. Soc., vol. 70, p. 425, 1936.

25. Brenner, Abner, *Electrodeposition of Alloy, Principles and Practice*, Vol. I , p.78, Academic Press,(1963)

26. 渡邊 徹, *アモルファスめっき法とその應用*, p. 151, 日刊工業新聞社, (1990).

27. Seim, H. J. and Holt, M. L., *J. Electrochem. Soc.* **96**, 205-213(1949)

28. Ernst, D.W. and Holt, M. L., *J. Electrochem. Soc.* **102**, 461(1955)

29. Jyoko Yukimi and Ohno Izumi and Haruyama Shiro, *J. Japan Inst. Metals.* **52**, 95-102(1988)

30. Yntema, L. F, , U.S. *U.S. Patent* 2,599,179 (1952)

31. Holt, M.L., *Met Finish.* **54**(9), 48 (1956)

32. Brenner, Abner, *Electrodeposition of Alloy, Principles and Practice*, Vol. II , p.443-448, Academic Press,(1963)

33. 渡邊 徹, *アモルファスめっき法とその應用*, p. 158-163, 日刊工業新聞社, (1990).

34. Brenner, Abner, *Electrodeposition of Alloy, Principles and Practice*, Vol. II , p.457, Academic Press,(1963)

35. Brenner, Abner, *Electrodeposition of Alloy, Principles and Practice*, Vol. II , p.459, Academic Press,(1963)

36. 屠振密, *電鍍合金原理與工藝* 國防工業出版社 1993. p. 330-331

37. 曾華梁 等, *電鍍工藝手冊*, p.555-556, 機械工業出版社, (1989)

38. 曾華梁 等, *電鍍工藝手冊*, p.527, 機械工業出版社, (1989)

39. Gabe, D.R. and Wilcox G.D., *Trans. Inst. Metal Finish.*, 1993, **71**(2), 71

40. Schmalzried, H., "Solid State Reactions", (Verag Chemie, 1981), pp. 87-89

41. Ng, W. Y., Man, H. C., Yeung, C. H., Siu, C. L. and Lee, C. Y., Electroplating and Finishing, 1999, **18**, 4

42. 電氣鍍金研究会編, 機能めっき皮膜の物性, 日刊工業新聞社, p.23-31(1987)

43. Lowenheim, Fredrick A., *Modern Electroplating*, (Wiley-Interscience, 1981), p. 9

44. Lowenheim, Fredrick A., *Modern Electroplating*, (Wiley-Interscience, 1981), p. 702

45. European Directive EN1811

46. Van, Orden, A. C., *CORROSION/91*, Paper 140, National Association of Corrosion Engineers, Houston, TX, (1991)

47. Mansfeld,. F. "The Polarization Resistance Technique for Measuring Corrosion Current", *Advances in Corrosion Science and Technology Vol. 6*, M.G. Fontana and R.W. Staehle, Eds.,(Plenum Press, New York, 1976). P. 163

48. Stern, M. *Corrosion*, **14(9)**, 440-444(1958).

49. Geary, A.L. and Stern, M., *Journal of the Electrochemical Society*, **104**, 56-63, (1957)

50. "Model 352/252 Softcorr II Corrosion Measurement & Analysis Softwore," EG & G, Princeton, NJ, (1991).

51. Link ISIS Progame, Oxford Instrument (UK) Ltd. (1994)

52. Marx, D.R., Bitler W.R., Bitler, W. R. and Pickering, H. W., "Metallic Barrier for Protection of Contacts in Electronic Circuits from Atmospheric Corrosion", Final Report on AES Project No. 29, *Plating and Surface Finishing*, June, pp. 69-72. (1977)

53. ASTM X-ray Diffraction Data Card No. 5-0727, No. 29-489